

Project Number: ME-RLN-0802

EXCESS MATERIAL UNLOAD MECHANISM REDESIGN

A Major Qualifying Project Report

Submitted to the Faculty

of the

WORCESTER POLYTECHNIC INSTITUTE

In partial fulfillment of the requirements for the

Degree of Bachelor of Science

By

Taylor LaLonde

Michael Sangermano

Joseph Wilkos

Date: January 15, 2009

Approved:

Professor Robert L. Norton. Advisor

Acknowledgements

Our MQP would like to thank the following individuals from WPI and the Sponsoring Company for their dedication and help throughout the course of this project:

- Professor Robert Norton
- Charlie Gillis
- William Motherway
- Ken Belliveau
- Ernie Chandler
- Dave Clancy
- Adriana Hera
- Corey Maynard
- Ping Xu

Abstract

This project investigates the dynamic behavior of an excess material unload station on an indexing machine used by the sponsor company. This station is used to remove material left over from operations performed previously in the machine. Failure to remove material at this station causes a stop in machine operation, which is undesirable. Investigation of potential causes for this failure included testing the machine with accelerometers, recording high-speed video of the machine in operation, and researching potential errors by discussing station operation with engineers and mechanics familiar with the machine. Results of this investigation showed that the likely root cause of this error was a related problem happening at an upstream station. With this information, it was decided to redesign the current station to achieve the same operation with a similar system. The proposed system redesign utilizes one less cam and five fewer links than the original design.

Executive Summary

The main goal of this project was to redesign components of the excess material removal station in order to reduce machine downtime caused by failed material removal. Other goals were to simplify the dynamics of the system and investigate pickoff tool design flaws. Different components of the system were analyzed to determine their impact on this problem. Analysis of the station found no major problems with this system, as the station demonstrated well-behaved motions and the probable root cause of the failure was found to occur at a different station. Because of this, a redesign of the system was initiated with the intent to simplify the system's dynamics.

The analysis process began by creating a dynamic model of the system to calculate the displacement, velocity, and acceleration of the slide and pickoff tool. This required developing a lumped mass and stiffness model of each linkage in the station. Effective stiffness calculations were determined by performing finite element analysis of each link and combining the stiffness in series for both linkage trains. Effective masses of the linkage trains were obtained by using Pro/Engineer CAD models to calculate the mass and then using conventional lumped model techniques to add the masses together. Two differential equations were created to model the system and they were solved using MATLAB. MATLAB provided graphs of the displacement, velocity, and acceleration of the two end effectors in the system: the slide and the pickoff tool. Data was also taken from the real excess material removal station using accelerometers and a signal analyzer. High-speed video was also taken of the station during standard operation to provide a visual understanding of system dynamics.

The accelerometer data indicated that the excess material removal station, as now designed, is a very well behaved system. There were no acceleration spikes in the system other

than those expected due to designed in impacts such as where the locating pin enters the nest. The high-speed video also did not indicate that the pickoff tool was having trouble removing the excess material. Discussions with engineers and mechanics revealed that the problems detected at this station were most likely due to errors happening upstream in the process. These errors happen at other stations where the excess material became misaligned or broken. This causes the pickoff tool at this station to be unable to remove the material.

The conclusion was made that there was no major problem with the excess material removal station's current design. Therefore, the project's focus was shifted to the secondary goal of designing a simpler system. The current system is very complex, as the pickoff tool has a pivot is that is carried on a slide. This makes this system a coupled, two degree of freedom system.

To simplify this system, a fourbar linkage was used. Instead of having a two-degree of freedom system driven by two cams, a fourbar linkage allows for a simpler system that has one degree of freedom and only one cam. The fourbar linkage design was adapted from a previous project's redesign of one of the sponsor company's other machines. This project was another WPI MQP from 2004 named "Redesign of a Cartridge Unload Mechanism" [Baird].

The redesigned excess material removal station is a cam-driven eightbar linkage. This design features a single cam that moves a linkage train that drives the fourbar linkage. The pickoff tool is attached to the coupler link of the fourbar. When the input link of the fourbar linkage is driven, the pickoff tool goes through the desired motion of moving in to remove the excess material and rotating downwards to dispose of the material in a scrap chute. A new cam was designed to drive this linkage. The new cam allows for adequate time in contact with the

excess material in order to achieve vacuum, and it provides sufficient clearance between the pickoff tool and the nests.

To implement this redesign, a new cam and new links would need to be manufactured. The existing mounting frame also requires a few changes. The cam would be placed in the same position as one of the cams in the original station. The new design is much simpler and requires five fewer links and one fewer cam than the current design.

There may not be economic justifications for implementing this redesigned system in the existing machines, as the current excess material removal station is most likely not the root cause of the pickoff failure. However, this new design could provide a simpler solution to part removal in future machines. This design also showcases the ability for simple linkage system to achieve complex motion. Such ability can be utilized in future system designs to create less expensive, similar systems.

Table of Contents

Acknowledgements.....	i
Abstract.....	ii
Executive Summary.....	iii
1 Introduction.....	1
1.1 Background.....	1
1.1.1 System Dynamics.....	3
1.1.2 Pickoff Tool.....	4
2 Goal Statement.....	5
2.1 Sub Tasks.....	5
3 Investigation of the Current Design.....	6
3.1 Modeling the System.....	6
3.2 Testing.....	7
3.2.1 Accelerometer Testing.....	7
3.2.2 High-Speed Video.....	8
3.2.3 High-Speed Video with Accelerometer Data.....	9
3.3 System Analysis.....	10
3.3.1 Basic Analysis.....	10
3.3.2 Analysis of Test Data.....	12
3.3.2.1 Acceleration Analysis.....	12
3.3.2.2 High speed Video with Accelerometer Data.....	15
3.3.3 Theoretical Models of Current Design.....	16
3.3.3.1 MATLAB Model.....	17
3.3.4 Discussions with Engineers and Mechanics.....	26
3.4 Investigation Conclusions.....	27
4 Station Redesign.....	28
4.1 Original Fourbar Linkage Design.....	28
4.2 Initial Redesign.....	29
4.3 Final Redesign.....	32
4.3.1 Final Redesign Overview.....	33

4.3.2	Design Component.....	35
4.3.2.1	Weldment and Height Adjustment Bracket.....	36
4.3.2.2	Connecting Rods.....	38
4.3.2.3	Bellcrank.....	38
4.3.2.4	Components Reused From Removal Station.....	39
4.3.2.5	Fourbar.....	40
4.3.3	Locating Considerations	44
4.3.3.1	Fourbar X position.....	45
4.3.3.2	Fourbar Y position.....	45
4.3.3.3	Fourbar Z position	46
4.3.4	Clearance.....	46
4.4	Cam Design	47
4.5	New System analysis.....	54
4.5.1	Basic Analysis.....	55
4.5.2	Theoretical Model of New Design.....	55
4.5.2.1	Dynacam Model	59
4.5.2.2	Fourbar Model	61
4.5.2.3	Sixbar Model	64
4.5.2.4	Fatigue Analysis	66
4.5.2.5	Tear Out Analysis.....	68
4.5.2.6	Gripper Force Analysis.....	69
4.5.3	Design Analysis Results	70
5	Conclusions.....	70
5.1	Existing Station Design.....	71
5.2	Redesigned Station.....	71
6	Recommendations.....	73
7	References.....	75
8	Appendices.....	76
8.1	Appendix A: High-Speed Video Shot.....	76
8.1.1	Shot 1	76
8.1.2	Shot 2	76

8.1.3	Shot 3	77
8.1.4	Shot 4	77
8.1.5	Shot 5	78
8.2	Appendix B: Effective Mass and Stiffness Calculations	79
8.3	Appendix C: MATLAB Code	84
8.3.1	Main MATLAB Code.....	84
8.3.2	Cam Systems Code	85
8.4	Appendix D: List of Drawings	86
8.5	Appendix E: Pin Fatigue Analysis MathCAD Sheet	87
8.6	Appendix F: Coupler COSMOSWorks Screenshots.....	92
8.7	Appendix G: Tear out Analysis MathCAD Sheet.....	93
8.8	Appendix H: Gripper Force Analysis MathCAD Sheet.....	94

Table of Figures

Figure 1: Current Excess Unload Station.....	2
Figure 2: Nest, Pickoff Tool, and Slide	2
Figure 3: Pickoff Tool Pick up and Blowoff Positions.....	3
Figure 4: Pickoff Tool Components	4
Figure 5: CAD Model of Scrap Removal Station.....	6
Figure 6: Accelerometer Placement.....	7
Figure 7: Pickoff Tool Accelerometer Placement	9
Figure 8: How the Part is Assembled	11
Figure 9: Finite Element Analysis of a Part.....	11
Figure 10: Rotate Linkage Acceleration vs. Cam Angle Graph.....	13
Figure 11: Slider Linkage Acceleration vs. Cam Angle Graph.....	13
Figure 12: High-Speed Video with Accelerometer Graph Screenshot.....	16
Figure 13: Lumped Parameter Model.....	17
Figure 14: Slide Displacement Function (MATLAB Input 's').....	20
Figure 15: Pickoff Tool Displacement Function (MATLAB Input 'sigma')	20
Figure 16: Slide Velocity Function (MATLAB Input 'sdot').....	21
Figure 17: Pickoff Tool Velocity Function (MATLAB Input 'sigmadot').....	21
Figure 18: Slide Position Data from MATLAB (x).....	22
Figure 19: Slide Velocity Data from MATLAB (xdot)	22
Figure 20: Slide Acceleration Data from MATLAB (xdotdot)	23
Figure 21: Pickoff Tool Position Data from MATLAB (theta).....	23
Figure 22: Pickoff Tool Velocity Data from MATLAB (thetadot)	24
Figure 23: Pickoff Tool Acceleration Data from MATLAB (thetadotdot)	24
Figure 24: Pickoff Tool Acceleration (Real Data vs. MATLAB)	25
Figure 25: Slide Acceleration (Real Data vs. MATLAB)	25
Figure 26: Previously Designed Fourbar Linkage Design.....	29
Figure 27: Portion of Coupler Curve of Fourbar Linkage Needed.....	30
Figure 28: Linkage in Full Down Position	31
Figure 29: Model of Belt and Nest System.....	33
Figure 30: Fourbar Assembly	34
Figure 31: Parts of Existing Station Not incorporated in New Design.....	35
Figure 32: Weldment	36
Figure 33: Height Adjustment Bracket.....	37
Figure 34: Connecting Rods	38
Figure 35: Bellcrank	38
Figure 36: Removal Station Components Incorporated in Redesign.....	39
Figure 37: Crank	40
Figure 38: Detail of Crank Bushing Hole.....	41
Figure 39: Coupler	42

Figure 40: Rocker	43
Figure 41: Axis Orientation of the Weldment	44
Figure 42: Slots for Adjustment in the X-direction	45
Figure 43: Clearance between Path of Nest and Pickoff Tool.....	46
Figure 44: First Cam Iteration S-V-A-J Diagram.....	47
Figure 45: Boundary Conditions Used In First Cam Iteration.....	48
Figure 46: S-V-A-J Diagram of Cam Function with Two Splines	49
Figure 47: S-V-A-J Diagram for Cam with Two Dwells	50
Figure 48: Knot Location of B-spline for Cam Rise.....	51
Figure 49: Knot Location of B-spline for Cam Fall	51
Figure 50: S-V-A-J Diagram for Cam with Shortened Stroke	53
Figure 51: S-V-A-J of Final Cam Design.....	54
Figure 52: 2D System	56
Figure 53: Fourbar Section Geometry	57
Figure 54: Sixbar Section Geometry.....	57
Figure 55: Bellcrank Fold	58
Figure 56: Final Theoretical Model Geometry	58
Figure 57: Dynacam Model Geometry	59
Figure 58: Dynacam Exported S, V, A Data	60
Figure 59: Fourbar Model Geometry.....	61
Figure 60: Theoretical Acceleration of Links 2, 3, and 4 from the Fourbar Model	62
Figure 61: Theoretical Force on Cam Lever Pivot from Fourbar Model	63
Figure 62: Fourbar Exported θ , ω , α Data	63
Figure 63: Sixbar Model Geometry	64
Figure 64: Theoretical Acceleration of Pickoff Tool Pin from Sixbar Model.....	65
Figure 65: Theoretical Force on Rocker's Pivot from Sixbar Model.....	66

List of Tables

Table 1: Mass Properties of Dynacam Model.....	60
Table 2: Mass Properties of Sixbar Model	65
Table 3: Pin Forces from the Sixbar Model.....	67
Table 4: Theoretical Forces on Fourbar Links.....	68
Table 5: Redesigned System Analysis Results	70

1 Introduction

The sponsor company uses an indexing machine to assemble a consumer product. To accomplish this, a moveable nest is indexed to several stations that place two materials, break one to a proper shape, weld the two to make an assembly, and then remove the products. The material break operation results in a small amount of excess material being left on the nest after the finished product is removed. This excess material is later removed at the excess material unload station that is the subject of this project.

This excess material unload device periodically fails to remove the excess material from the moving nest. This failure triggers an automatic stop when detected by sensors at the next station. Once a stop occurs, a mechanic must manually remove the material. This stoppage is a significant contributor to machine downtime. It is believed that this problem can be addressed through a redesign of the excess material removal station.

1.1 Background

This station operates with the input of two cams that power two, separate linkage trains. One of these linkage trains (labeled slider linkage in Figure 1) operates a slide. Figure 2 shows the slide in more detail. This slide carries the pickoff tool's moving pivot and moves the pickoff tool into and out of the nest to pick up the excess material with two vacuum pickoffs. As it moves forward, the rotate cam must supply motion to the rotation pickoff tool to keep it stationary with respect to the slide. As the slide translates from the nest, the rotate cam causes the pickoff tool to rotate downwards to place the excess material over a scrap chute, where it is blown off. The other linkage train (shown as the rotate linkage train in Figure 1) rotates the pickoff tool.

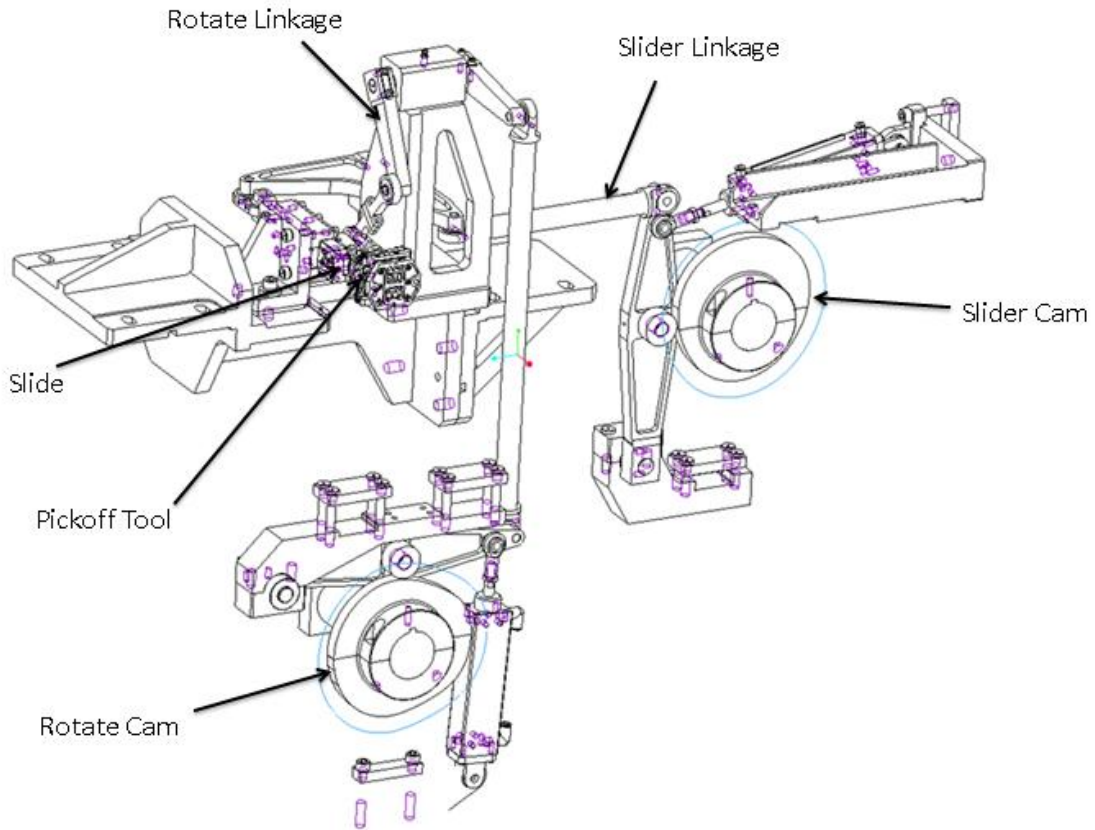


Figure 1: Current Excess Unload Station

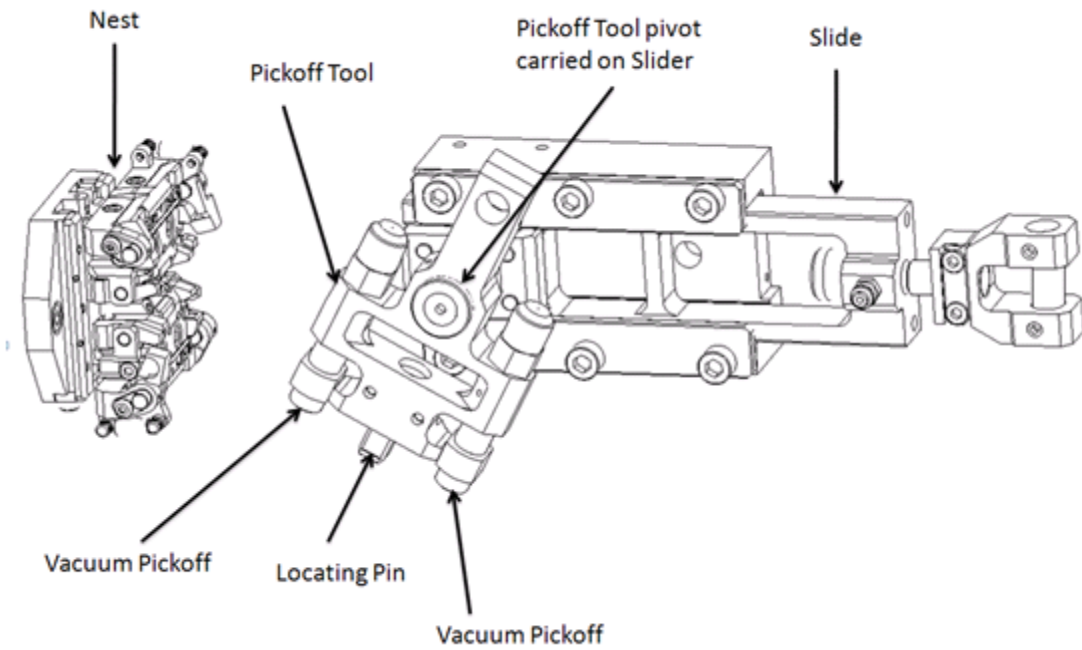


Figure 2: Nest, Pickoff Tool, and Slide

Figure 3 shows the slide and pickoff tool in the pickoff and blowoff positions.

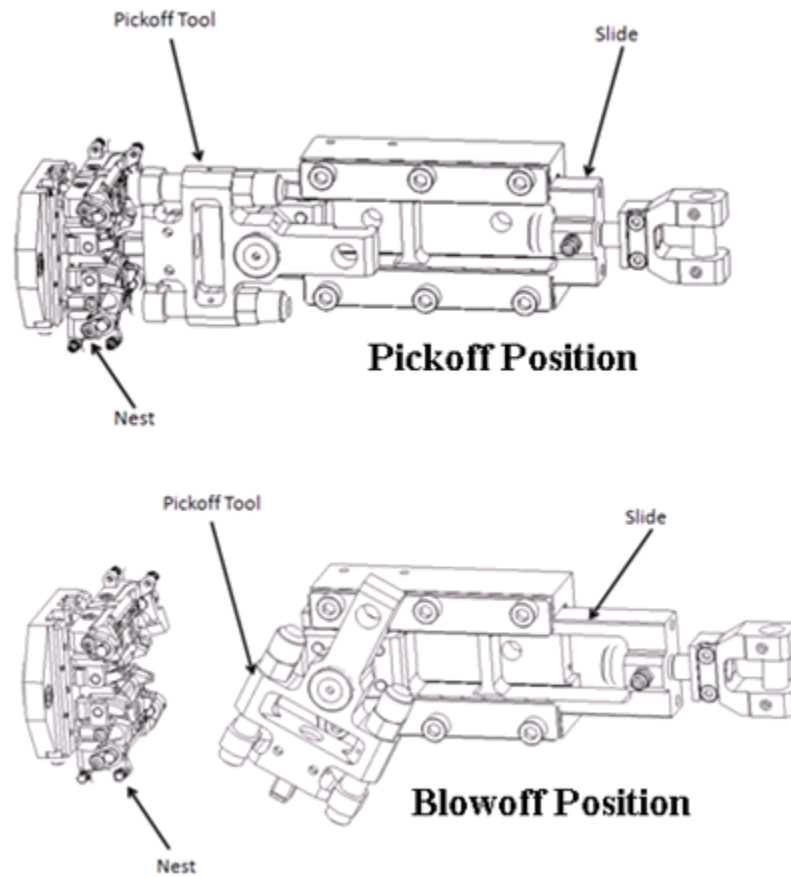


Figure 3: Pickoff Tool Pick up and Blowoff Positions

1.1.1 System Dynamics

The two coupled linkage trains cause the dynamics of this system to become very complicated. This complication comes from the fact that the pivot of one rocker in the rotate linkage is carried on the slide of the slider linkage, coupling their motions. This effectively gives the rotate train two inputs. Because of this, many conventional analysis packages cannot be used to analyze the system. This is because many of these programs utilize a single-input model to calculate results. Another problem that these two linkage trains present is that they must be in proper phase in order to work. The rotate cam must chase the motion of the slide to keep the pickoff tool horizontal as it enters the nest. This must happen because the pickoff

tool's pivot is moving, as the rotate linkage geometry is constantly changing. The rotate cam therefore cannot dwell during that part of the cycle and must chase the slide motion to keep the pickoff tool from rotating. Slight variances in phase will cause unexpected and unwanted movements in the linkage's end effectors. Such variation is unacceptable on such an indexing machine, making this station require some calibration at setup time.

1.1.2 Pickoff Tool

The pickoff tool in this station is comprised of several parts as shown in Figure 4. A metal frame serves as the main structure of this part (labeled A in Figure 4). There is also a metal locating pin inserted into one end of the frame that aligns it to the nest (labeled B in Figure 4). Above and below this pin are two vacuum grippers (labeled C in Figure 4). The grippers on this tool are used to remove the excess material from the nest. Two vacuum grips are needed because each nest holds two pieces of excess material.

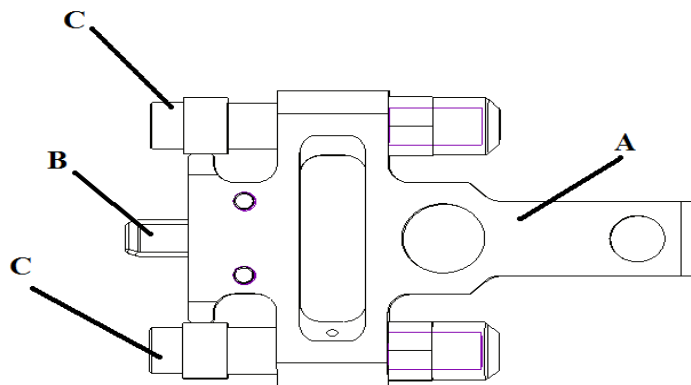


Figure 4: Pickoff Tool Components

To remove the excess material, a vacuum seal is made once the pickoff tool reaches the nest. This vacuum seal is vital to a successful pickoff of the excess material. Magnets on the nest at either end of the part hold the excess material. To overcome the force of these magnets, the suction force must be greater than that of the magnetic field. As such, a proper seal between the product and vacuum head must be made in order for a successful pickoff to occur.

2 Goal Statement

The goals of this project are to model and analyze the current excess material unload station and to search for potential areas where improvements could be needed. With this investigation, a redesign of this station or components of this station is to be performed.

2.1 Sub Tasks

The complex dynamics in this system, caused by the translating pivot and dual cam design, are a potential cause for error in this system. As such, solutions that serve to simplify the dynamics of this system will be investigated.

Another possible cause for error in this system could be the pickoff tool design. Failure in the pickoff tool could be due to an inadequate seal between the vacuum grippers and the product. To address this problem, new pickoff tool designs can be investigated.

Lastly, all system redesigns should be geared to simplifying the overall system, ideally leading to less mechanism and only one cam. Such a change will provide a system that is less expensive and easier to maintain.

3 Investigation of the Current Design

The system was modeled in the 3D CAD package Pro/Engineer, and then tested using accelerometers, and its function was recorded with high-speed video equipment. These data provided a basis for system analysis.

3.1 Modeling the System

The parts were modeled and assembled using drawings given to us by the sponsor. The CAD model gives us a better understanding of how the linkages in the system move and interact with each other. In addition to learning more about the model, the CAD model provides mass properties and kinematic data of individual parts. Figure 5 shows the final CAD model of the excess material removal station.

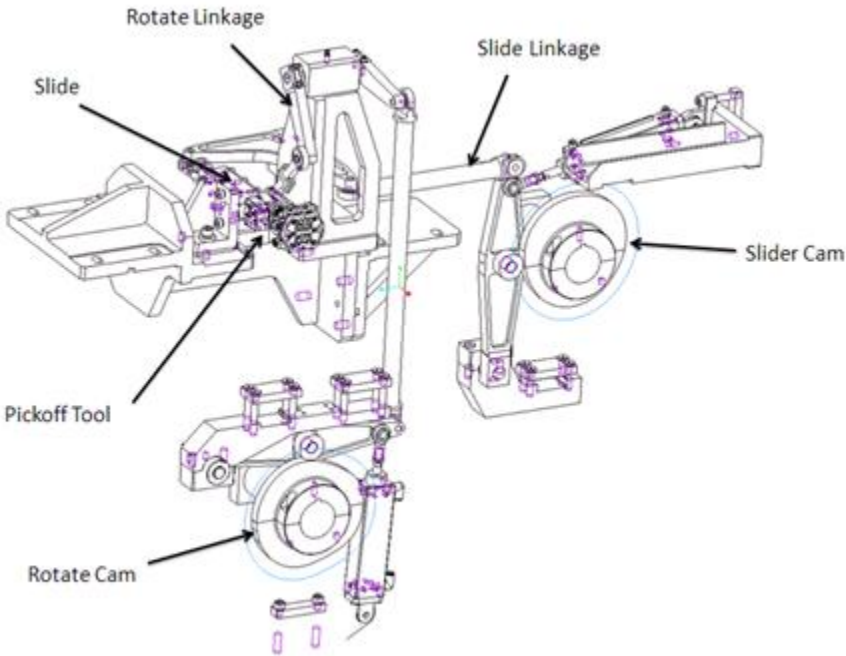


Figure 5: CAD Model of Scrap Removal Station

3.2 Testing

While CAD models are useful for understanding part function, actual testing on this system was necessary to obtain an understanding of the dynamics of the actual system.

Accelerometers and high-speed video were used to help provide such insight.

3.2.1 Accelerometer Testing

To facilitate the accelerometer testing, Dytran accelerometers, model numbers 3056A2 and 3055B4, were used in conjunction with a Hewlett-Packard dynamic signal analyzer (DSA), model number 35670A. These accelerometers were placed on various links on the station (as shown in Figure 6) to help provide an overall view of the station's dynamics. The links analyzed were the lever actuators (A and B), vertical cam lever (C), the horizontal cam lever (D), the bellcrank (E), and the slide (F). Accelerometer model 3056A2 was used at position A, B, C, and D. Accelerometer model 3055B4 was used at positions D and F.

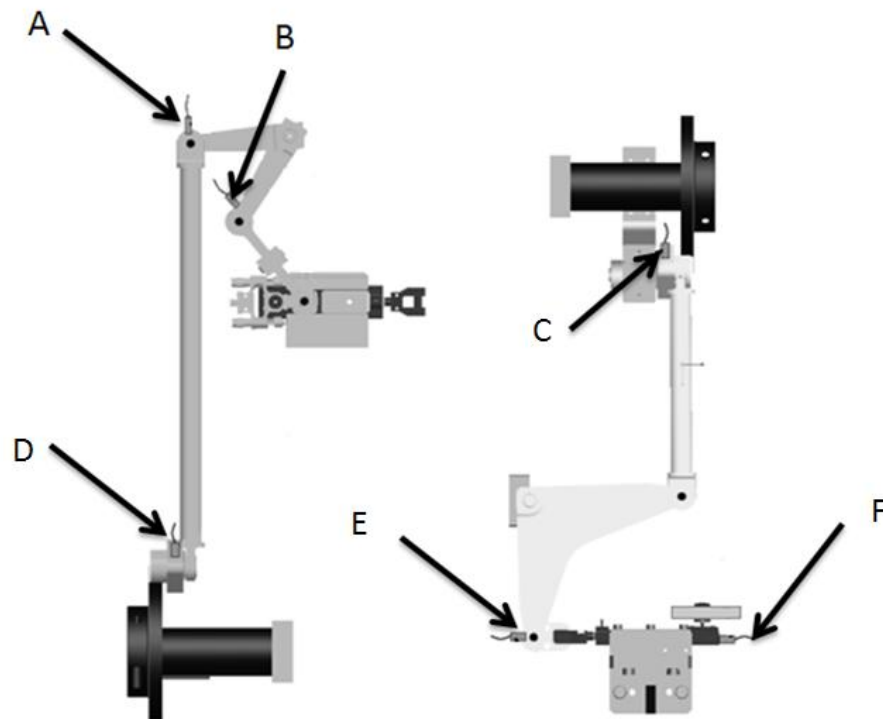


Figure 6: Accelerometer Placement

The basic procedure for accelerometer testing was straightforward. First, two accelerometers were placed on separate links at the radius of a pin on each rotating link or on the translating slides. The accelerometers were held in place with magnets attached to the accelerometer. Cables connected to the DSA were then connected to the accelerometers. A machine trigger (trigger fires when nests start to move) was also connected to the DSA, as it would provide the analyzer with a signal for each completed system cycle. This allowed the DSA to correctly time phase and average the recorded data.

The DSA is able to read data from two accelerometers at a time, meaning that to obtain acceleration data from the six chosen links, three separate tests were needed. Each one of these tests took 2048 samples at a sample rate of 2.56 kilo samples per second and used 25 averages to reduce the noise in the data. Conversion factors of 100 mV/g (for 3056A2) and 50 mV/g (for 3055B4) were also programmed into the DSA. This was done to allow the DSA to return results in g, as the raw acceleration data is in volts. The resulting data from the DSA was saved to a disk to allow the recorded data to be further analyzed by a computer.

3.2.2 High-Speed Video

To gain a visual understanding of the system movement, high-speed video was taken of the slide and pickoff tool with the machine operating under standard conditions. To set up the video, a high-speed camera was placed on a tripod and aimed at the desired location. Extra lighting was also needed as to ensure a quality video. When the shot was in frame and the machine was running, the video was taken. Because there are 2000 frames per second in these high-speed videos, only eight seconds of video could be taken at a time due to the large file size (500 MB per second of footage). Different angles were shot in each of the videos: a close up of the slide and pickoff tool from the side (Shot 1), a close up of the slide and pickoff tool from a

slight angle (Shot 2), a behind shot of the slide and pickoff tool (Shot 3), a zoomed out shot of the slide and pickoff tool (Shot 4), and a further zoomed out shot that also shows the lever actuators (Shot 5). See Appendix A for a screenshot from each of these videos.

3.2.3 High-Speed Video with Accelerometer Data

The high-speed video software used by the sponsor company has the capability to read accelerometers and automatically phase the data with the videos. Synchronized results provide exact phasing information, taking much guesswork out of acceleration data interpretation. Due to the value of these results, a second high-speed video recording session was arranged to allow such data to be taken.

The set up for this testing was essentially the same as for the previous high-speed video testing, with the only difference being where the accelerometers were attached to the machine. These accelerometers were attached to the slide and to the pickoff tool. The slide accelerometer was placed in the same position as in the previous accelerometer testing (position F in Figure 6). The accelerometer attached to the pickoff tool was placed in line with the pin connection next to the pickoff tool's pivot. See Figure 7 to see the pickoff tool accelerometer's placement.

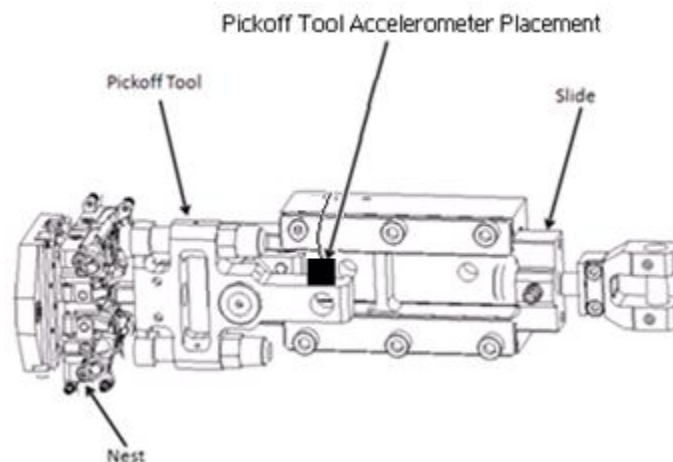


Figure 7: Pickoff Tool Accelerometer Placement

The high-speed video recorder's receiver was then connected to these accelerometers with cables to allow for data collection by the high-speed video software. This did not require a machine trigger as the data was automatically phased with the recorded video. The downside to this technique is that the data is not averaged or scaled based on the transducer calibration factor, meaning that there may be noise in the measured data. The resulting values were not in g but in volts.

3.3 System Analysis

The excess material removal station was analyzed using two different methods. A dynamic model was created in MATLAB to calculate the accelerations of the pickoff tool and slide using differential equations derived by the project advisor. This data was analyzed alongside high-speed video that was taken in conjunction with the accelerometer testing.

3.3.1 Basic Analysis

The dynamic model requires mass and stiffness data of the linkages to calculate the accelerations. The masses of the parts in the system were calculated by attributing the applicable material and density to the part and performing a mass properties analysis in Pro/Engineer. The stiffness values were calculated with help of finite element analysis software, using COSMOSWorks in SolidWorks. The part files were imported into COSMOSWorks from Pro/Engineer and the applicable material properties were assigned to the parts. The parts were constrained at their pivot points by using the “fixed restraint” command. Applicable forces were then applied to the pins at the point of connection to the mating link to take into account the twist of the link. The direction of these forces depended on how the part was loaded in the system. The displacement was calculated and the stiffness, or k , value was obtained by dividing the applied force by the displacement. Stiffness values were found for all parts in the linkages.

Figure 8 shows one of the parts, a lever actuator, of those that were chosen for finite element analysis (FEA). The force on its pin is caused by a connecting rod, and is applied in the direction of the conrod (see Figure 9 for a screenshot from this FEA).

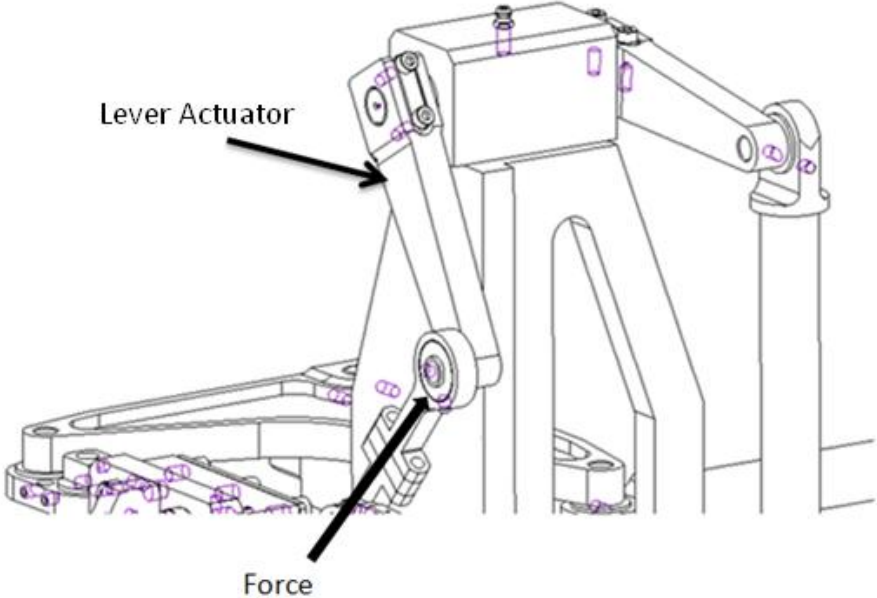


Figure 8: How the Part is Assembled

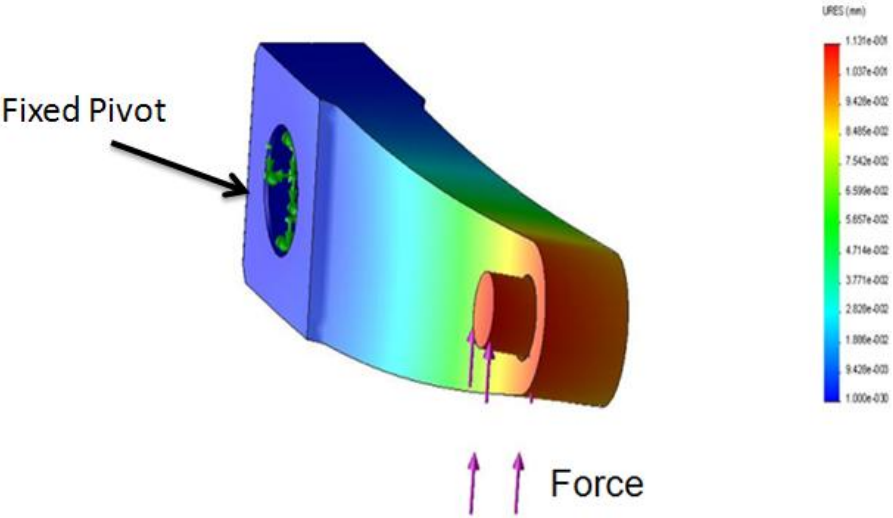


Figure 9: Finite Element Analysis of a Part

The masses were then lumped together using conventional lumped model techniques as detailed in Appendix B to obtain the effective mass of the entire linkage. The correct mass and second moments of mass were obtained from the mass properties analysis in Pro/Engineer. The second moments of mass were taken about the pivot points in each rotating link. These values were used to calculate effective mass of the lever by dividing the second moment of mass by the square of the radius to the applied force on the lever. These masses were combined using the proper lever ratios to get the effective mass of each linkage train.

The stiffness coefficients of each link were combined in series for each linkage train to find their effective stiffness coefficients. Details of this process are shown in Appendix B.

3.3.2 Analysis of Test Data

The high-speed videos and the data collected from the accelerometer testing were analyzed to provide an understanding of the system's dynamics.

3.3.2.1 Acceleration Analysis

The first step taken in the analysis of the accelerometer data was to combine the results of the various accelerometer tests into two Excel spreadsheets. The accelerometer data from the links in the slider linkage were stored in one spreadsheet, while the data from the links in the rotate linkage were stored in the other. This was done as to allow for the accelerations of connected links to be directly compared. Another reason for this separation was to keep the data in each sheet readable and easy to work with, as with too much data on one sheet it became difficult to interpret the results.

The two sets of accelerations were graphed and moving averages were taken of the resulting plots. The moving averages allowed trends in the data sets to be more easily seen, as

they eliminated much of the data's noise. Annotated versions of these graphs can be seen in Figure 10 and Figure 11. Cam angle zero in these graphs is not at machine zero, but rather at the point where the trigger happened to be in the cycle.

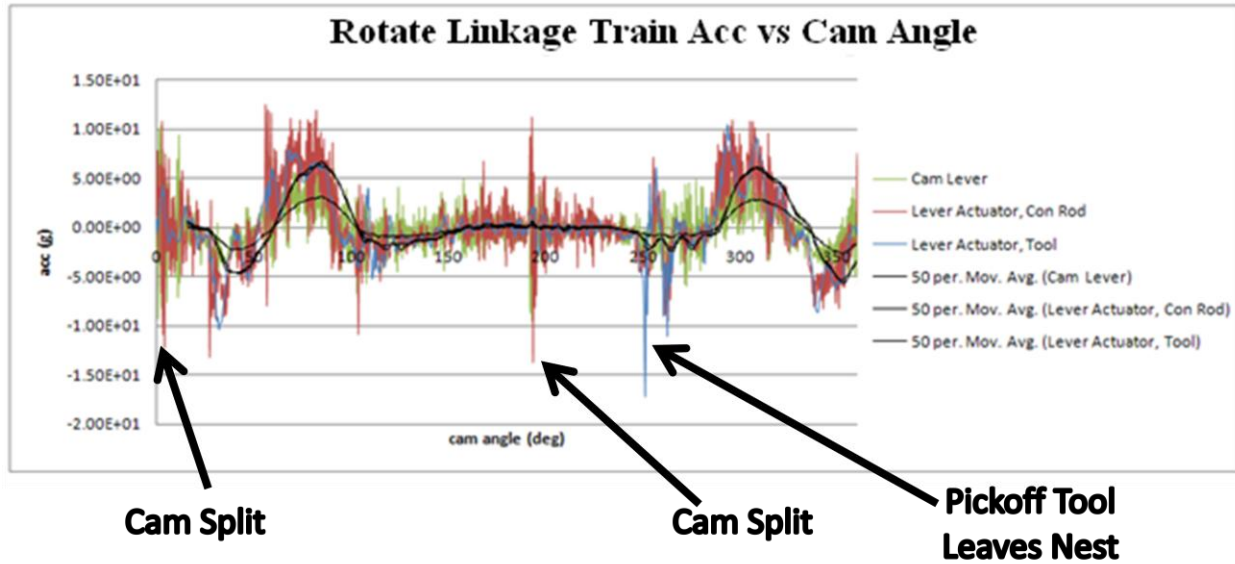


Figure 10: Rotate Linkage Acceleration vs. Cam Angle Graph

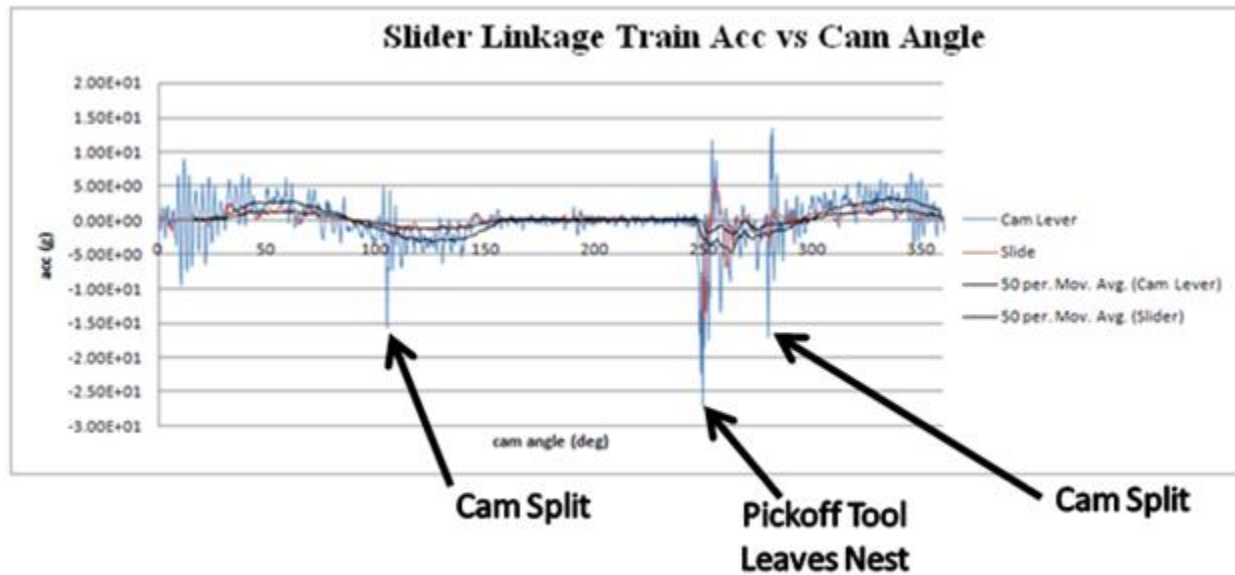


Figure 11: Slider Linkage Acceleration vs. Cam Angle Graph

The largest recorded spike in acceleration in the rotate linkage occurs when the pickoff tool leaves the nest. In this spike, the maximum acceleration is 16.9 g. This acceleration was recorded on the lever actuator that is connected to the pickoff tool through a short conrod

(acceleration of this lever actuator is shown in blue series on Figure 10). Two peaks can be seen at cam angles 75 degrees and 300 degrees. These peaks occur when the lever actuator is chasing the slide to keep the pickoff tool horizontal. Two more spikes in acceleration can be seen at cam angle 10 degrees and 190 degrees. These spikes were attributed to the cam splits, as they both occur when these splits reach the follower. Further evidence that these spikes are caused by the cam splits is that these spikes are more prominent in the cam lever (green series in Figure 10) than in the pickoff tool-side lever actuator. This is significant because the spike in acceleration should be attenuated as it passes through the system. The fact that these spikes are 180 degrees apart also indicates they are due to the split.

Most of the spikes and peaks of the rotate linkage's acceleration data are not of much concern due to the fact that they occur when the pickoff tool is either not holding the excess material or has already made vacuum with the excess material. The one peak during the dwell is of some interest, as it could have an impact on the gripping process.

The largest recorded spike in acceleration in the slider linkage again occurs when the pickoff tool leaves the nest. In this spike, the maximum acceleration is 38 g. This acceleration occurs on the cam lever (blue series in Figure 11). Two other acceleration spikes were measured on the cam lever; one near cam angle 100 degrees and the other at cam angle 280 degrees. The timing of spikes corresponds with when cam splits reach the follower. This conclusion is again backed by the fact that the spikes are more prominent closer to the cam and that they occur 180 degrees apart.

The spikes and peaks in this linkage are due to known design features. The cams are split for ease of assembly and this always produces an acceleration spike when the follower

encounters them. The locating pin is designed to contact and move the nest into position. There are no spikes during the pickoff dwell, meaning that the actual pickoff process is not interfered with. One area of possible concern is the spike in acceleration from the cam slit near cam angle 100 degrees. Due to this jump's proximity to pickoff tool nest entry, this could potentially cause an issue in proper nest locating. This area does not, however, cause any major concerns. The acceleration spike is significantly muted in the slide, meaning the actual pickoff tool movement is not affected to a great degree. Also, the floating nest is able to align itself with the pickoff tool, and the grippers of the pickoff tool are spring mounted. These springs allow the grippers to meet the nest's surface at varying speeds and positions and still guide themselves to the proper end orientation.

Some acceleration spikes in both systems seem to be due to spikes in the other system. For example, the spike near cam angle 100 degrees in Figure 10 may be caused by the cam split in the slider linkage. Crossover effects such as this increase the difficulty of system analysis from a practical and theoretical standpoint and could lead to unintended dynamic effects.

3.3.2.2 High speed Video with Accelerometer Data

The recorded video and accelerometer data was played simultaneously to confirm our previous assumptions about phasing of the accelerometer data (see Figure 12). Previous phasing and interpretation of acceleration spikes and peaks were based on logic and visual inspection of the high-speed video. Based on the phasing in this linked video, our previous analysis was confirmed.

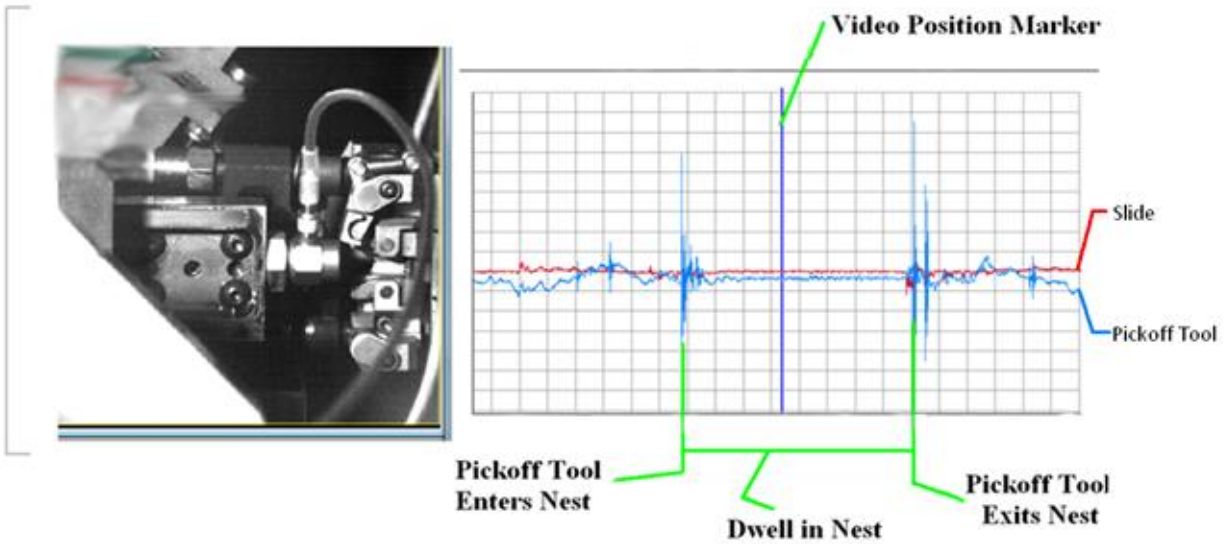


Figure 12: High-Speed Video with Accelerometer Graph Screenshot

This video also provided us with a more accurate measurement of the acceleration of the pickoff tool. The measurement is more accurate because it is on the pickoff tool rather than on an adjacent link. This acceleration graph (blue in Figure 12) shows that there is no acceleration spike in the middle of the dwell. This had been an area of concern based on the cam split spike from the rotate linkage accelerometer data, as the spike may have been affecting the pickoff ability of the system. The measured accelerations of the pickoff tool during dwell in the nest are well behaved, with almost no visible spikes. These findings imply that the dynamics of the system are not a significant cause of pickoff failure, as there are no measured accelerations or visible problems with the system's movements at the time when the tool is picking up the parts.

3.3.3 Theoretical Models of Current Design

Theoretical models of this design were created to provide a tool that could be used to test design alterations. This tool allows one to quickly and inexpensively test proposed design changes.

3.3.3.1 MATLAB Model

The system is a coupled, two degree of freedom cam-driven system. Due to the large rotation angle of the pickoff tool, angular acceleration needs to be calculated rather than the linear acceleration for that part. The motion is complicated to model because the pivot of the pickoff tool is carried on the moving slide. The lumped parameter model is shown in Figure 13, where m_1 represents the mass of the cam follower, k_1 represents the effective stiffness of the air cylinder, and c_1 represents the effective damping of the air cylinder. The parameters m_2 , k_2 and c_2 all represent the variables associated with the slider linkage above the cam and its lever arm.

The pickoff tool variables are a little different. Since the model is measuring the angular acceleration of the pickoff tool, the second moments of mass about the link's pivot need to be known. The variables are defined as follows: j_1 , d_1 , m_{I1} and I_1 represent the stiffness, damping, mass and second moment of mass, respectively, of the rotate cam follower and its air cylinder. The parameters j_2 , d_2 , m_{I2} and I_2 represent the variables associated with the pickoff tool's linkage.

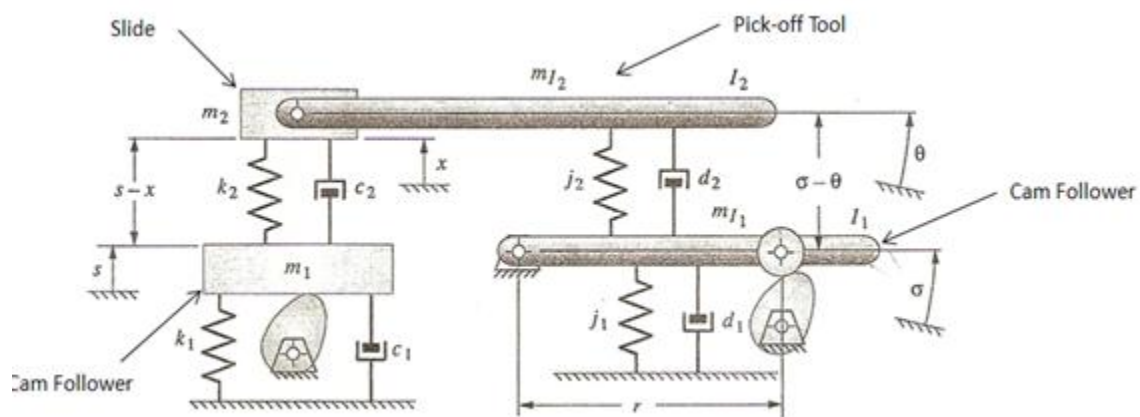


Figure 13: Lumped Parameter Model

The dynamic model uses the differential equations 1 and 2 shown below (Full MATLAB code can be found in Appendix C). These equations are second order differential equations (O.D.E.'s) and are used calculate the displacement, velocity, and acceleration of the slide and the same parameters for the rotating pickoff tool.

$$m_2\ddot{x} + c_2\dot{x} + k_2x + (m_1q \cos \sigma)\ddot{\theta} = c_2\dot{s} + k_2s \quad (1)$$

$$(I_2 + m_1q^2 \cos^2 \sigma)\ddot{\theta} + d_2\dot{\theta} + j_2\theta = d_2\dot{\sigma} + j_2\sigma \quad (2)$$

State Space Solution:

$$\text{Let: } y_1 = x, \quad y_2 = \dot{x}, \quad \phi_1 = \theta, \quad \phi_2 = \dot{\theta}$$

$$m_2\dot{y}_2 + c_2y_2 + k_2y_1 + (m_1q \cos \sigma)\dot{\phi}_2 = c_2\dot{s} + k_2s \quad (3)$$

$$(I_2 + m_1q^2 \cos^2 \sigma)\dot{\phi}_2 + d_2\phi_2 + j_2\phi_1 = d_2\dot{\sigma} + j_2\sigma \quad (4)$$

$$\dot{y}_1 = y_2 \quad (5)$$

$$\dot{\phi}_1 = \phi_2 \quad (6)$$

The MATLAB model utilizes the Runge-Kutta fourth-order method to solve the ordinary differential equations. The differential equations 1 and 2 are second order and the Runge-Kutta routine can only solve first order equations. In order to get around this, the equations were converted to state space form as shown in equations 3, 4, 5, and 6. There were two equations and two unknowns in equations 1 and 2, but when the state space solution is applied, there become four equations and four unknowns (equations 3, 4, 5, 6). The new unknowns become the second derivatives that the Runge-Kutta could not handle and are just converted to first derivatives of dummy variables.

The MATLAB code uses the displacement and velocity data from the cam followers as inputs. The displacement is represented in the model as “s”, for the displacement of the cam follower in the slider linkage, and “σ” for the angular displacement of the cam follower in the pickoff tool’s linkage. The variables x and θ represent the slide’s displacement and pickoff tool’s

rotation. In the MATLAB code, velocity in the system is designated as \dot{s} , \dot{x} , $\dot{\sigma}$ and $\dot{\theta}$ and acceleration is designated \ddot{s} , \ddot{x} , $\ddot{\sigma}$, $\ddot{\theta}$.

Equations 3, 4, 5, and 6 were entered into MATLAB to calculate the displacement, velocity, and accelerations of the end effectors in the system. The MATLAB code needs values for all of the variables in the system (mass, spring constants, second moment of mass etc.) and inputs for the driving data. The driving data for the code was taken from two different sources. Our Pro/Engineer model provided driving data and we also recreated the cams in DYNACAM and used their s and v functions for the driving data.

The cam profile data points were given to us by the sponsor company and they were imported into Pro/Engineer to create the cam. When the data points were imported, the spline fitted to the data had a minor glitch in it. Pro/Engineer had trouble connecting both ends of the spline and this caused a large anomaly to appear in both of the final cams. Because of this, the Pro/Engineer output had some undesirable spikes in the velocity and position used as input. This caused error in the MATLAB model, so instead of relying on Pro/Engineer to supply the driving data, we recreated the cams in DYNACAM using the timing diagrams provided by the sponsor. DYNACAM calculated the displacement and its derivatives of the recreated cam functions and the data was exported to a “.dat” file. Figure 14, Figure 15, Figure 16, and Figure 17 show graphs of these data used as inputs for the MATLAB. These files were imported into MATLAB and used to calculate the displacement, position, velocity and acceleration outputs of the two end effectors in the system (see Figure 18, Figure 19, Figure 20, Figure 21, Figure 22, and Figure 23 for graphs of this data).

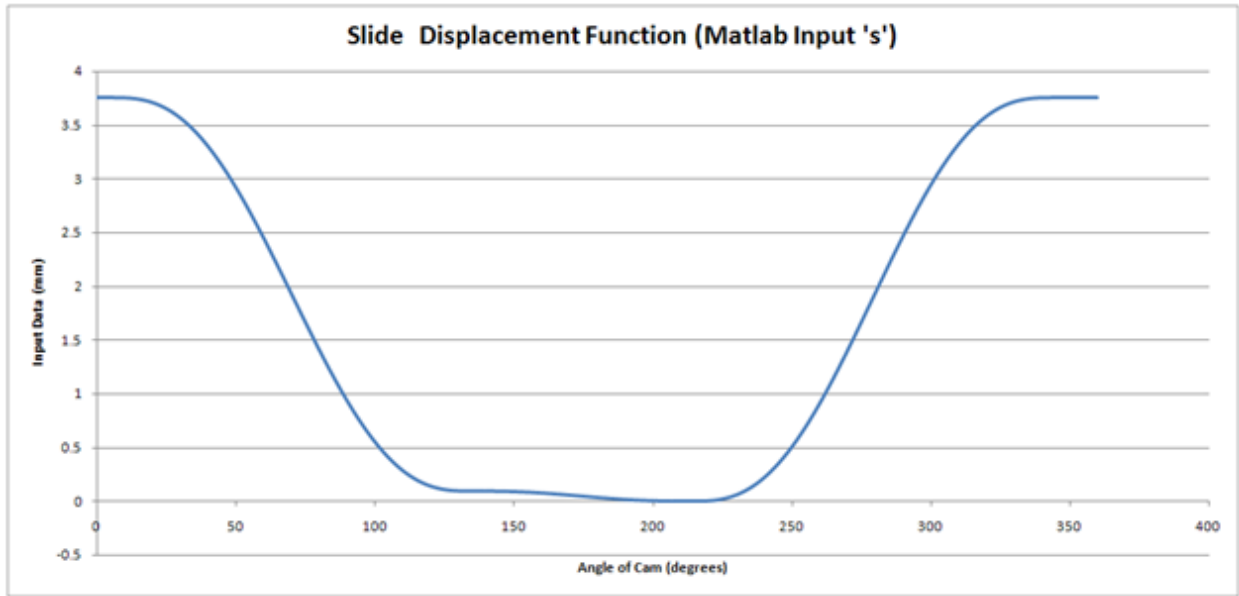


Figure 14: Slide Displacement Function (MATLAB Input 's')

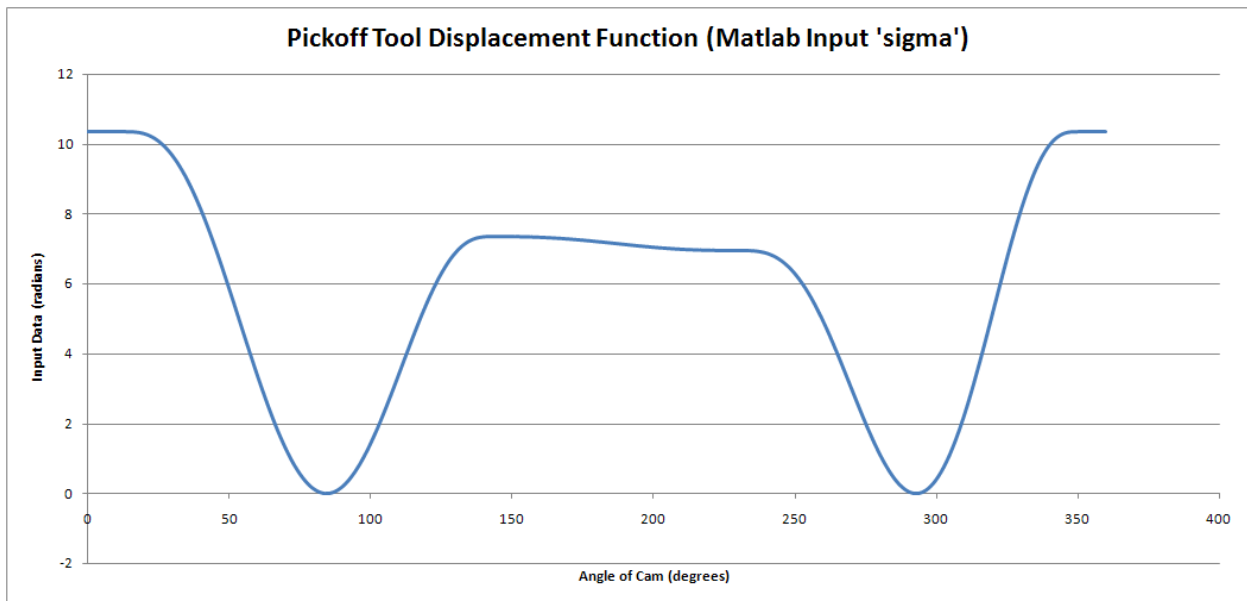


Figure 15: Pickoff Tool Displacement Function (MATLAB Input 'sigma')

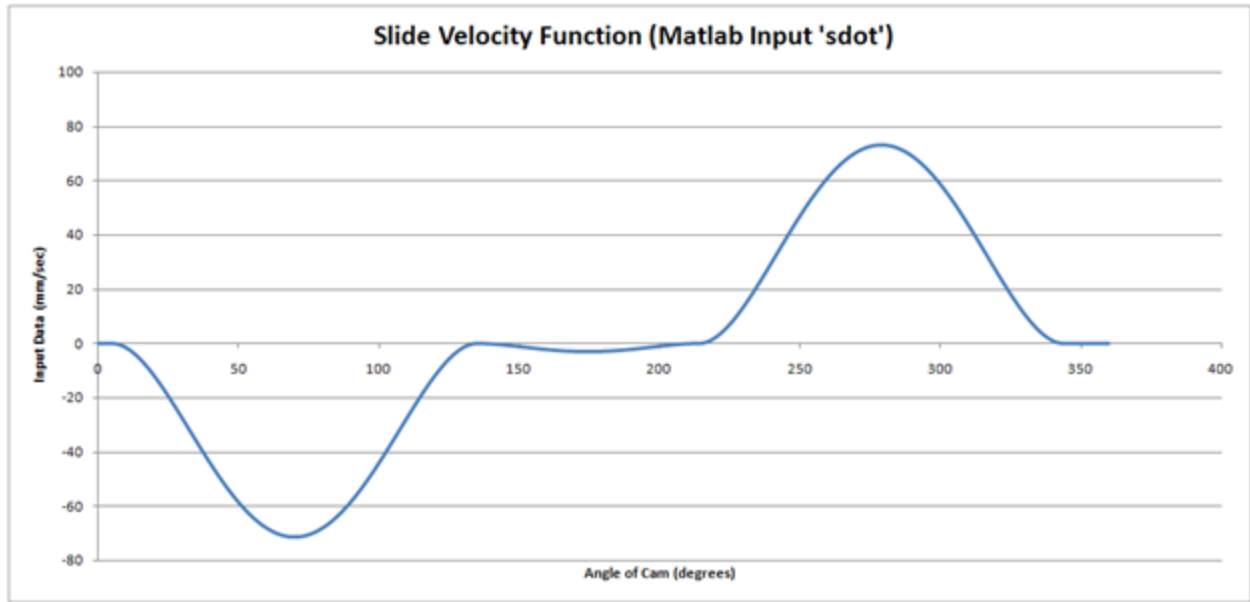


Figure 16: Slide Velocity Function (MATLAB Input 'sdot')

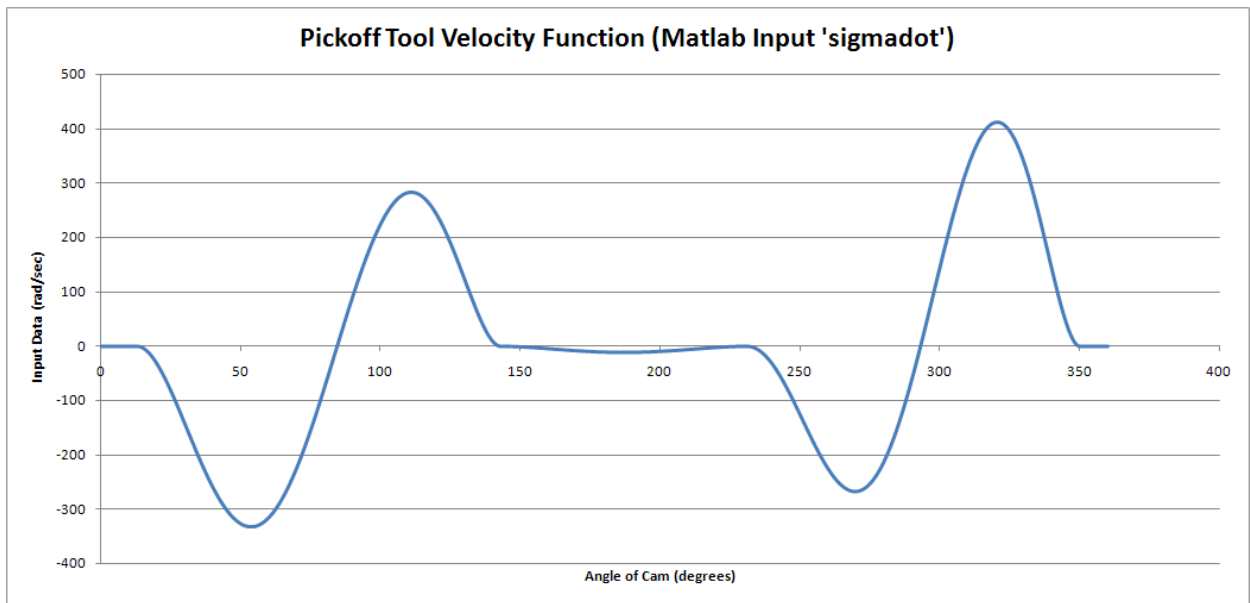


Figure 17: Pickoff Tool Velocity Function (MATLAB Input 'sigmadot')

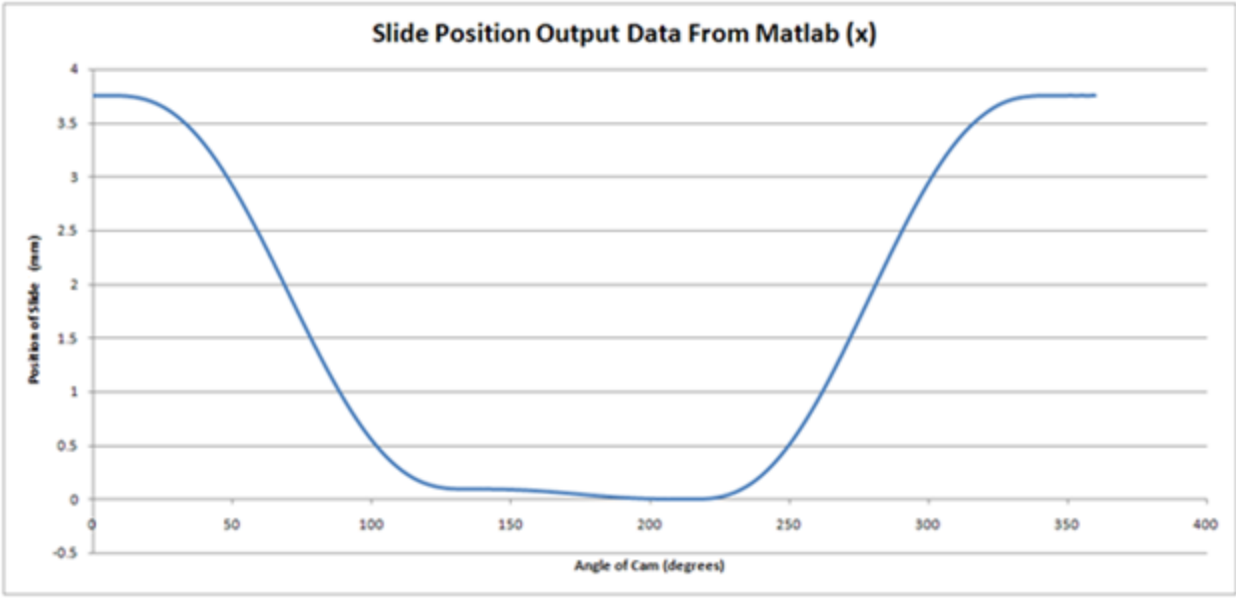


Figure 18: Slide Position Data from MATLAB (x)

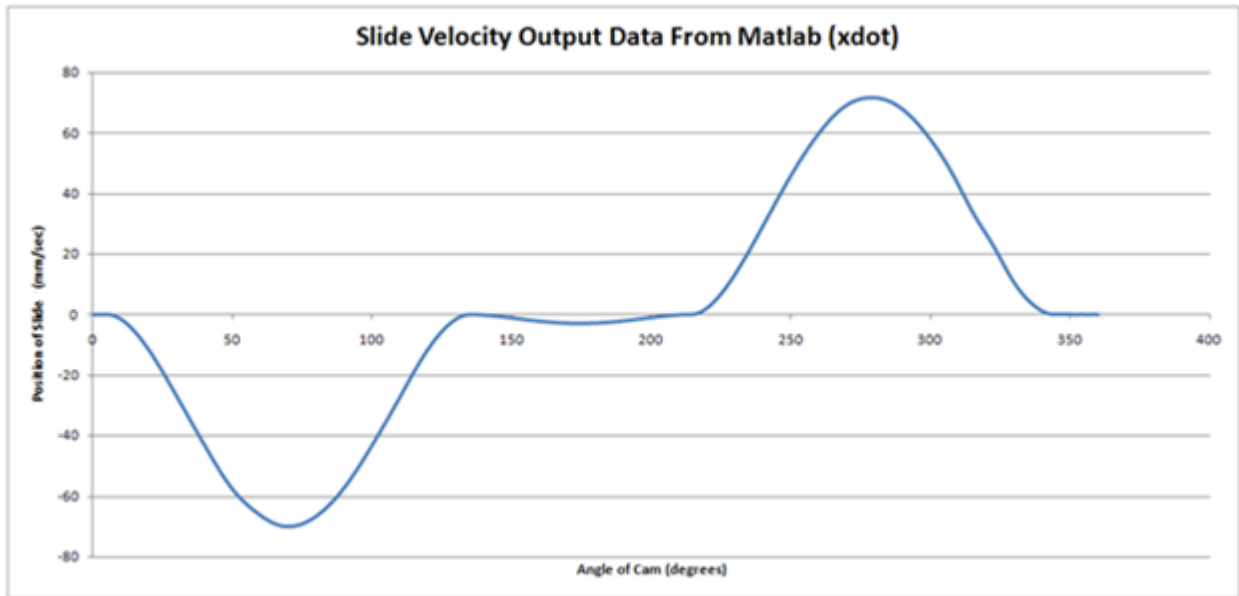


Figure 19: Slide Velocity Data from MATLAB (xdot)

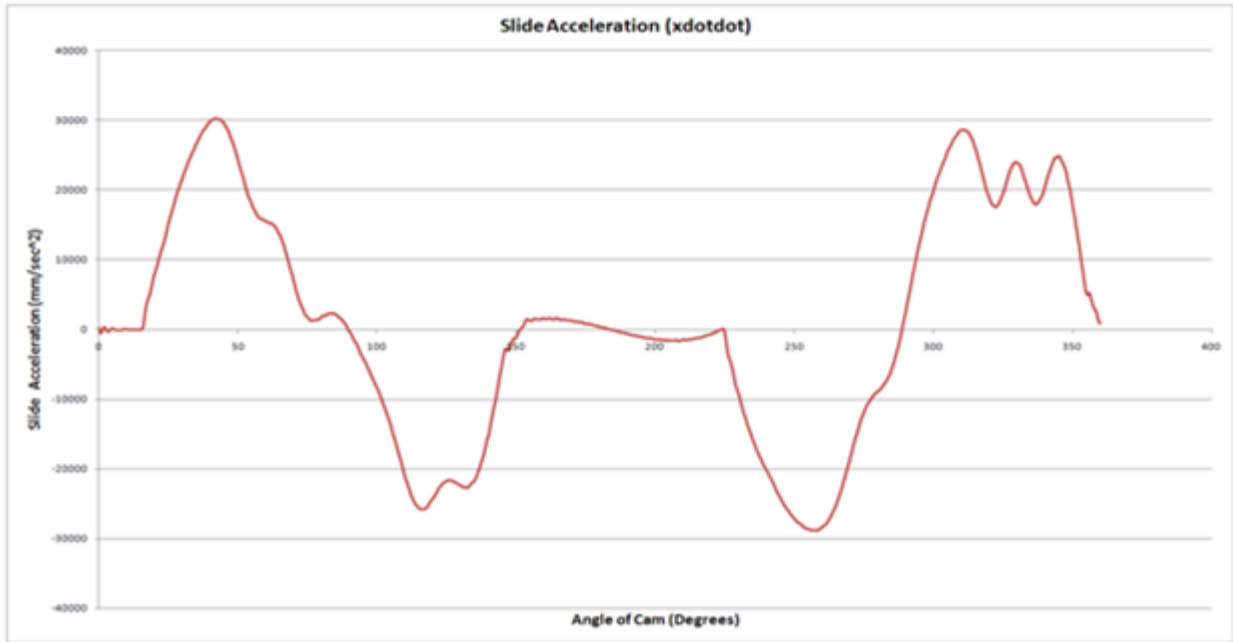


Figure 20: Slide Acceleration Data from MATLAB (xdotdot)

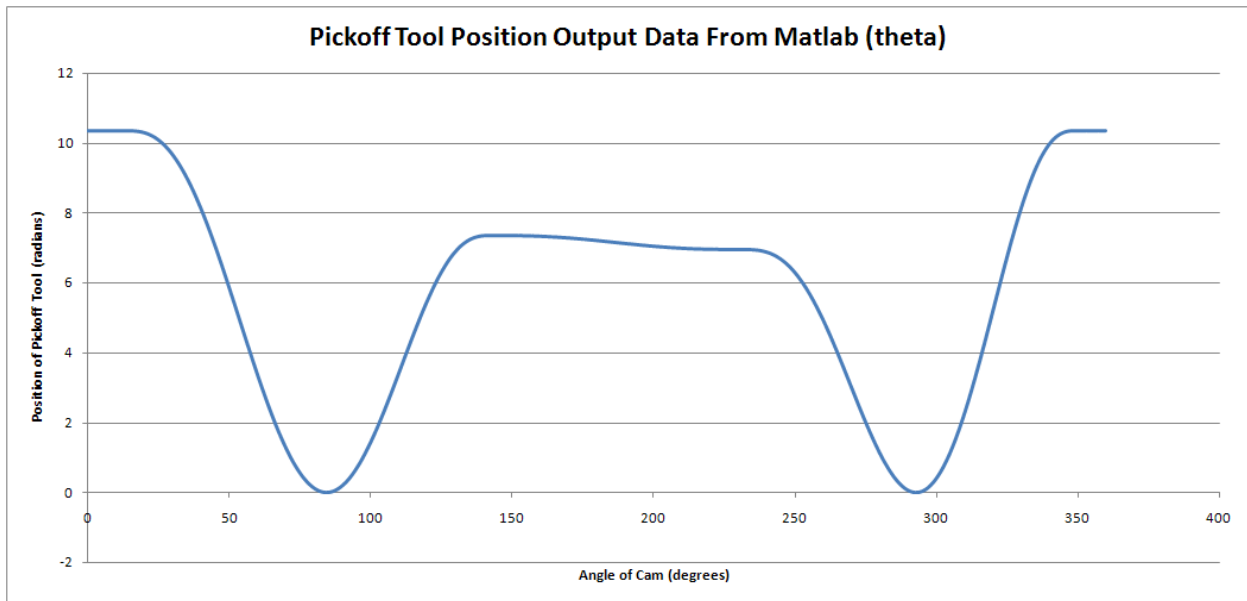


Figure 21: Pickoff Tool Position Data from MATLAB (theta)

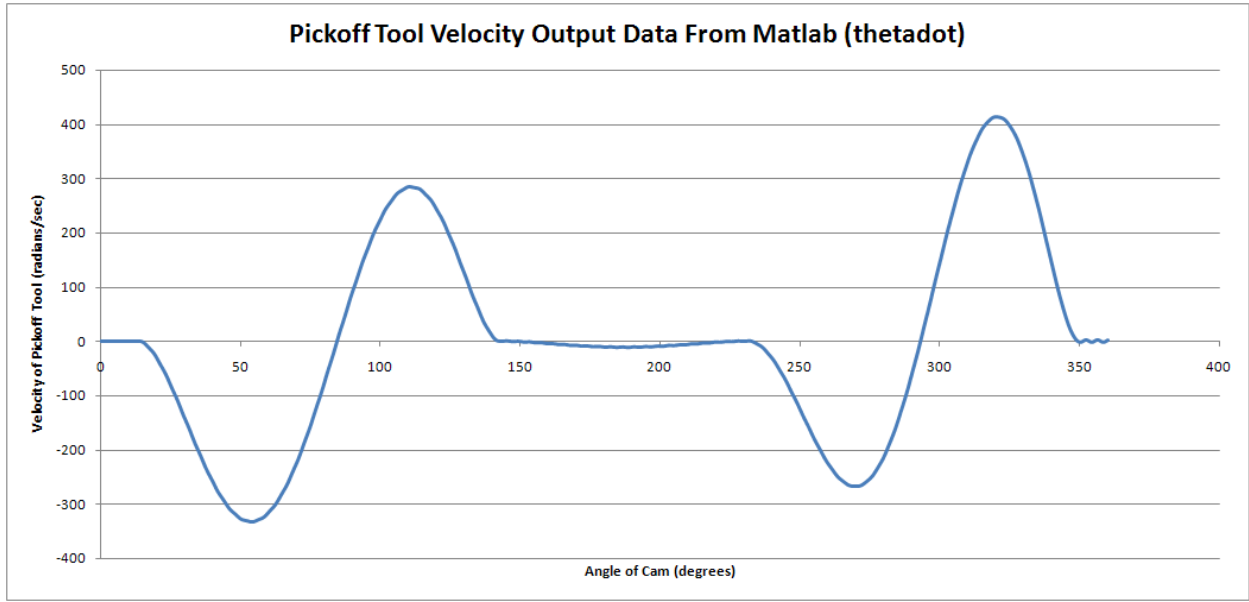


Figure 22: Pickoff Tool Velocity Data from MATLAB (thetadot)

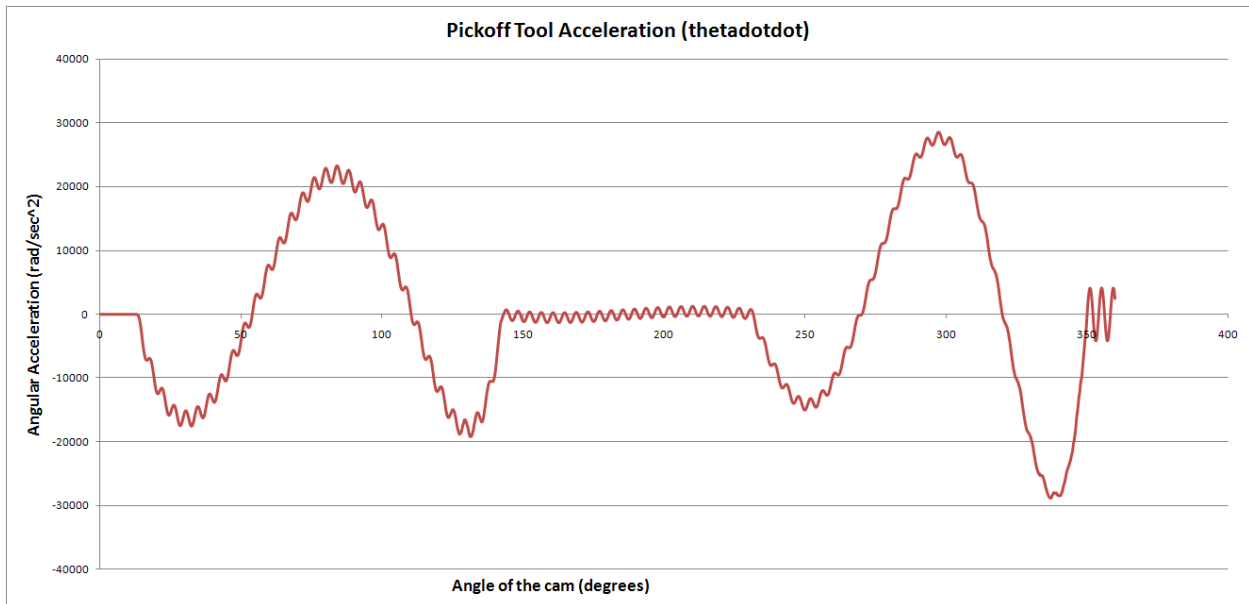


Figure 23: Pickoff Tool Acceleration Data from MATLAB (thetadotdot)

3.3.3.1.1 Comparison between MATLAB Data and Accelerometer Data

Figure 24 and Figure 25 show graphs of the measured data versus the MATLAB output.

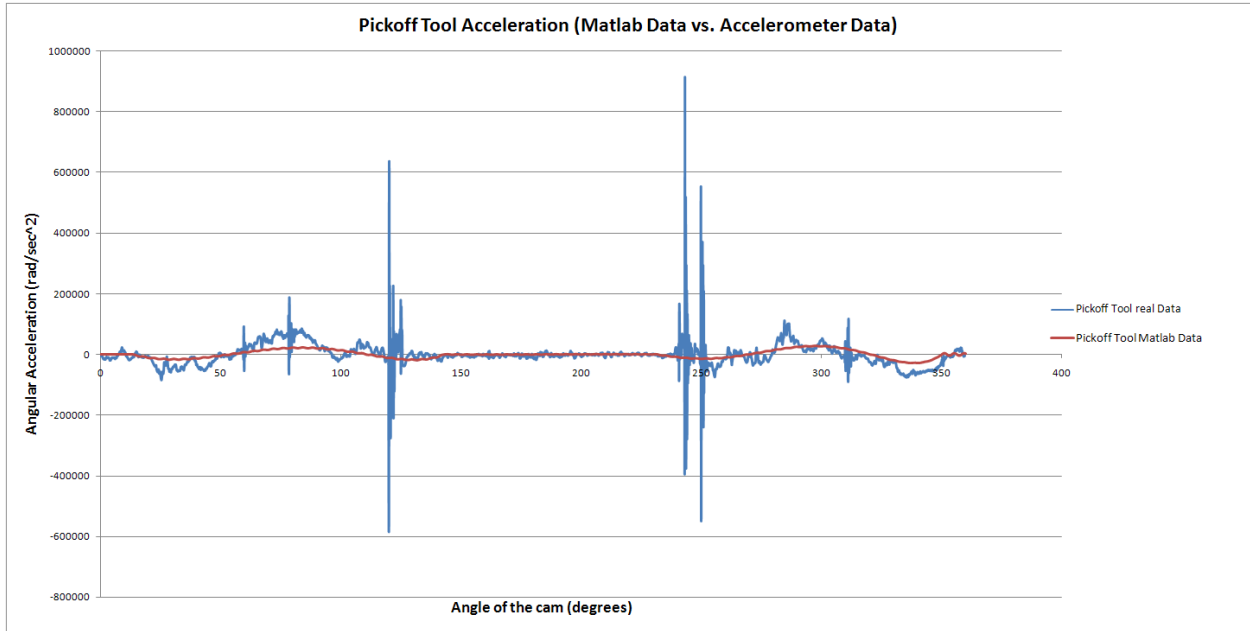


Figure 24: Pickoff Tool Acceleration (Real Data vs. MATLAB)

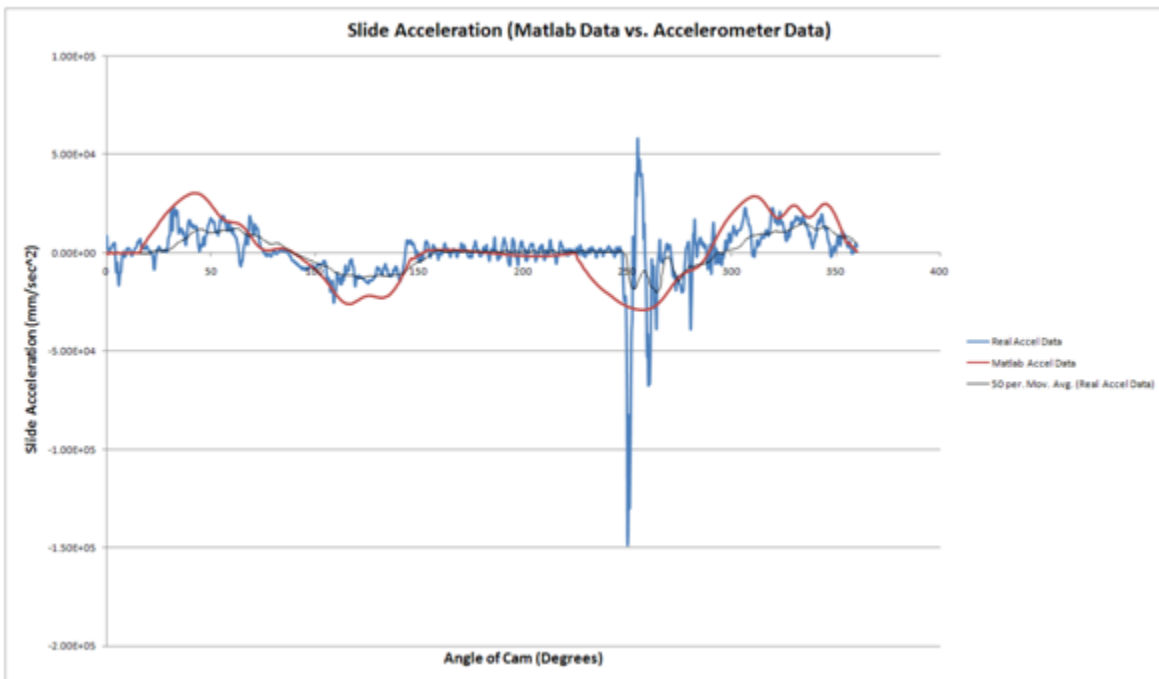


Figure 25: Slide Acceleration (Real Data vs. MATLAB)

The MATLAB code does not take into account impacts, as it is a purely dynamic model. The big spikes in the pickoff tool's acceleration in the accelerometer data are from when the tool enters and exits the nest. The large spike in the slide data is at the end of the dwell and is due to

the pickoff tool exiting the nest. As seen in the figures above, the MATLAB simulation has similar shape to that of the experimental curves but the pickoff tool's simulated acceleration magnitude is lower than that measured and the slide acceleration is slightly higher. The model still needs refining so that it can reflect the real system more accurately.

3.3.4 Discussions with Engineers and Mechanics

In addition to measuring the accelerations in the system and viewing high-speed video of the system operating, we took the time to talk to other engineers and mechanics that worked with this machine. We asked them what they believed was causing the pickoff tool to miss the excess product. They reported that the problem could be caused by an error happening upstream in the process. A station upstream could be misplacing the product, causing the pickoff tool to be unable to remove it. The station upstream is unable to notify the operator that the product has been misplaced so it does not cause the system to stop until it reaches the excess material removal station. If the product was misplaced (placed crooked or broken) the pickoff tool would have no way to remove it, but the error is attributed to this station.

The next question we asked the mechanics and engineers was whether the design of the pickoff tool itself was contributing to the problem of not removing the product. The engineers reported that the pickoff tool rarely had to be replaced or repaired. They assured us that the pickoff tool design has not been a contributing factor to the pickoff tool being unable to remove excess product since an entire redesign that added the spring-loaded ends to the tool. The current pickoff tool appears not to have a problem removing excess material if it is in the correct place.

3.4 Investigation Conclusions

The results of our investigations showed us that the dynamics of this system did not have a significant effect on this system's ability to pickoff excess material. This conclusion was reached from the relatively low accelerations during the pickoff event (impacts excluded) and high-speed videos that showed no noticeable vibrations. Much circumstantial evidence provided by engineers and mechanics indicated that the problems experienced by this system may be caused by upstream errors in the machine. These facts led us to the conclusion that this system was not the root cause of the pickoff failures and thus not itself a main contributor to machine downtime.

With this conclusion, we decided to focus on our secondary project goals. As discussion with engineers had effectively ruled out the pickoff tool as a cause for error, our remaining design goals were to simplify the system and the system's dynamics. To this end, a complete redesign of the system was pursued. This redesign was performed with the intent to reduce the complexity of the system to have one cam and fewer links. The resulting system is proposed as a simpler alternative to this common application of part removal from or placement on a stationary nest on the Sponsor's machines. The proposed design could be a superior approach for future machine designs.

4 Station Redesign

When it was determined that no major improvements could be made on the current station, an alternative solution was investigated. In order to remove the excess material from the nest, a tool with vacuum applied suction to the product. The tool then translated away from the nest and rotated downward to position where it could safely blow-off the product into a scrap chute. It was this same effective motion that was desired in a possible redesign of the station. A previous group of WPI students, for the project Redesign of a Razor Cartridge Unload Mechanism [Baird], had developed a linkage that had a pickoff tool rotating through a similar motion and it was suggested that the feasibility of adapting that design for the excess product removal station be investigated.

4.1 Original Fourbar Linkage Design

The four bar linkage that was designed in the previous group's project needed to accomplish two tasks. The pickoff tool first had to pick up the good product and then transfer it to a chute where the product was removed. The coupler curve for this previous linkage is shown in Figure 26. Here the pickoff tool is carried on the coupler of a fourbar linkage. The fourbar's motion has both rotation and translation, and thus is able provide the necessary motion from a single input.

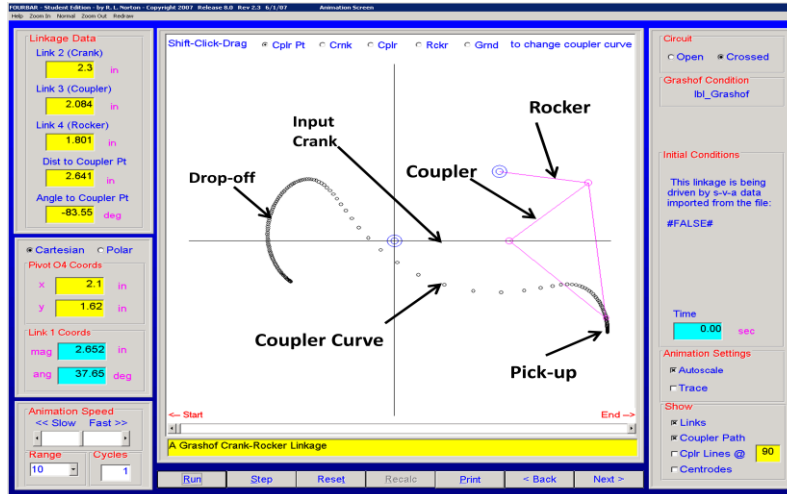


Figure 26: Previously Designed Fourbar Linkage Design

In Figure 26 the linkage is shown in the position where it dwells to pick up the product at the nest. After the pickoff tool dwells in the nest, it moves vertically out of the nest. That allows for clearance between the pickoff tool and the nest before the pickoff tool begins to rotate. Next the pickoff tool begins to rotate and translate horizontally to move the product to the unload chute. The product is removed from the pickoff tool by swiping it against a stationary part causing it to fall into an offload chute. That is the reason for the curvature at the end of the pickoff tools motion on the left. In order to move the product to the correct locations in that application, the crank of the fourbar linkage had to rotate through 109 degrees. This resulted in the coupler rotating through 158 degrees. Since the crank for that linkage had to rotate through such a large angle, a second stage was added to reduce the required input angle. This made the earlier design of the system an eight bar linkage, as the cam lever and its conrod were added.

4.2 Initial Redesign

In order to determine if this fourbar linkage would fit into the existing mounting of the present excess material removal station, the CAD model of the previous linkage was merged with the CAD model of the current machine's excess material unload assembly. In order to

utilize the linkage and the current pickoff tool, the linkage had to be rotated 90 degrees from its original orientation. This resulted in the pivot points of the crank and rocker being below the existing mounting surface of the existing base weldment causing an interference with that surface. Therefore, in order to utilize this linkage on the excess material removal station, the base weldment would need to be redesigned.

By mounting the fourbar linkage into the excess material removal station, it was determined that the linkage did not need to use the full motion of the original coupler curve. The only section of the coupler curve that was needed from the previous design was the section where the tool pulls out straight from the nest (labeled pickoff point) up to where the tool had rotated about 80 degrees. The portion of the coupler curve used in the new design is shown in Figure 27, with the orientation of the coupler in full down position shown in Figure 28.

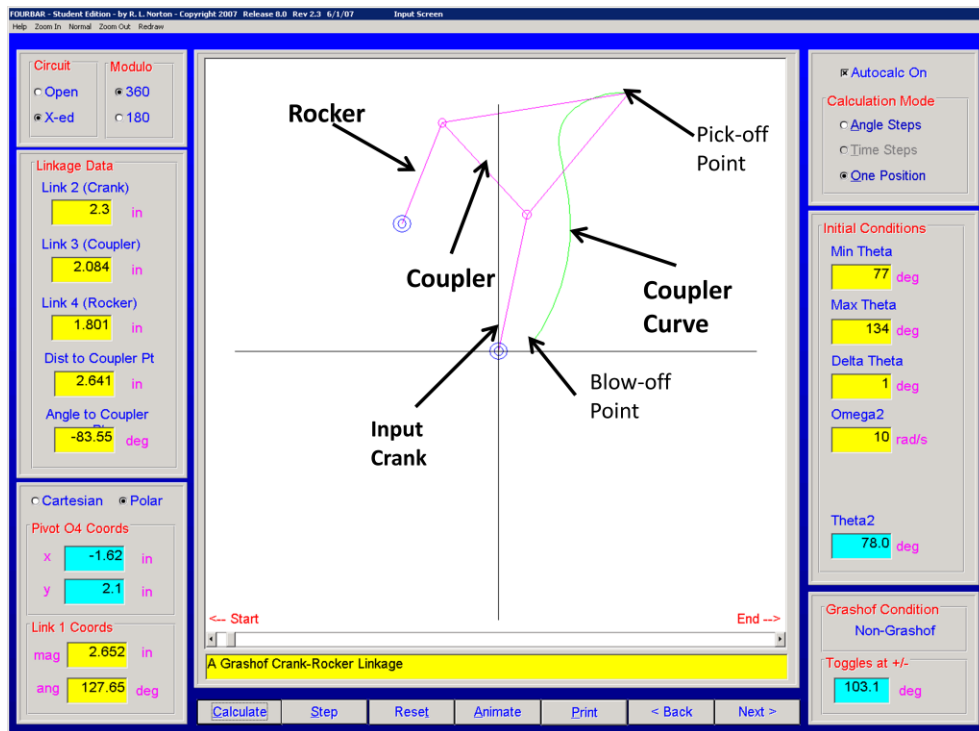


Figure 27: Portion of Coupler Curve of Fourbar Linkage Needed

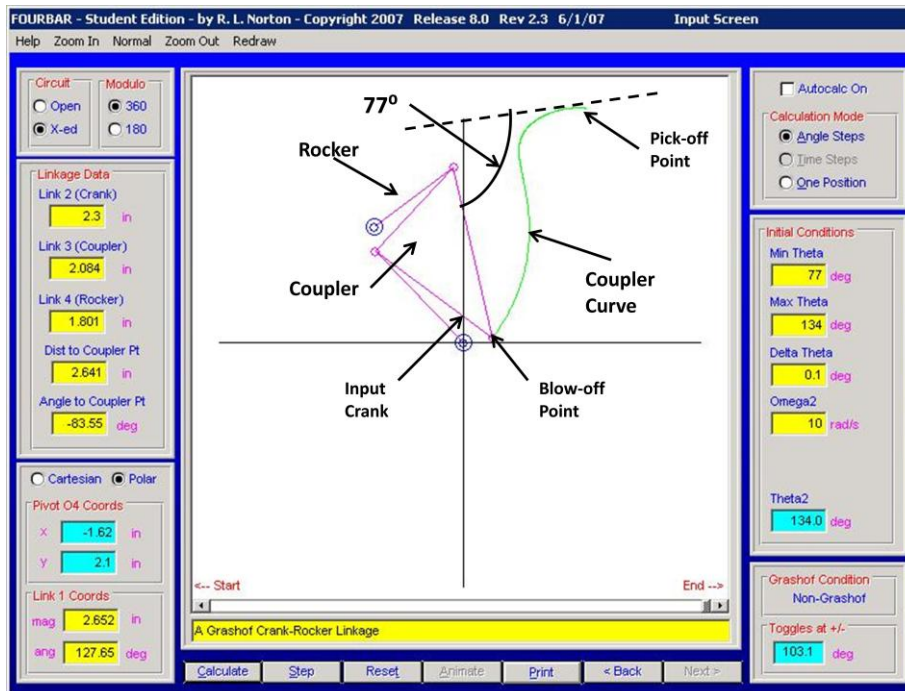


Figure 28: Linkage in Full Down Position

In Figure 27, the linkage is rotated 90 degrees to show how it would be mounted in the new design. Since the new design reduced the angle of rotation of the input crank to fifty-seven degrees (within reasonable range for driving from a cam-link dyad), the intermediate fourbar linkage stage of the previous design was eliminated. The new system also reduces the overall degrees of freedom from two to one, so only one cam is now needed. That also eliminates the coupled motion of the previous design as this single linkage both moves and rotates the pickoff tool to a position where it can blow-off the excess material into the scrap chute. Because the pickoff tool is carried on the coupler, it has complex motion (rotation and translation) needed to both move and rotate the part. A final advantage of the system is that it reduces the number of moving links from thirteen to seven.

4.3 Final Redesign

After it was determined that this coupler motion would work well for the redesign, the linkage was mocked up in the removal station. Since the links interfered with the middle mounting section of the base weldment, it had to be redesigned. The only section of the weldment that was redesigned was the middle section, which ensured that the mounting points of the weldment to the machine's main frame remained the same.

Another major part of the redesign was to attempt to use as many of the same parts from the existing station as possible. In fitting the linkage to the weldment, it was determined that the location of the slider cam offered the best arrangement to drive the linkage. This initially allowed the slider cam's follower, its mounting point, connecting rod, and bellcrank to be used in the new design reducing the number of new parts needed. Other parts that were retained from the existing station in the redesign were the pickoff tool, the scrap chute, and its mounting brackets.

After the linkage was placed on the redesigned weldment and the pickoff tool was aligned with the nest, a servo function was applied to the fourbar to see how the pickoff tool would interact with the nest and to determine if there were interferences between pickoff tool and nest. This showed that during part of the pickoff tools motion there was very little clearance between it and the nest as it moved into position. Since the nest was stationary in that first run, a model of the nest and the belt was added to the system, as shown in Figure 29.

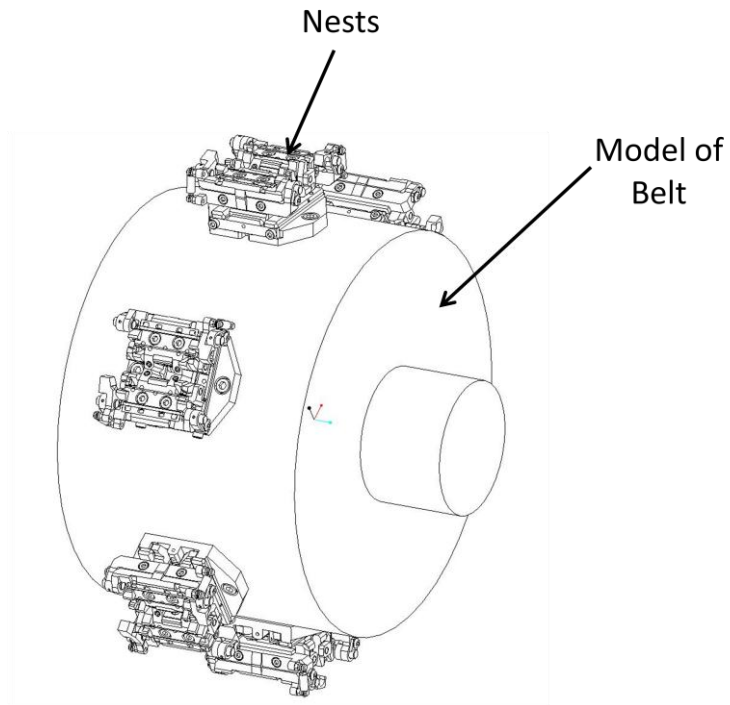


Figure 29: Model of Belt and Nest System

In order to properly gage the amount of clearance between the nest and the pickoff tool the belt was given the correct mod-sine function for its indexing motion as currently used on the machine. By analyzing the motion of the belt in conjunction with the motion of the fourbar linkage it was determined that linkage motion could be timed with the design of a cam provide more clearance between pickoff tool and nest.

4.3.1 Final Redesign Overview

The complete assembly of the redesigned removal station is shown in Figure 30

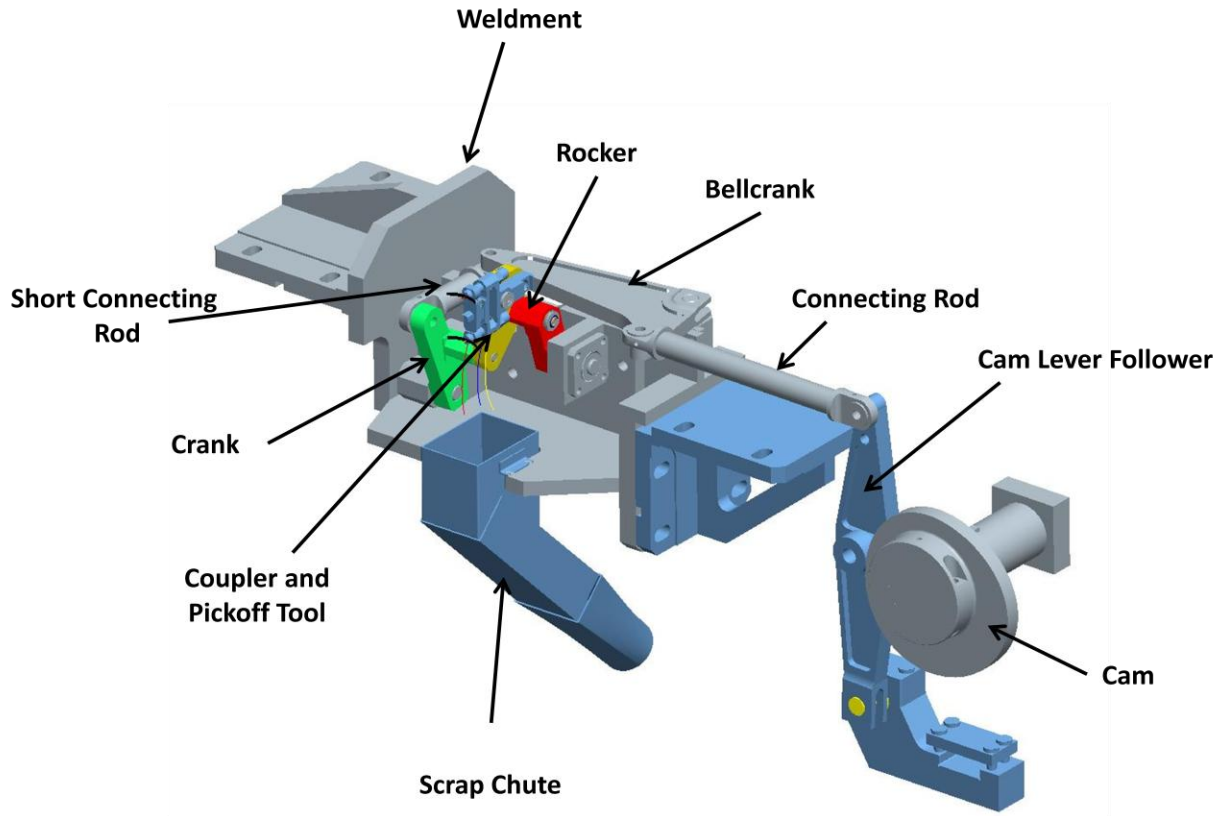


Figure 30: Fourbar Assembly

This redesign reduced the total number of moving components from thirteen, in the existing station, to seven. The components that are no longer incorporated in the new design are shown in Figure 31.

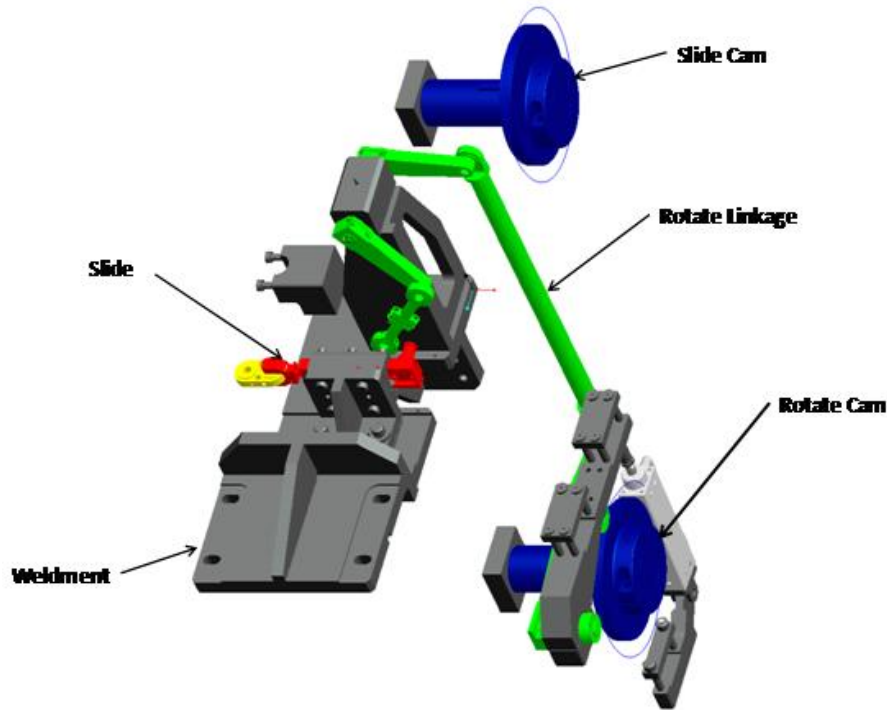


Figure 31: Parts of Existing Station Not incorporated in New Design

The major simplification in the redesign comes from the removal of the rotate cam system, eliminating the coupled motion and reducing the degrees of freedom from two to one. The redesign also simplifies the adjustment of the system. With the coupled motion of the existing system many of the adjustments are interactive, affecting multiple systems. The redesign eliminates that problem by having each adjustment orthogonal to, and independent of, the other.

4.3.2 Design Component

This section details each individual part of the redesign. Along with creating a CAD model of the entire redesign, drawings were created for each of the new or redesigned parts. Those drawings were made using Geometric Dimensioning and Tolerancing (GD&T), which is a method used to describe the geometric requirements for parts and assemblies. Using GD&T defines the allowable variation in form and size of individual features, as well as the allowable variation between features. When dimensioning a part using GD&T the method of a part's

assembly was used to determine the main reference planes as well as the tolerances of the features. See Appendix: D for a list of the drawings.

4.3.2.1 Weldment and Height Adjustment Bracket

The redesigned weldment is shown in Figure 32.

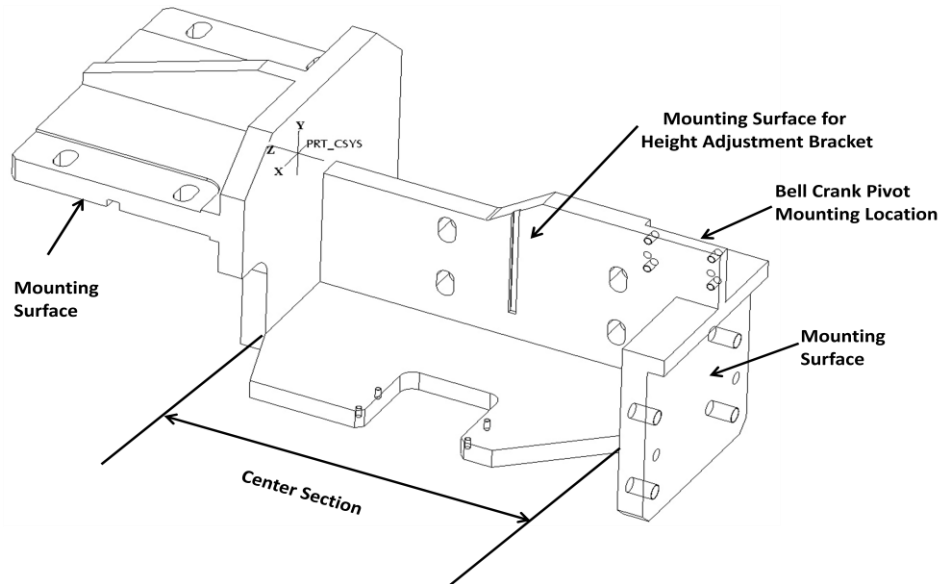


Figure 32: Weldment

As previously mentioned, the mounting location of the weldment to the frame of the machine was maintained as in the current removal station weldment, as was its present means for horizontal adjustment. This allowed the mounting features to remain the same, as the only section of the weldment that was redesigned was the center section connecting the two mounting surfaces. In the center section, there is now a horizontal and vertical surface. The vertical surface is used to mount the height adjustment bracket, which is shown in Figure 33.

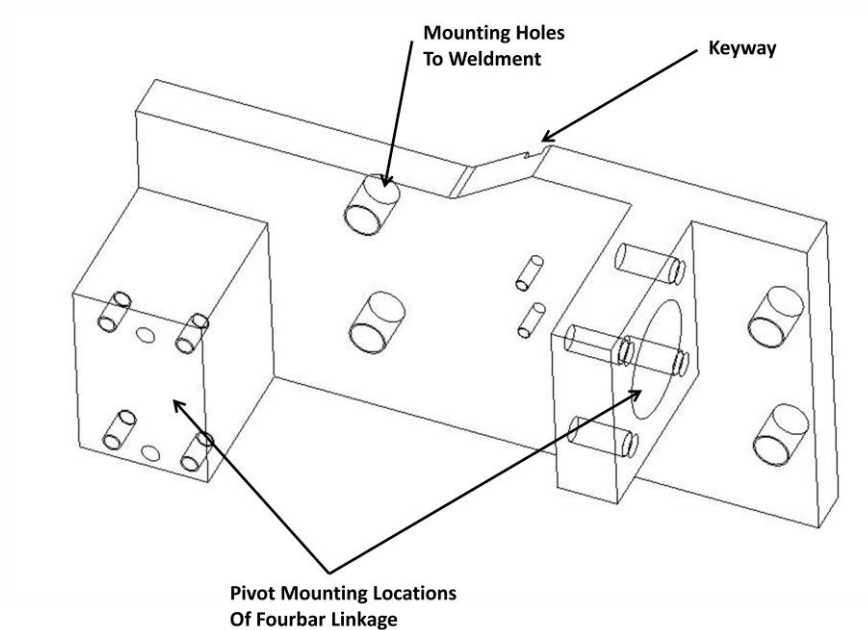


Figure 33: Height Adjustment Bracket

The height adjustment bracket carries the fixed pivots of the fourbar linkage, which allows for the locations of the pivots to be held within tight tolerances to each other ensuring the correct coupler motion of the linkage. In order to mount and allow for vertical adjustment, four slots were added to the weldment allowing for a maximum displacement of ten mm. Also, to rotationally locate the height adjustment bracket on the weldment a key slot was added. That key is secured to the height adjustment by screws into two threaded holes in the key. Also, the position of the key, when fully inserted, was designed so that it was centered within the bracket. That reduced any rotation in the setup of the bracket allowing for the use of only one jackscrew to adjust the height. The vertical surface of the weldment is also where the pivot for the bellcrank is mounted. The bellcrank pivot-bearing block is mounted to the back side of the vertical surface as shown in Figure 32

4.3.2.2 Connecting Rods

In order to simplify the design of the components used to drive the fourbar linkage, two standard connecting rods of different lengths were used. The two connecting rods are shown in Figure 34.

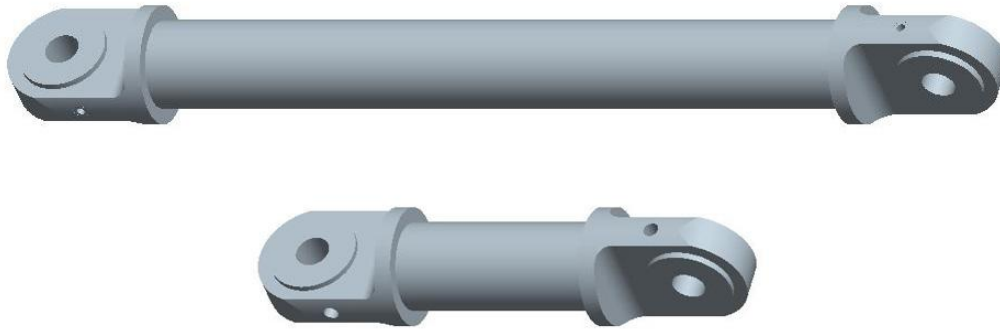


Figure 34: Connecting Rods

The length total length between pivot points of the shorter connecting rod is 116.5 mm and is 271 mm on the longer connecting rod. The bearing housings on both of the connecting rods are mounted 90 degrees to each other.

4.3.2.3 Bellcrank

The design of the bellcrank is shown in Figure 35.

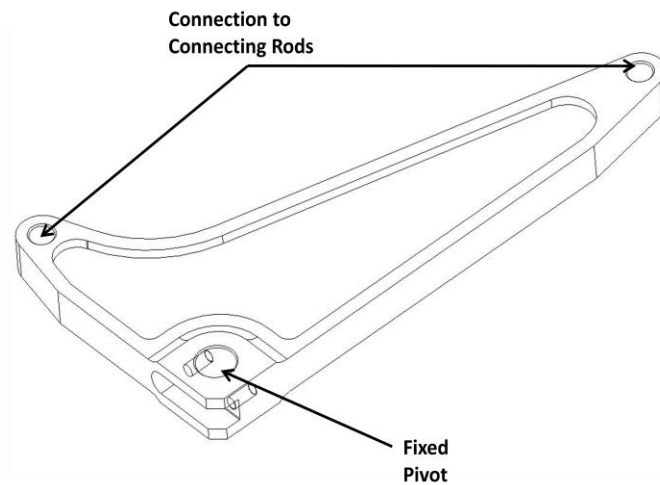


Figure 35: Bellcrank

The basic design features of the bellcrank were maintained from the existing bellcrank used on the removal station. Since the lever ratio of the crank needed to be increased to allow for a shorter stroke in the cam, the lengths from the pivot to the connection points of the connecting rods were altered. The shorter side of the bellcrank, whose connecting rod is attached to the follower, was shortened to 100 mm. The other leg of the bellcrank, whose connecting rod is attached to the crank, was lengthened to 218 mm. Those changes resulted in a lever ratio of 2.18, increased from 1.11 on the old design.

4.3.2.4 Components Reused From Removal Station

One of the design considerations for this redesign was to incorporate as many of the same components from the removal station as possible. Figure 36 shows all the removal station components that were reused for the new design.

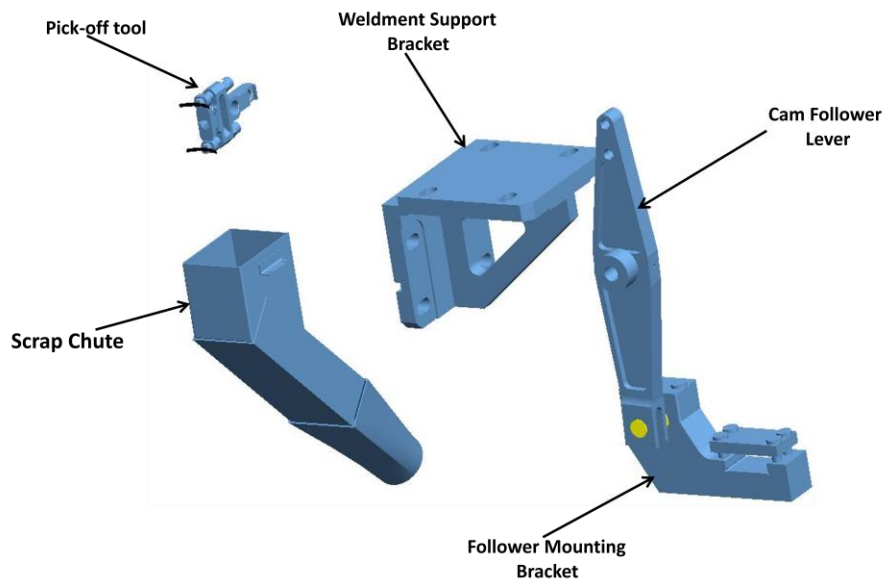


Figure 36: Removal Station Components Incorporated in Redesign

The existing removal station components incorporated in the new design include the pickoff tool, scrap chute, support bracket for the weldment, cam follower lever, and the follower mounting bracket.

4.3.2.5 Fourbar

The fourbar in the redesigned system consists of a crank, a coupler, and a rocker. This system is powered by the short conrod and is used to achieve the desired motion of the pickoff tool.

4.3.2.5.1 Crank

The design of the crank was based on the crank used in the fourbar linkage of the previous MQP. The final design of the crank is shown in Figure 37.

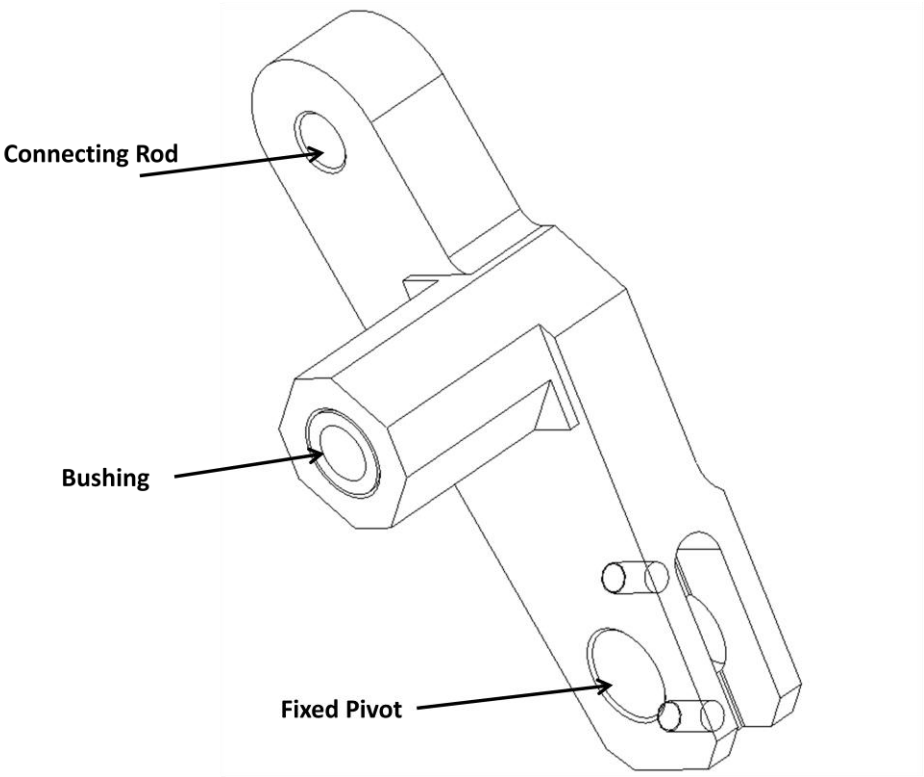


Figure 37: Crank

The crank uses a standard design feature to mount the fixed-pivot bearing, which determined the height and width of the crank. There are two mounting points on the crank, other than the fixed pivot, one for the connecting rod, connection between link 5 and 6, and the other for the coupler, connection between link 6 and 7. The distance from the pivot point to the attachment point of the connecting rod was increased in order to make the conrod horizontal halfway through the stroke of the crank. That point was also rotated 13.3 degrees so that the plane between that point and pivot was vertical half way through the stroke of the fourbar linkage.

A boss was added to the connection point of the coupler in order to accommodate the increased lever ratio of the bellcrank. That also had the added benefit of increasing the bearing ratio on the pin. The hole for the pin has a clearance fit of H7 to allow the pin to rotate freely. Also, the crank contains a bronze bushing, which is the length of the boss, which is press fit. Since it would be difficult to machine a hole to press fit tolerances over the length of the boss, the hole was divided into three sections, shown in Figure 38.

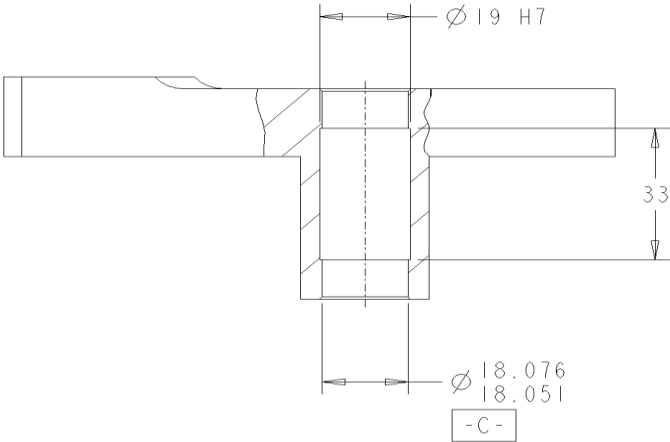


Figure 38: Detail of Crank Bushing Hole

Each end of the hole is held to press fit tolerances while the center has a slightly larger diameter and held to the tolerance of a clearance fit. Having a bushing the entire length of the boss enables the bushing to be easily replaced by pressing out. Since the crank will be machined from a solid piece of material, the boss was made with chamfered edges rather than round to simplify machining. Also, the chamfers do not go all the way to the surface of the part. The reason for the chamfers is to reduce the mass of the crank.

4.3.2.5.2 Coupler/ Pickoff tool

The coupler serves as the link connecting the crank to the rocker, as well as the part to which the pickoff tool mounts. The coupler assembly is shown in Figure 39.

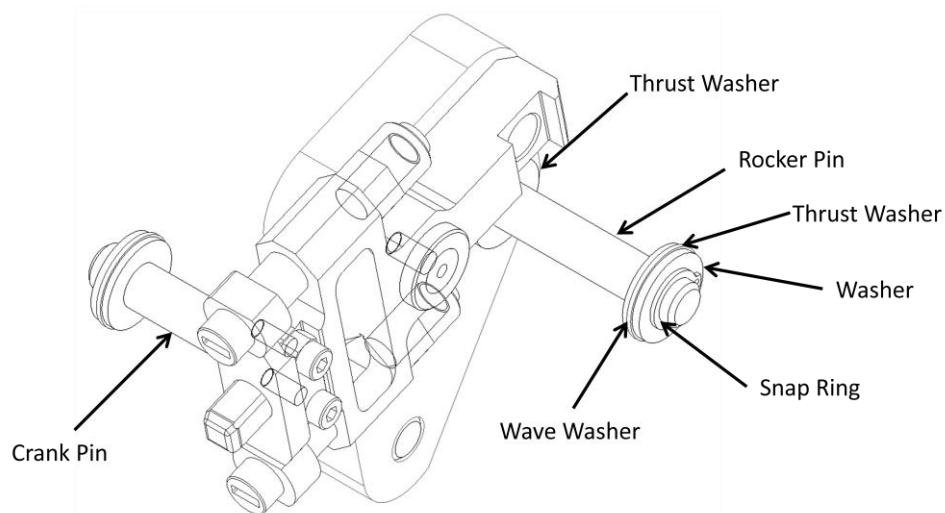


Figure 39: Coupler

The coupler contains two pins, which are press fit in, and each pin serves as the connection between either the crank or the rocker. Since the pin is press fit in the coupler, the pins will have zero rotation in respect to the coupler but will be rotating with respect to the rocker and the crank. Bronze thrust washers were added to either end to reduce the friction between the contact surfaces. Wave washers are used to load the coupler axially to the crank and rocker, preventing

any lateral motion. In order to compress the wave washer a standard washer is used and a snap ring is used to secure the assembly.

The pickoff tool is mounted using a similar method as used on the present removal station. The 10 mm diameter hole has a pin press fit and is threaded on the opposite end, bolting the pickoff tool in that location. The larger diameter hole also has a press fit pin, but has a slightly different mounting method. The pickoff tool is placed on the pin and an end cap is placed on the pin. Then the end cap is secured to the pin with a screw.

4.3.2.5.3 Rocker

The rocker contains features similar to that of the crank and is shown in Figure 40.

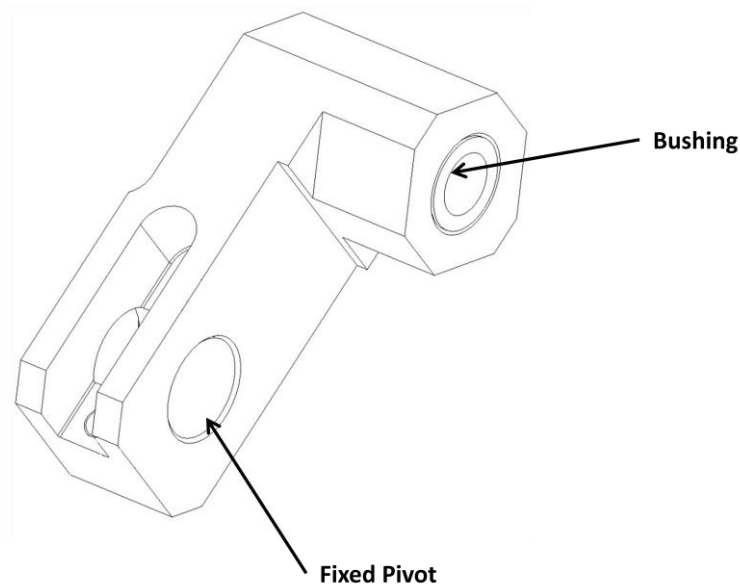


Figure 40: Rocker

The rocker uses the same standard design feature to mount to the pivot bearing at its fixed pivot. The rocker also contains a boss with chamfered edges around the hole for the pin. The reason for the boss on the rocker was to increase the bearing ratio and reduce wear on the bushings.

4.3.3 Locating Considerations

Between assembly machine setups there are many slight variations in the location of the frame rails, belt and nest. So, when redesigning the weldment, adjustability for the location of the pickoff tool needed to be considered. Since the pickoff tool may not be entering the nest perfectly horizontal, the pickoff tool needs to compensate for slight angular variations. To accomplish that the pickoff tool maintains the same spring loaded vacuum ports. The three axes considered for adjustability are shown in Figure 41.

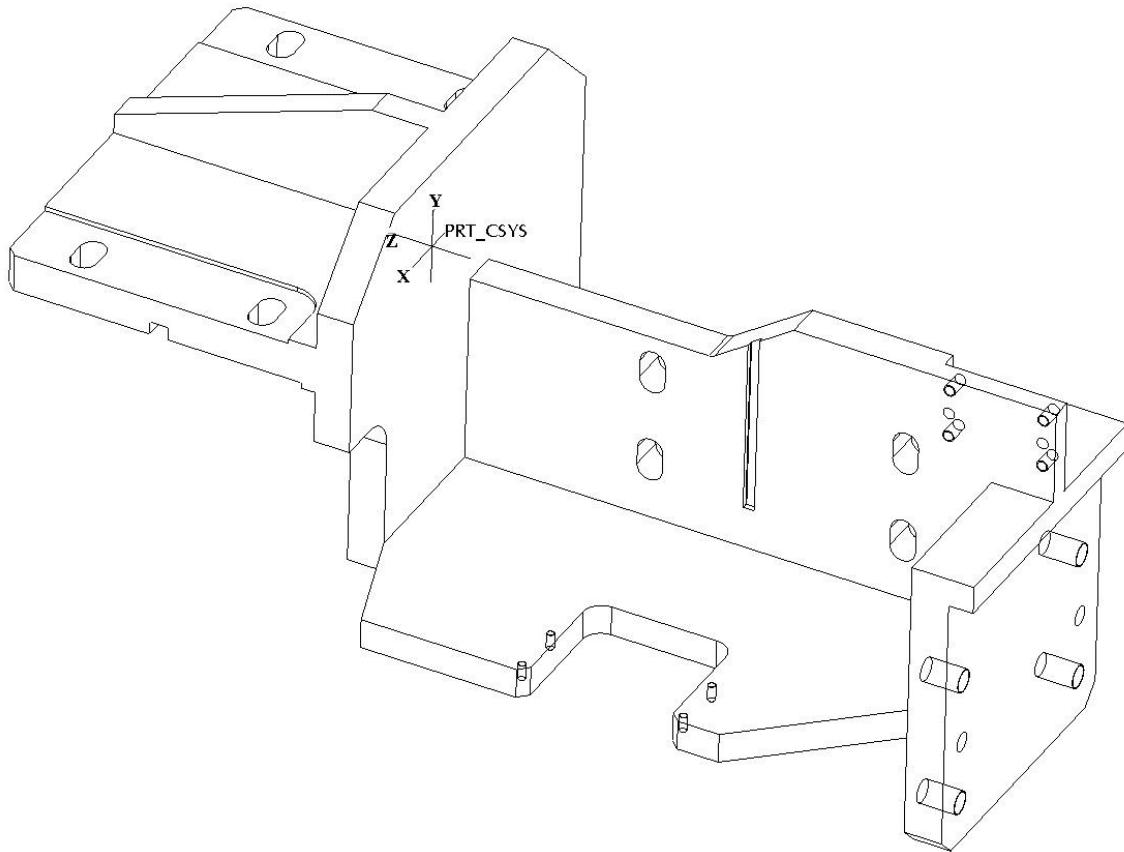


Figure 41: Axis Orientation of the Weldment

4.3.3.1 Fourbar X position

The redesigned weldment maintained the same adjustability in the x-direction as the previous one. As shown in Figure 42, at either end of the weldment there are four slots, which are the mounting locations to the machine chassis.

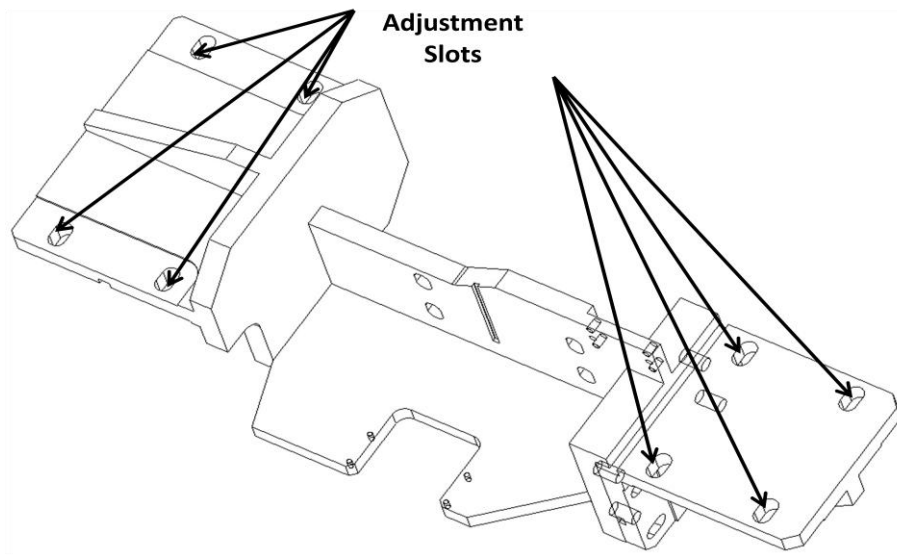


Figure 42: Slots for Adjustment in the X-direction

To control the displacement of the adjustment, jackscrews are mounted at either end, and to prevent rotation there is a slot machined into the left mounting face.

4.3.3.2 Fourbar Y position

In order to keep the adjustability settings independent of each other, a height adjustment bracket was added to the weldment. This bracket uses the same slot style mounting as the weldment. Also, the height adjustment bracket uses a keyway to prevent rotation of the bracket and allows for the use of only one jackscrew to adjust the height, see Figure 32.

4.3.3.3 Fourbar Z position

There is no direct adjustment in the z-axis. This is because the machines are accurate to themselves, which means that the location of the belt to the machine chassis will be consistent with all machines. So, the keyway in the height adjustment bracket not only serves as a method to prevent rotation but also locates the pickoff tool along the z-axis. Also, the nest floats in the z-direction and the locating pin forces it to the correct alignment with the pickoff tool.

4.3.4 Clearance

One of the challenges in determining the timing of the pickoff tool in respect to the nest was clearance between the two. Figure 43 shows the paths of the two points on the pickoff tool and nest that are most likely to interfere. The point chosen on the nest was the area where the excess material is secured and the point chosen on the pickoff tool was the upper most point of the top vacuum point.

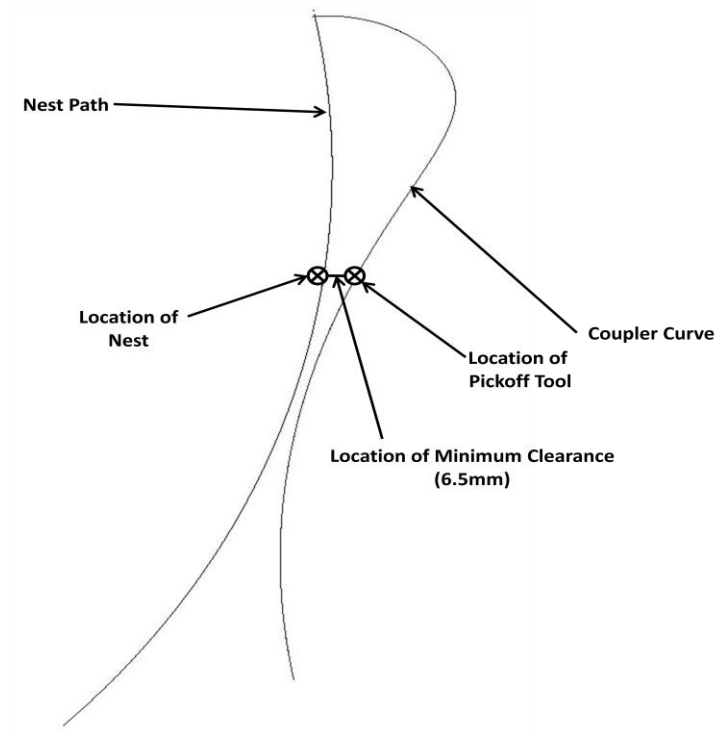


Figure 43: Clearance between Path of Nest and Pickoff Tool

As shown in Figure 43, the two paths never intersect except where the pickoff tool enters the nest to remove the excess material. The smallest distance between these two paths, other than the pickoff position, is 1.8 mm. Since the two are never at that position at the same time, the closest one to the other dynamically is 6.5 mm, which occurs while the pickoff tool is in its upward motion.

4.4 Cam Design

After the position of the links and design of the weldment were established, a preliminary cam was designed for the system. The total stroke of the cam was determined by running the servo function on the crank and measuring the minimum and maximum angles of the cam follower arm. The follower arm needed to rotate approximately 15.5 degrees to achieve the required coupler motion. When designing the cam function, the timing diagram from the slider cam was used as a basis to determine the length and time the pickoff tool should be in dwell to establish vacuum on the product. This was duplicated in the new design.

The first iteration of the cam design used two segments, a dwell and a spline (Figure 44).

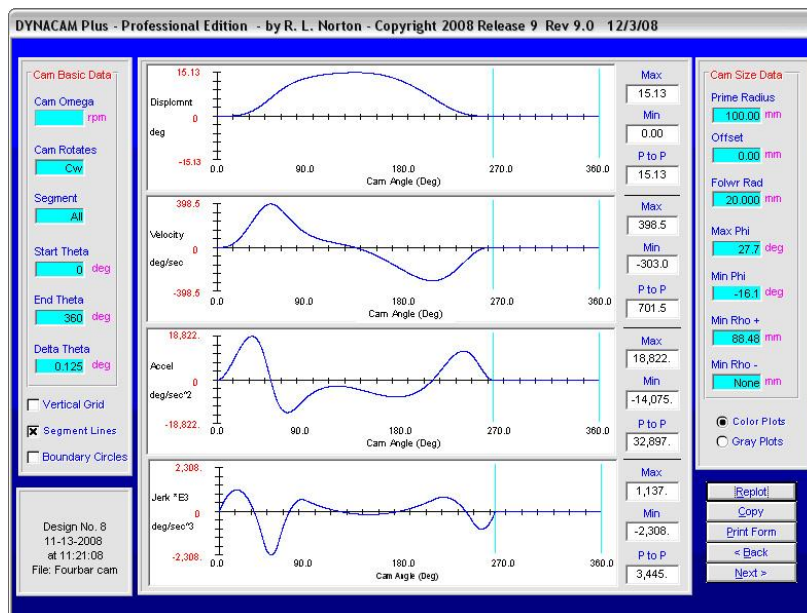


Figure 44: First Cam Iteration S-V-A-J Diagram

The function utilized a spline function for the rise and fall and a dwell when the pickoff tool was in the nest. The spline function had ten boundary conditions, as shown in Figure 45.

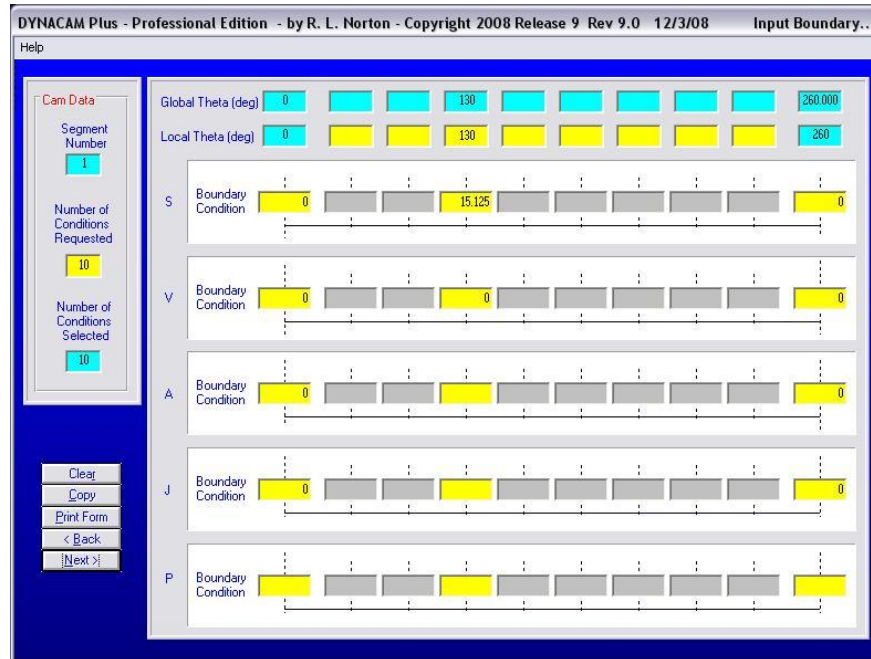


Figure 45: Boundary Conditions Used In First Cam Iteration

Eight of the boundary conditions were used to make the displacement, velocity, acceleration, and jerk zero at each end of the function. The two other boundary conditions were used to set the displacement to 15.5 degrees at 130 degrees into the cam motion and set the velocity to zero at this point. The jerk was constrained to zero at the dwell interfaces to minimize vibrations.

When that cam was applied to the system, the pickoff tool came close to interfering with the nest on both the downward and upward motions. Many iterations were tried to obtain a longer dwell at the maximum displacement using a single spline and additional boundary conditions. However, a long enough dwell could not be obtained and the pickoff tool still had very little clearance on the upward motion. The spline function was then split into two sections. The resulting S-V-A-J diagram is shown in Figure 46.

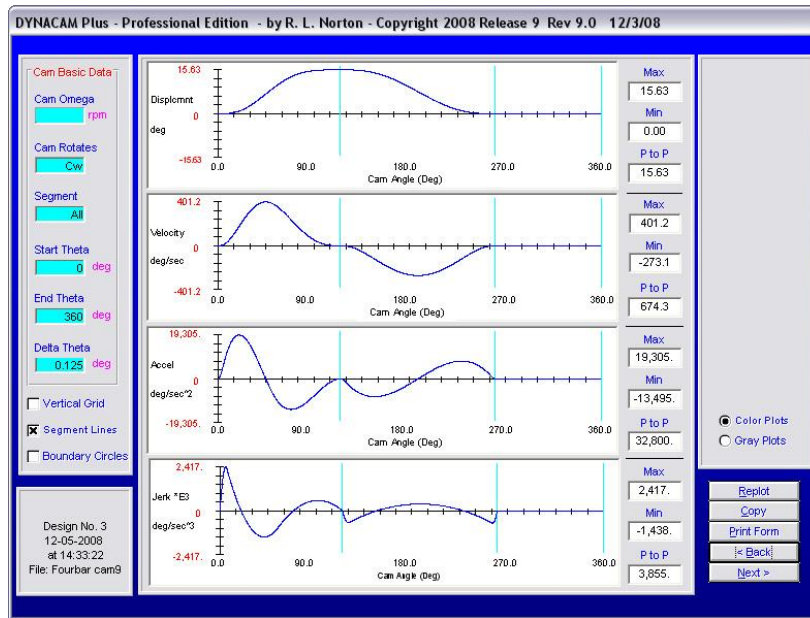


Figure 46: S-V-A-J Diagram of Cam Function with Two Splines

Splitting the spline into two segments allowed for more control over the length of the dwell at maximum displacement and allowed for the rise and fall to occur at over different lengths. The resulting motion of the pickoff tool still had very little clearance with the nest on the upward motion. To add more control over the length of the dwell, more boundary conditions were added. This still made it difficult to obtain a long enough dwell.

In order to improve the clearance, a dwell of 25 degrees was added at maximum displacement, 115 degrees. The resulting S-V-A-J diagram is shown in Figure 47.

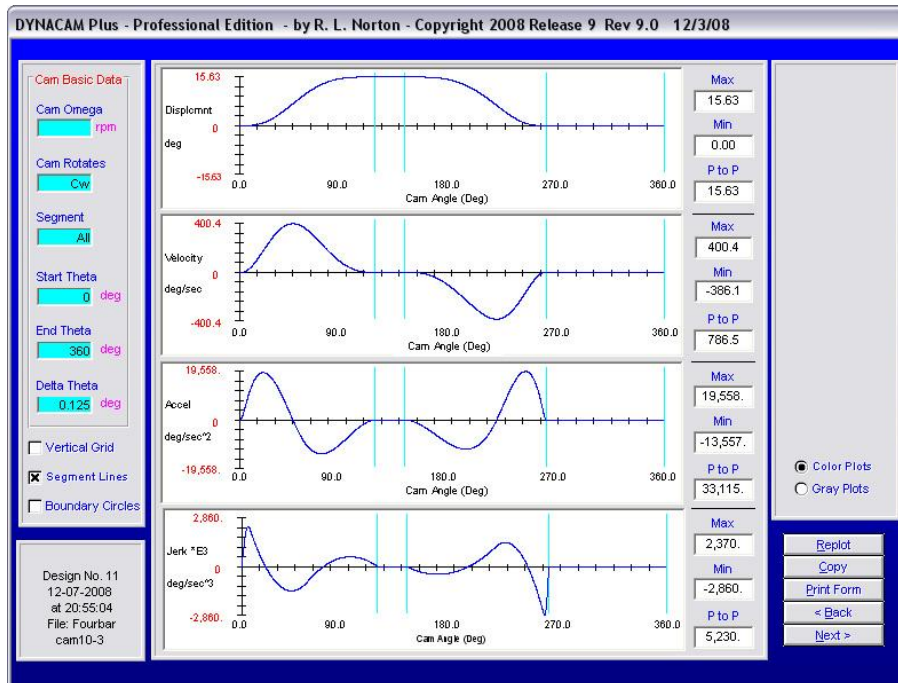


Figure 47: S-V-A-J Diagram for Cam with Two Dwells

By adding this dwell, it became less challenging to increase its duration through the manipulation of the spline functions. In order to obtain the displacement function shown in Figure 47, the knots for both the rise and fall were placed closer to ends of the functions that had zero displacement as shown in Figure 48 and Figure 49.

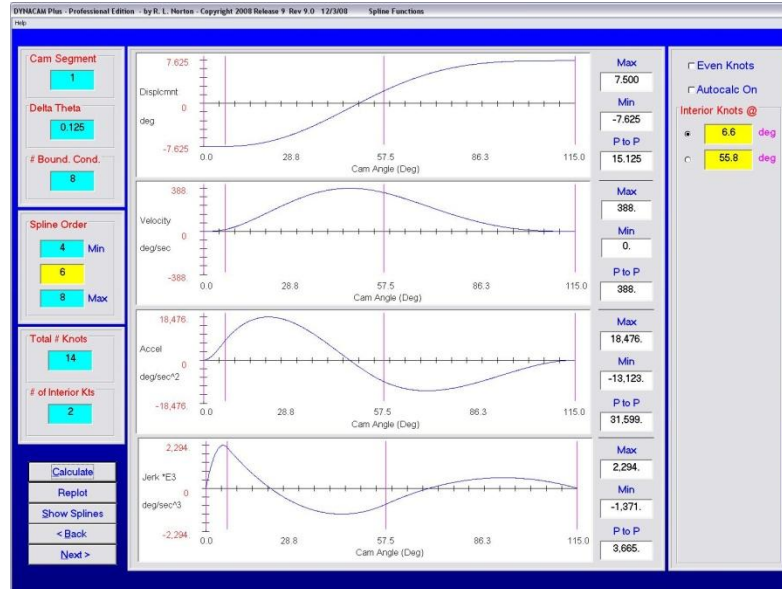


Figure 48: Knot Location of B-spline for Cam Rise

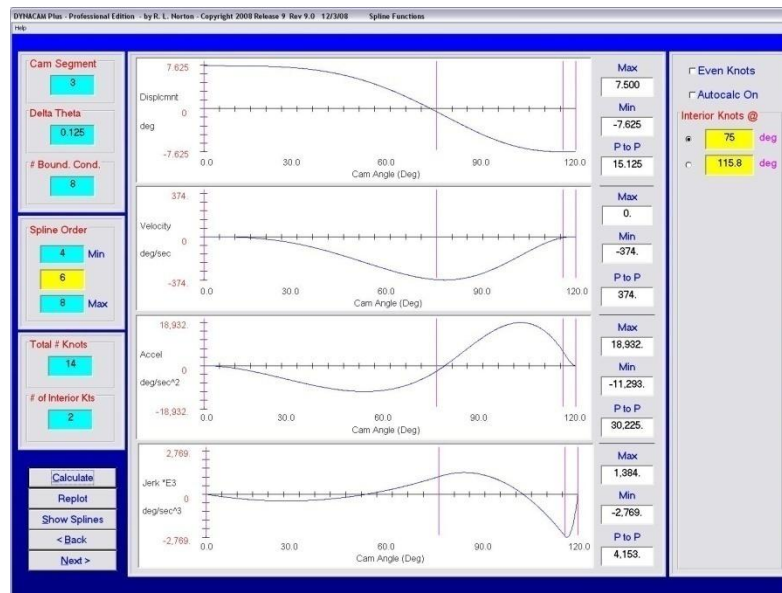


Figure 49: Knot Location of B-spline for Cam Fall

The increased dwell allowed the nest more time to return to its static position thus allowing for more clearance between the nest and pickoff tool.

After testing many iterations of a cam function with a rise, fall, and two dwells, it was determined that the cam function shown in Figure 47 was the best option. The next step was to size the cam. In order to maintain the cam position of the removal station, the zero displacement

of the cam had to be when the follower arm was at negative 7.625 degrees. That resulted in a prime radius of 81.8 mm and a maximum radius of 127.8 mm. However, it was soon discovered that in order to fit the cam profile on the sponsor's standard cam blank the range for the prime radius of the cam had to be between 95.5 mm and 119 mm. That meant that the stroke of the new cam was approximately twice that which would fit on the cam blank. This required the total lever ratio of the links driving the fourbar linkage to be doubled to reduce the angular displacement of the follower to be within the cam blank limits. The simplest way to accomplish that was to adjust the lever ratio of the bellcrank. On the current removal station, the lever ratio of the bellcrank was approximately 1.11. In order to obtain a lever ratio of approximately 2.2, one end of the bellcrank was shortened to 100 mm and the other end lengthened to 218 mm, resulting in a lever ratio of 2.18.

With the lever ratio increased, the total angular displacement of the cam was reduced to 7.5 degrees, which resulted in a prime radius of 95.5 mm and a maximum radius of 118.4 mm. The resulting S-V-A-J diagram for that cam is shown in Figure 50.

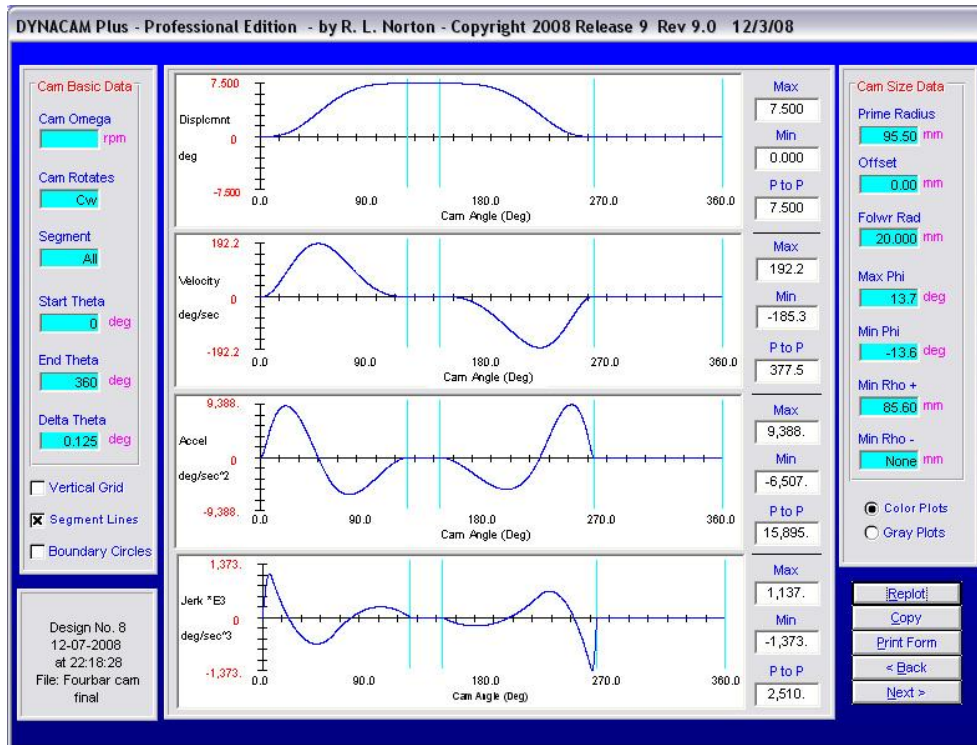


Figure 50: S-V-A-J Diagram for Cam with Shortened Stroke

Reducing the total angular displacement of the cam by half caused the maximum acceleration to also be reduced by half, but unfortunately will cause the effective mass of the follower train as felt at the cam roller to quadruple, versus the previous design.

One final suggestion was provided regarding the design of the cam that allowed for a further reduction of the cam's acceleration. The suggestion was that the length of the dwell at zero displacement was unnecessarily long and that it could be reduced. That dwell was made one hundred degrees in the previous iterations because that is the length of the dwell on the removal station, so it was assumed the dwell needed to be that long. However, other stations that use vacuum to transfer parts have dwells for as little as twenty degrees. So, many iterations of different length dwells were investigated to determine which function gave the pickoff tool the most clearance. Through those iterations it was determined that a dwell of fifty degrees would

provide the most clearance between the nest and the pickoff tool and is still long enough to ensure a good vacuum seal on the material.

The S-V-A-J diagram of the final cam design is shown in Figure 51.

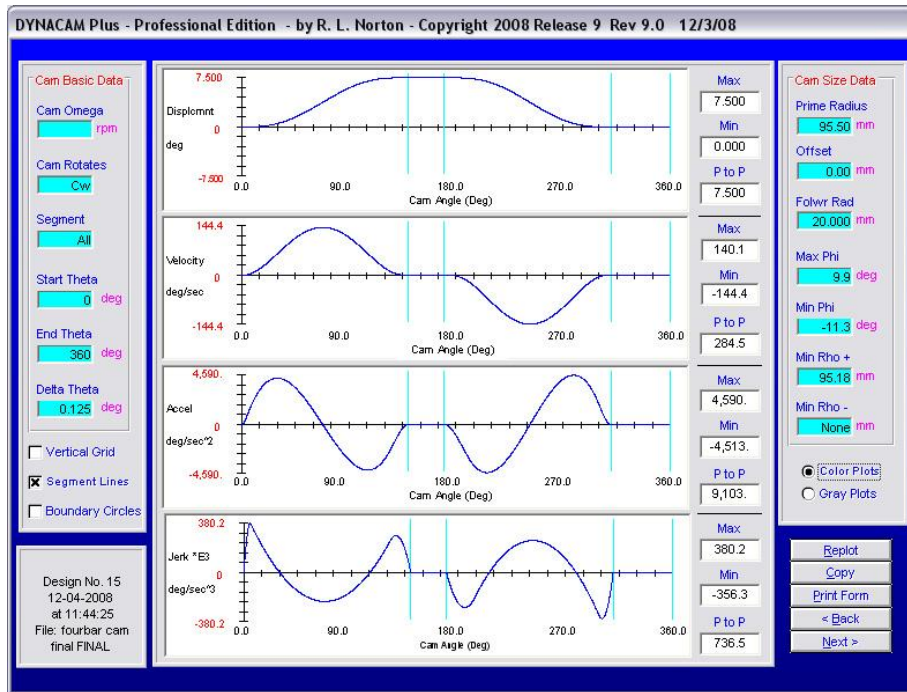


Figure 51: S-V-A-J of Final Cam Design

Reducing the length of the dwell at zero displacement decreased the maximum acceleration by approximately half. Finally, to maximize the clearance of the pickoff tool on its upward motion, the length of the dwell at peak displacement was increased by 5 degrees.

4.5 New System analysis

To understand the theoretical motion of this new design, system properties were found and a theoretical model of the system was created.

4.5.1 Basic Analysis

Basic analysis of this new design was performed to find masses and stiffnesses of the new links. This analysis was performed in the same way as with the analysis of the current design. As such, the masses were found using mass properties in Pro/e and stiffnesses were found using the FEA package COSMOSWorks. The effective mass and stiffness of the system was also calculated. These calculations can be seen in Appendix B.

4.5.2 Theoretical Model of New Design

To analyze our design, a theoretical model was needed. This was to be used to calculate forces and accelerations of the linkage, allowing further analysis to be performed on the design. For this design, an appropriate theoretical model was created using the programs Dynacam, Fourbar, and Sixbar.

These programs can only calculate 2D systems. Because of this, the redesigned linkages had to be modified so that they folded into one plane. To do this, some parts were rotated 90 degrees about the axis of their connecting rod as necessary to rotate them into one plane. The geometry of this 2D system can be seen in Figure 52.

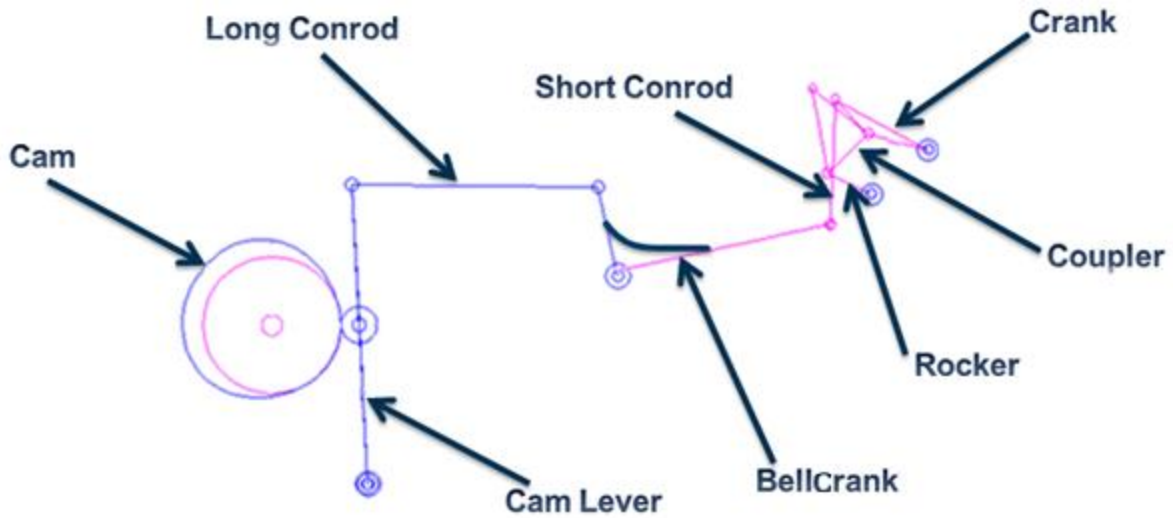


Figure 52: 2D System

As indicated by their names, Dynacam, Fourbar, and Sixbar are designed to analyze cams, fourbar linkages, and sixbar linkages. This linkage is an eightbar, as there are seven moving links plus the ground. As such, these programs required the linkage to be broken up into two sections. The first section is to be analyzed in Dynacam and Fourbar. This section is a cam-driven fourbar linkage that goes from the cam and cam lever to the first half of the bellcrank. This leaves a sixbar linkage to be analyzed in Sixbar. This section is comprised of the remaining parts, from the second half of the bellcrank to the crank and rocker. The geometry of the cam-driven fourbar can be seen in Figure 53. The geometry of the sixbar can be seen in Figure 54.

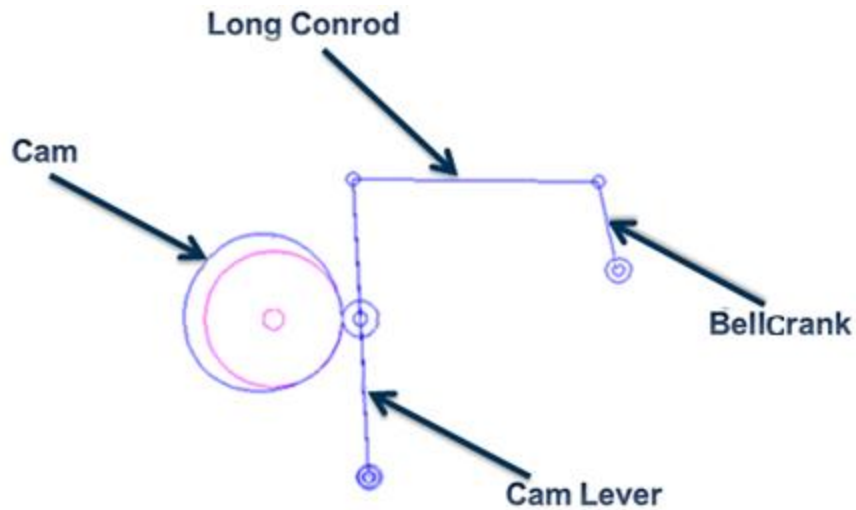


Figure 53: Fourbar Section Geometry

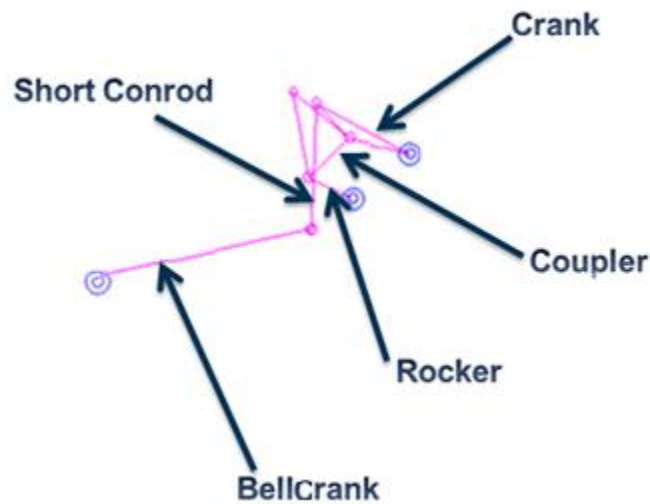


Figure 54: Sixbar Section Geometry

Another change to model geometry was to modify the bellcrank angle. The bellcrank is essentially two "links," merged into one and connected at a pivot. These two "links" are set 90 degrees apart. To allow the Sixbar model to interpret the output from the Fourbar model, the bellcrank was folded in upon itself. For a graphic of this shift, see Figure 55. The final geometry of the theoretical model can be seen in Figure 56.

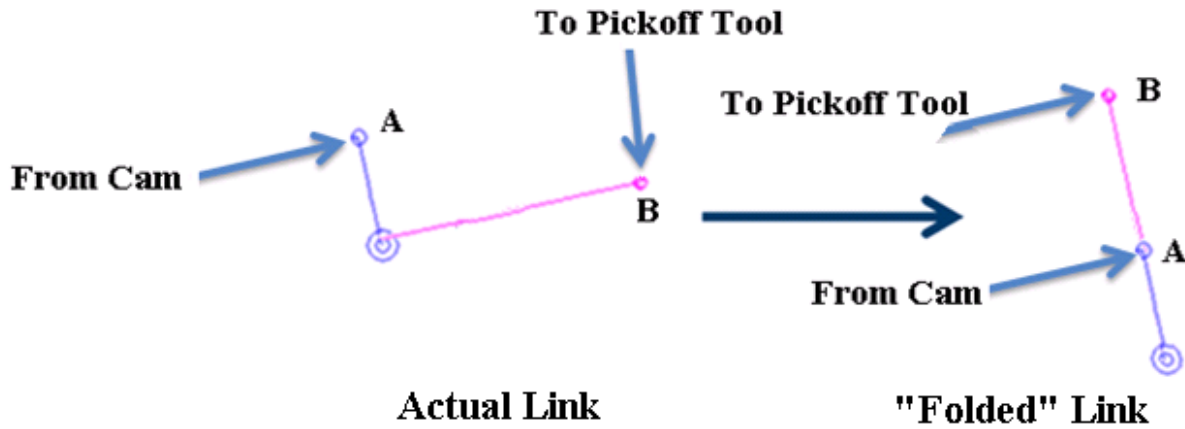


Figure 55: Bellcrank Fold

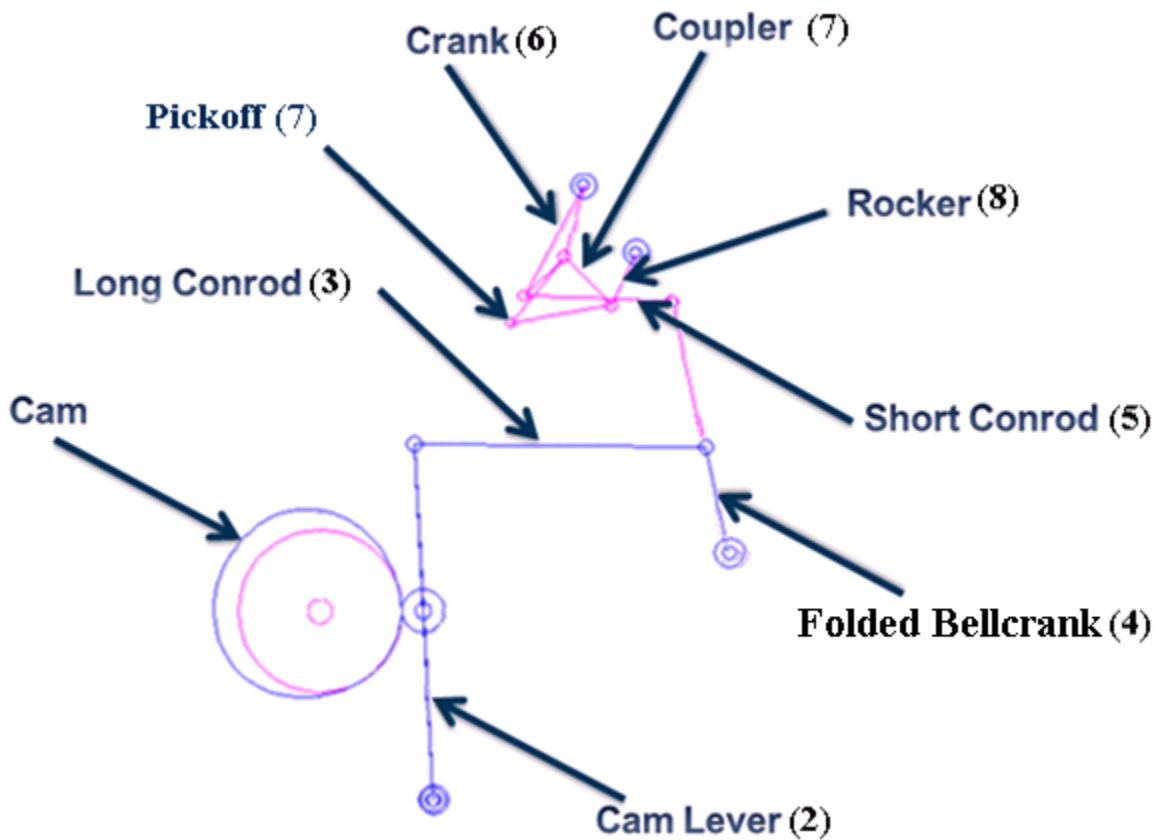


Figure 56: Final Theoretical Model Geometry

The programs used also do not take into account impacts. As such, actual test data taken from this system would differ from this theoretical model, as there would be spikes in accelerations at pickoff tool entry. Where there is a deliberate impact.

4.5.2.1 Dynacam Model

The first step in this process was to set up the fourbar first stage of the linkage train in the Dynacam file that was used to design the cam. The linkage data necessary to create the geometry for this part of the model were the pivot positions of the cam lever and bellcrank relative to the cam center and the linkage lengths. The resulting system can be seen in Figure 57.

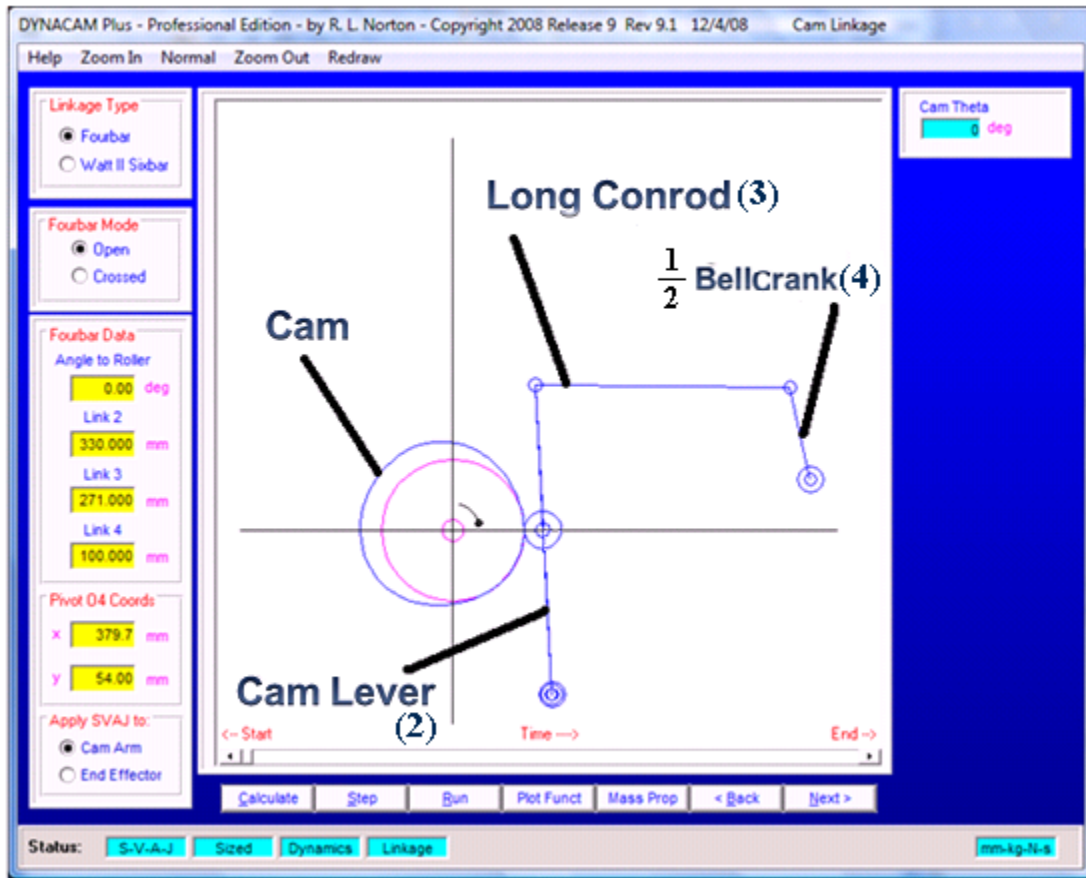


Figure 57: Dynacam Model Geometry

With this system geometry, data for the mass properties of these links was needed. This was necessary as to allow for dynamic calculations of the system. See Table 1 for the input values.

Table 1: Mass Properties of Dynacam Model

	Link 2	Link 3	Link 4	units
Distance to CG from Pivot	149.71	135.50	49.82	mm
Angle to CG in LRCS	0	0	-4.806	deg
Mass of link	1.645	0.499	0.394	kg
Mass Moment Inertia about CG	16952.09	5574.88	457.02	kg-mm ²

From this model, position, velocity, and acceleration (S, V, A) data was calculated and then exported. Graphs of this data can be seen in Figure 58.

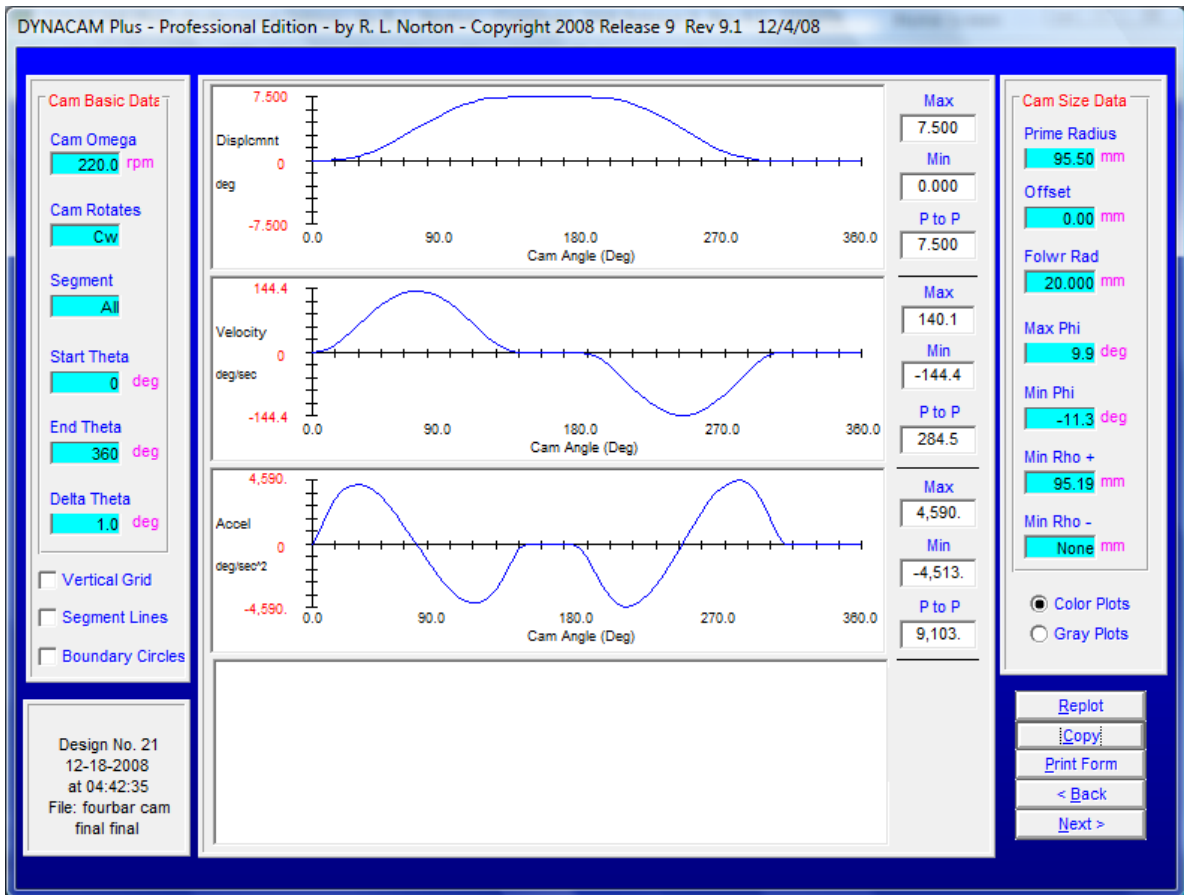


Figure 58: Dynacam Exported S, V, A Data

4.5.2.2 Fourbar Model

The results of the Dynacam analysis were imported into program Fourbar. This program allows for a more detailed analysis of the linkages and exports its output to be sent to Sixbar as an input for the next stage. To set up this model, the exported Dynacam data was imported to Fourbar. This imported the geometry of the system and properties of the links, as well as the driven S, V, A for link 2, meaning no additional data was needed. The result is shown in Figure 59. This geometry and the labels shown in this figure are the same as in the Dynacam model. The one difference between these models is that Fourbar does not show the cam profile as it already has the applicable driving data.

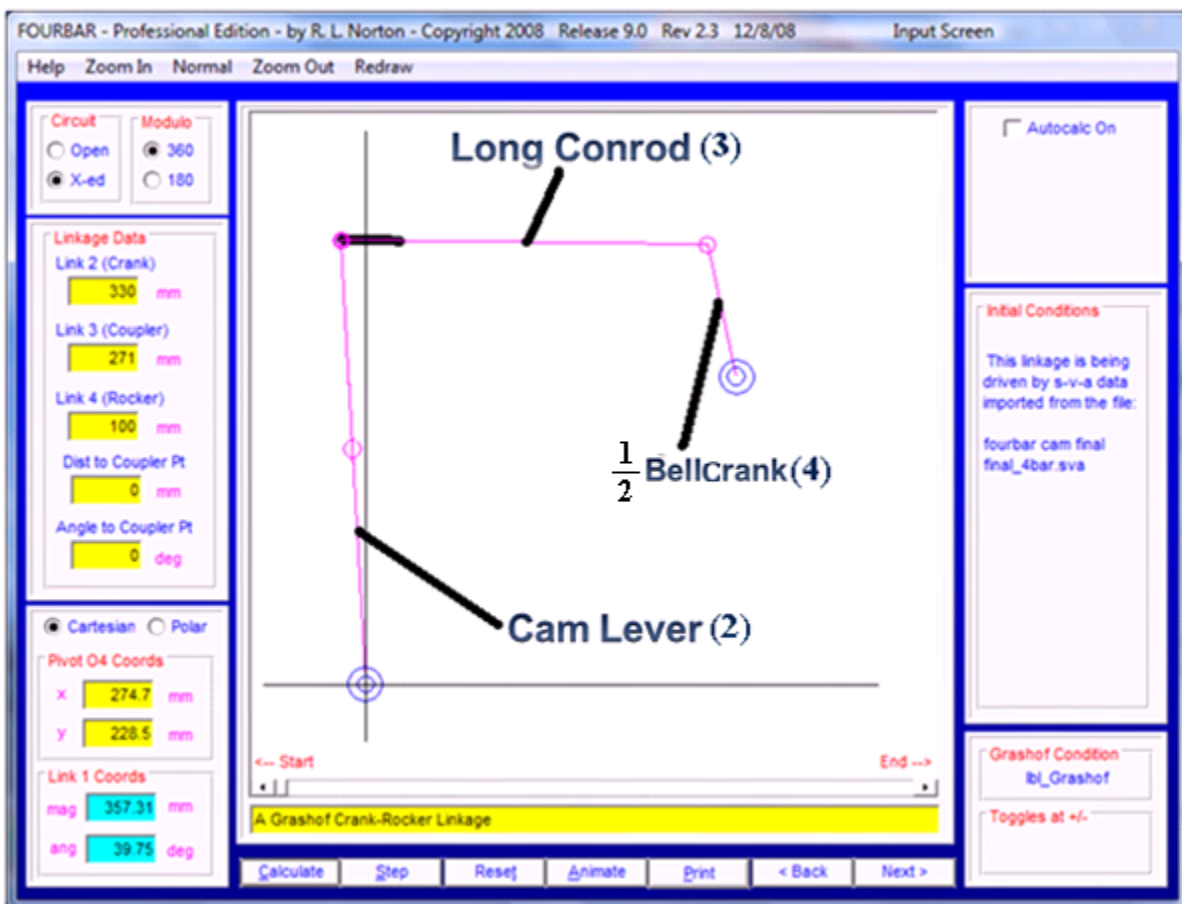


Figure 59: Fourbar Model Geometry

Using the geometry, the imported Dynacam results, and the mass properties of the links, Fourbar provides force and acceleration data of the links, pivots, and coupler points. This theoretical data gives us a portion of the results needed from this analysis. See Figure 60 and Figure 61 for example acceleration and force graph from Fourbar.

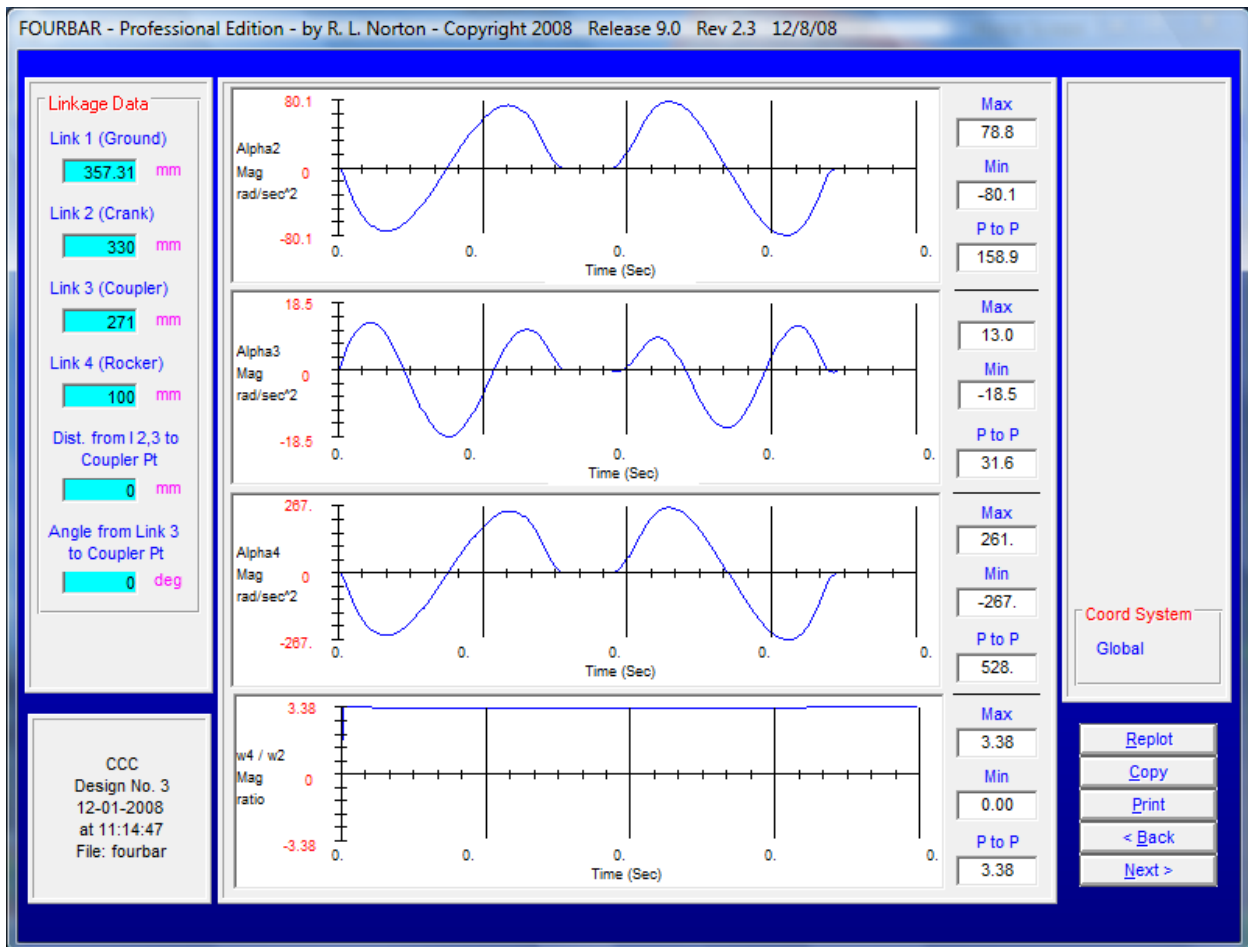


Figure 60: Theoretical Acceleration of Links 2, 3, and 4 from the Fourbar Model

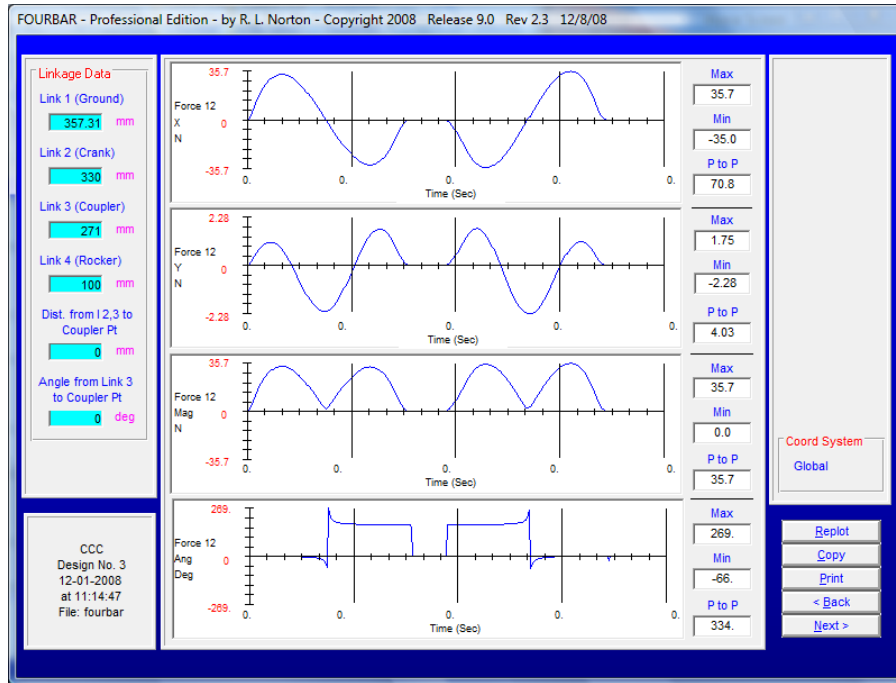


Figure 61: Theoretical Force on Cam Lever Pivot from Fourbar Model

From this model, theta, omega, and alpha (θ , ω , α) data was calculated and then exported.

Graphs of this data can be seen in Figure 62.

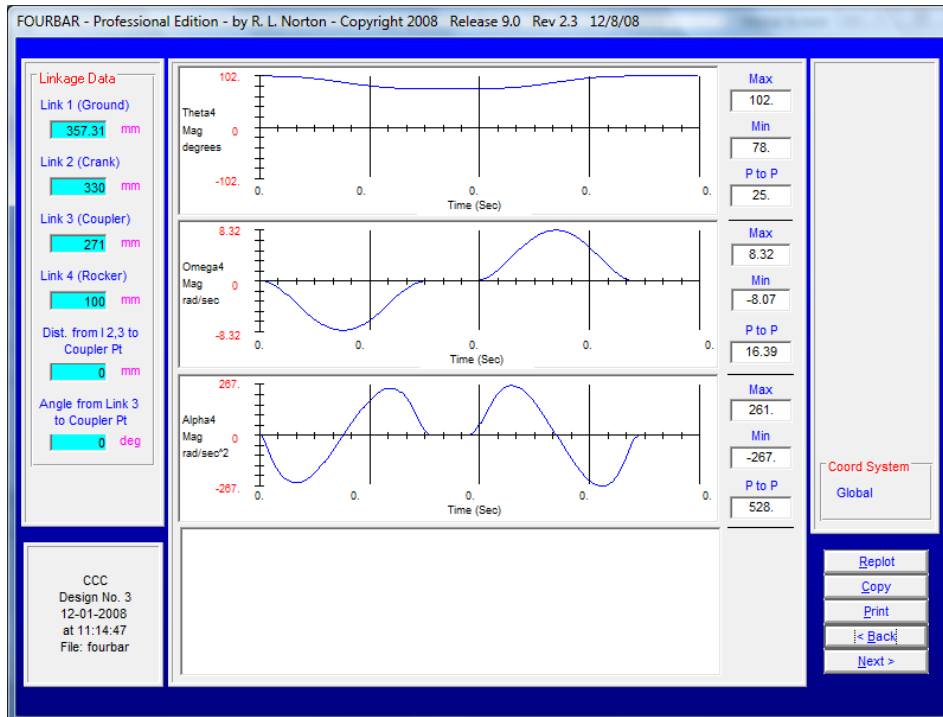


Figure 62: Fourbar Exported θ , ω , α Data

4.5.2.3 Sixbar Model

The Fourbar model's exported data gives Sixbar the driving data needed to analyze the rest of the system. With this driving data, the geometry of the system had to be created in Sixbar. The needed data were the crank and rocker pivots relative to the bellcrank pivot, the lengths of the linkages, and the angles and distances to the coupler points. See Figure 63 for the final geometry of this system.

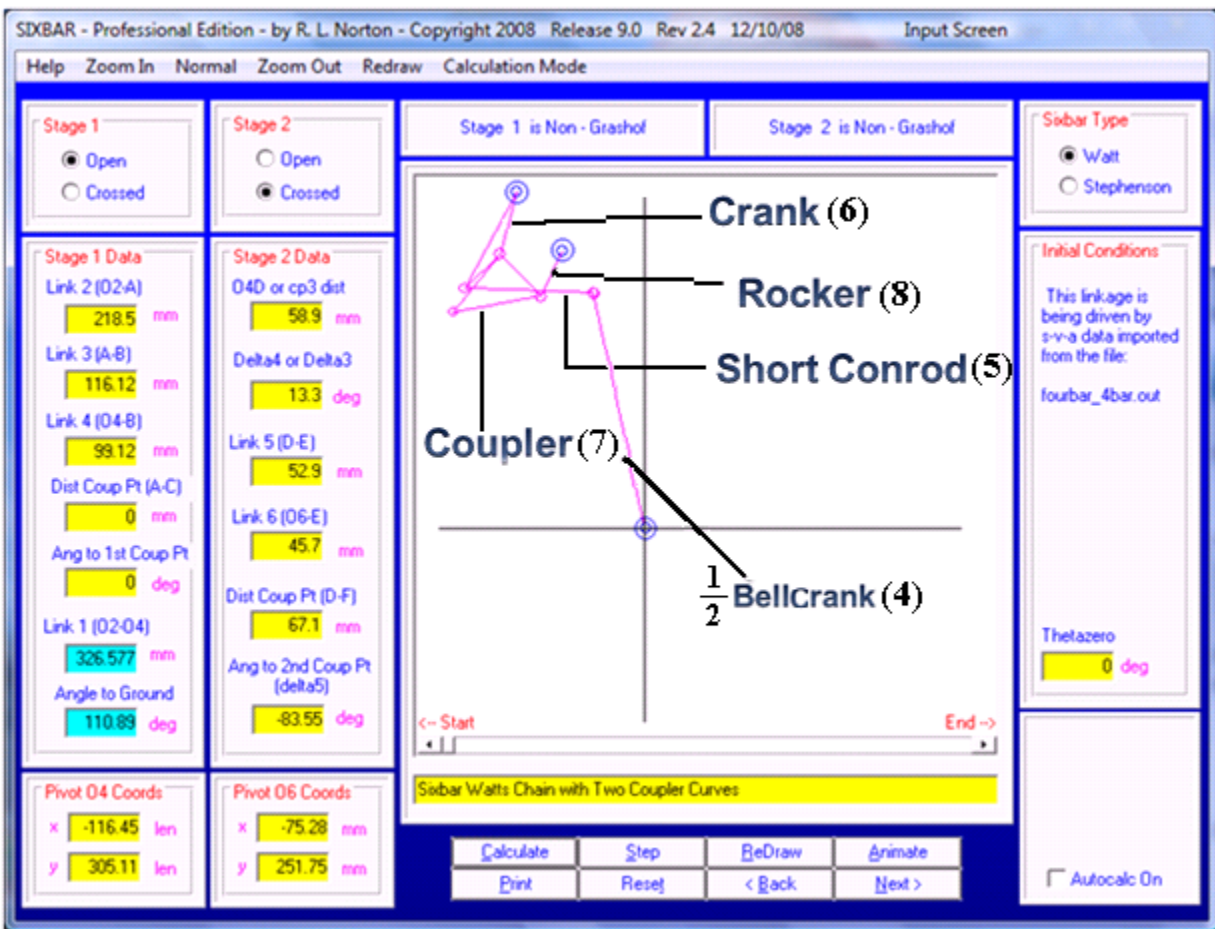


Figure 63: Sixbar Model Geometry

To calculate the forces and accelerations on the system, mass properties of the links were again needed. See Table 2 for a print out of this data.

Table 2: Mass Properties of Sixbar Model

	Link 2	Link 3	Link 4	Link 5	Link 6	units
Mass of Link	0.9036	0.3397	0.7743	0.9860	0.3928	kg
Mass Moment of Inertia vs. CG	0.003867	0.000769	0.000790	0.001291	0.000215	kg-m ²
Distance to CG from Pivot	104.240	59.742	52.088	36.913	25.926	mm
Angle to CG in LRCS	4.183	0.000	-7.978	143.410	0.000	deg

With both the mass property data and the geometry of the system set up in Sixbar, forces and accelerations could be calculated for all link centers of gravity's and pivots. An example of these theoretical acceleration and force results from the model can be seen in Figure 64 and Figure 65.

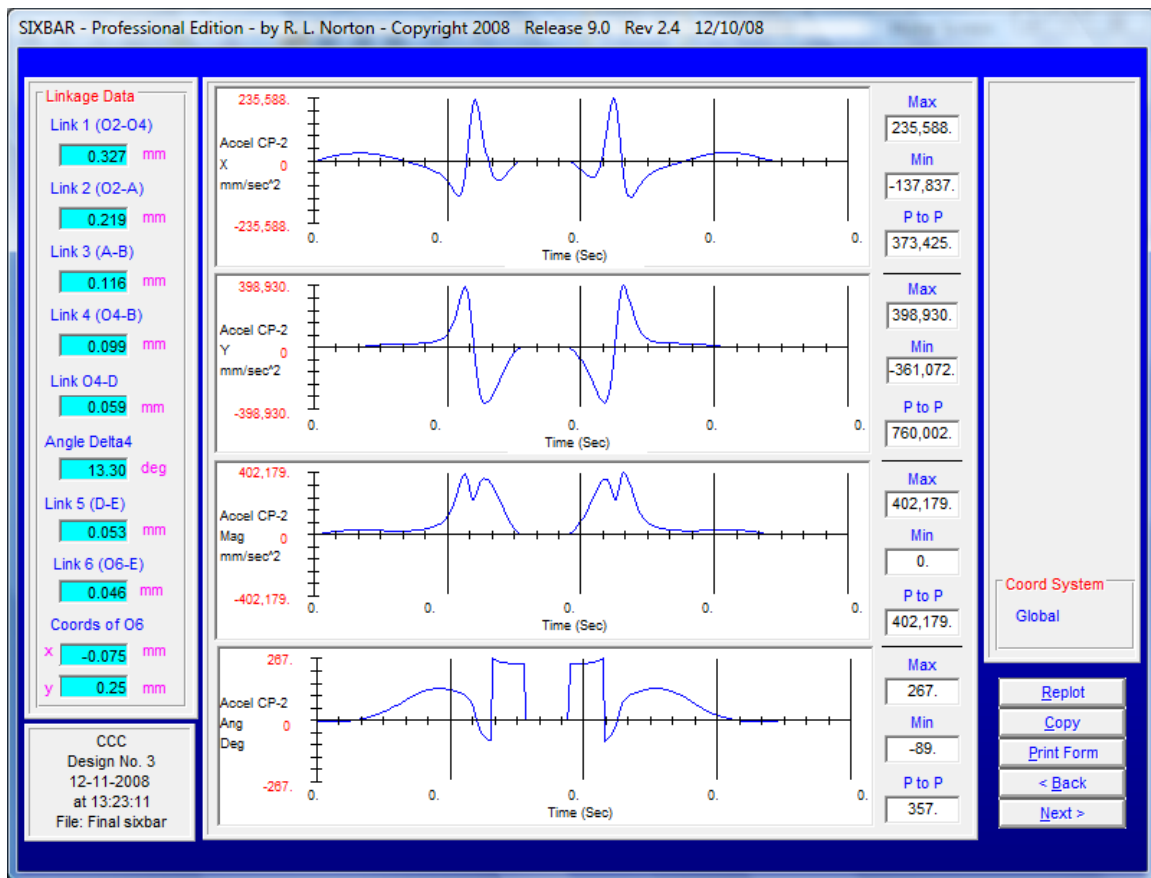


Figure 64: Theoretical Acceleration of Pickoff Tool Pin from Sixbar Model

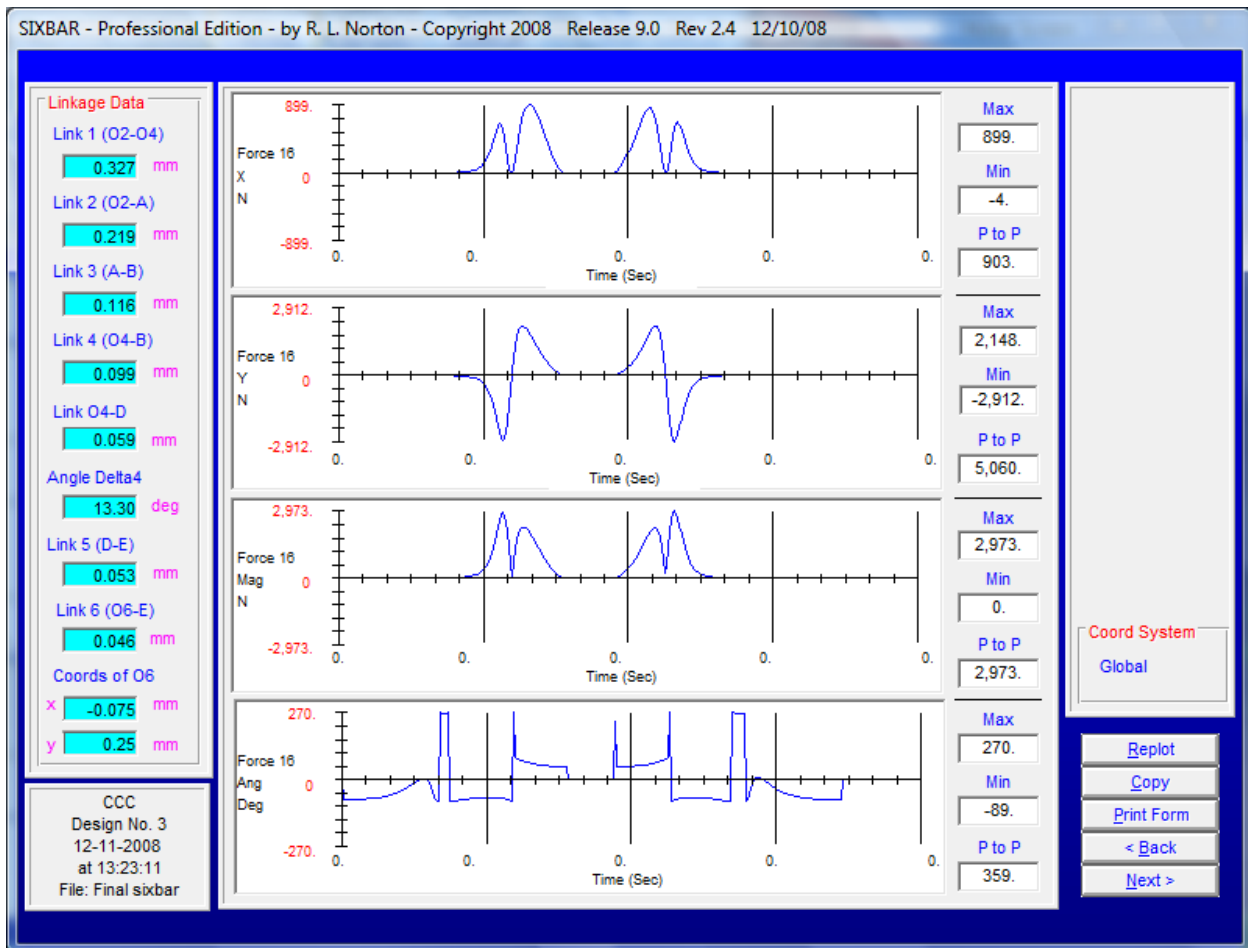


Figure 65: Theoretical Force on Rocker's Pivot from Sixbar Model

4.5.2.4 Fatigue Analysis

The indexing machine is designed to produce product rapidly. Because of this, all components of the machine must be designed to last for millions of cycles. To consider this, fatigue analysis was performed on the pins in this system and other components of the system to ensure that they would be reliable for an infinite life.

4.5.2.4.1 Pin Analysis

The pins are the weakest links in this system, and the largest shear forces are applied to them. To find which pin had the largest shearing force applied to it, the theoretical magnitude

force results from the Sixbar model were analyzed. See Table 3 for the resulting forces from this analysis.

Table 3: Pin Forces from the Sixbar Model

Connecting Member 1	Connecting Member 2	Pin Diameter (mm)	Force Magnitude (N)
Ground	Bellcrank	15.92	1106
Ground	Crank	15.92	2975
Ground	Rocker	15.92	2973
Bellcrank	Short Conrod	10	1085
Short Conrod	Crank	10	1069
Crank	Coupler	14	2816
Coupler	Rocker	14	2992

All pins are made out of SAE 1095 steel normalized at 1650 degrees Fahrenheit. The largest force found in this model was that of the coupler-rocker pin. Because of this fact, this pin was chosen for detailed fatigue analysis. This pin analysis was performed in the equation solver program MathCAD. The full pin analysis can be seen in Appendix E.

The results of this analysis showed that the pin would reach infinite life with a safety factor of 2.689. This analysis provides confidence in the system’s design, as its weakest component lasts for infinite life.

4.5.2.4.2 Component Analysis

Fatigue analysis was also performed on some of the newly designed links in this system. This analysis was completed using the FEA program COSMOSWorks. The first step in this analysis was to find the forces acting on each linkage. This was done by taking the accelerations of the center of gravity of various links from the Sixbar model and multiplying them by the masses of the applicable links. The resulting forces can be seen in Table 4.

Table 4: Theoretical Forces on Fourbar Links

Link Name	Mass of Link (kg)	Acceleration X, Y Components from Sixbar Model (mm/s²)	Force X, Y (N)
Crank	0.774	30256, 17795	23.4, 13.8
Coupler	0.871	185004, 122637	161.1, 106.8
Rocker	0.390	-201016, 106336	-79.0, 41.8

These forces were applied at the center of gravity of the links to the entire link. The links were then restrained at their pins and meshed. After a static study to determine stresses on each link, fatigue analysis was performed. The results of this fatigue analysis showed if the parts reached infinite life and gave a safety factor at infinite life.

The resulting maximum stress on the rocker was 0.1925 MPa. This part reached infinite life with a minimum safety factor of 397. The resulting maximum stress on the coupler was 1.098 MPa. This part reached infinite life with a minimum safety factor of 67.2. Screenshots of the resulting stress and safety factor plots of the coupler can be seen in Appendix F.

Only the rocker and coupler were analyzed in COSMOSWorks. The results from the analysis of those two parts showed very low stresses and very high safety factors. Due to the fact that these were the parts with the largest forces acting upon them, it was deemed not necessary to perform analysis on the remaining parts.

4.5.2.5 Tear Out Analysis

To determine if the pins would tear out of their components, tear out analysis was performed. The coupler-rocker pin was again investigated because it has the highest force acting upon it with the least material supporting it. The side where the pin connects to the coupler was focused on, as there was the least amount of material around the pinhole in this link.

To perform this analysis, the area under the pin was calculated. The force on the pin was then multiplied by this area value to find the tear out stress. This tear out stress was then compared to the yield strength of the coupler material to find the safety factor of the connection.

Based on this analysis, the tear out stress for this pin is 21.94 MPa. This analysis concludes that the pin does not tear out with a safety factor of 22.6. This tear out analysis was performed in the equation solver program MathCAD. See Appendix G for full tear out calculations.

4.5.2.6 Gripper Force Analysis

To ensure that the gripper force is sufficient to hold the excess material at all points from pickoff to drop off, the maximum acceleration of the grippers was investigated. These accelerations were taken from the Sixbar model by plotting the x and y components of the gripper's local coordinate system acceleration. The results of this analysis showed that the highest accelerations of the excess material were 63.1 g pulling directly away from the gripper and 37.8 g pulling to the side of the gripper. These accelerations values were multiplied by the mass of the excess material to find the forces acting on this excess material. These forces are 0.04 N and 0.02 N, respectively.

The force of the gripper was then found by finding the area of the vacuum head and multiplying it by -10 psi. This force value was found to be 0.024 N.

The factors of safety were then found by dividing the gripper force by the maximum force for each direction. The force of the gripper was also multiplied by the static coefficient of friction for steel on steel (0.15 [Weber]) for the side pull factor of safety calculation. The

resulting factor of safety was 33.7 pulling directly away from the gripper and 8.4 pulling to the side.

The result of this gripper analysis shows that the grippers will be able to deal with the accelerations of this system. This gripper analysis was performed in the equation solver program MathCAD. The full analysis can be seen in Appendix H.

4.5.3 Design Analysis Results

The masses and stiffnesses of all the new links in this system can be seen in Table 5. The found maximum stresses and safety factor at infinite life can also be seen in Table 5.

Table 5: Redesigned System Analysis Results

Link	Mass (kg)	Stiffness (N/m)	Max Stress on Link (MPa)	Safety Factor at Infinite Life
Cam Link	1.645	5.12e6	-	-
Long Conrod	0.499	4.64e7	-	-
Bellcrank	1.403	8.10e6	-	-
Short Conrod	0.3397	4.3e08	-	-
Crank	0.7743	7.92e7	-	-
Coupler	0.9860	5.48e7	0.4897	67.2
Rocker	0.3928	1.31e8	0.3427	218.2
Effective:	9.994	2.36e7	-	-

5 Conclusions

For this project, two systems, the existing station and a complete redesign of this station, were analyzed. Through experimentation, theoretical models, and analysis, the following conclusions can be provided.

5.1 Existing Station Design

Through analysis of both experimental data and a theoretical model, it was determined that there was not much opportunity for improvement to the existing station. Both the experimental and analytical data showed small or negligible accelerations at critical points in the system's cycle except for designed-in impacts. Also, when interviewing operators and other people familiar with the machine, it was stated that this station is probably not the root cause for most of the material removal failures. It was universally suggested that the problem might be upstream. The main theorized culprit for the issues in this station is a material breaking station. At that station, improper breaks result in the excess material being improperly placed in the nest. This causes the excess material to be improperly seated for removal, meaning that the excess removal station is unable to remove such material, and that it will be blamed for this type of upstream error because the only detector is there.

5.2 Redesigned Station

The redesign offers many advantages over the existing station. First, it eliminates the coupled motion of the slide and rotation of the pickoff tool. By removing the coupled motion, the redesign reduces the degrees of freedom in the system from two to one. This results in only one cam being needed to drive the system. The redesign also simplifies the total number of moving parts from thirteen to seven. The final advantage of the new system is that it has a direct adjustment for the alignment of the pickoff tool. On the existing system the set-up for the angle of the pickoff tool was dependent on the height at which it the pickoff tool was placed, so if either of those were altered the other would also need to be adjusted accordingly. On the redesign, each adjustment is independent allowing for any one of them to be altered without affecting the others.

There are some disadvantages to the redesigned system. The main disadvantage is the high accelerations experienced in the pickoff tools motion. These high accelerations are caused by the large displacement the pickoff tool must traverse on its way to blowing-off the material into the scrap chute. These accelerations, however, do not necessarily affect the system adversely. As shown by the gripper force equations, the excess material will not be flung off the grippers due to these accelerations. Also, as shown by the fatigue equations, this system is designed to last for infinite life even with these accelerations. The links have very low stress levels.

Another possible disadvantage to the system is the small clearance the pickoff tool has with the nest at one point in its motion. While the minimum clearance between the two is 6.5 mm, that still seemed to be a topic of concern with some of the engineers. Problems could arise if the system is placed incorrectly in the system, as the pickoff tool could smash into a nest if placed too close to the indexer. However, the likelihood of a nearly 7mm error in placement is quite remote.

The main drawback of this system is that it is probably not economic to replace the current excess material unload station in existing machines. This is because the root cause of this system's error may be from an upstream station. Because of this, the redesign may not substantially affect machine downtime. Future versions of this machine or similar machines may benefit from this design, as this system should be less expensive to produce and take less time to set up.

6 Recommendations

- Further investigate Material Break Station – To track down the root cause of this machine failure, the material break station should be investigated. This station was identified as causing this problem by many operators and engineers. If the analysis of this station clears it, other stations in the system should be investigated.
- Install observation device – A device such as a camera could be installed to help track down this error. Such a camera would take a picture of each nest as it passes through the material break station. Pictures of nests that later failed excess material unload could be analyzed to determine if material placement is even a real issue. Camera placement could also be used to track down the root cause of the failure, as pictures of failed nests may give insight as to where in the system the error is starting. Such a camera could be moveable and temporary.
- The redesigned system should not be used to replace the current design in existing machines– Because the current system may not be the cause of the machine downtime, it would be ineffective to replace this system. The redesign also utilized a similar motion, meaning that, if the error is caused by the general motion, this system will not address these problems.
- The redesigned system should be used for future excess material unload stations or other stations that require a similar motion – This system features a simple linkage to achieve a complex motion. This station may be more economical to utilize compared to a more complex station in future systems

- In general, simple linkages should be utilized over complex ones and should be investigated as valid design solutions in the design of all machines. In many cases, such as this one, simple, one-DOF systems are just as effective as a complex, multi-DOF system.

7 References

Baird, Timothy and Michael DiDonato. "Redesign of a Cartridge Unload Mechanism". WPI 2004.

Norton, Robert L. Cam Design and Manufacturing Handbook. Industrial Press 2002.

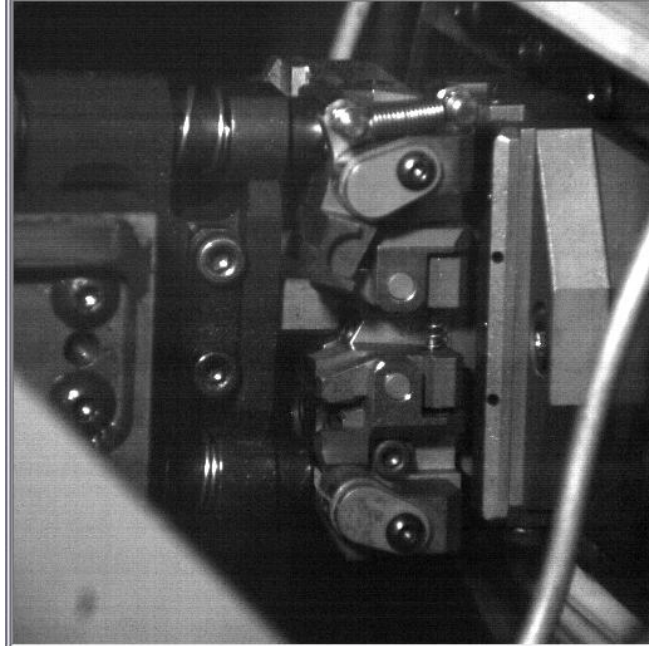
Norton, Robert L. Machine Design: An Integrated Approach. Prentice Hall 2005.

Weber, Robert L and others. College Physics- 4th Edition. USA: McGraw-Hill, 1965: 66.

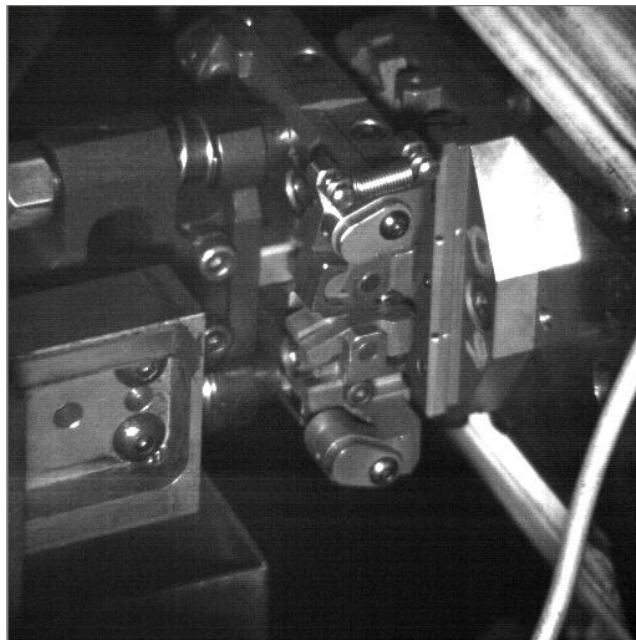
8 Appendices

8.1 Appendix A: High-Speed Video Shot

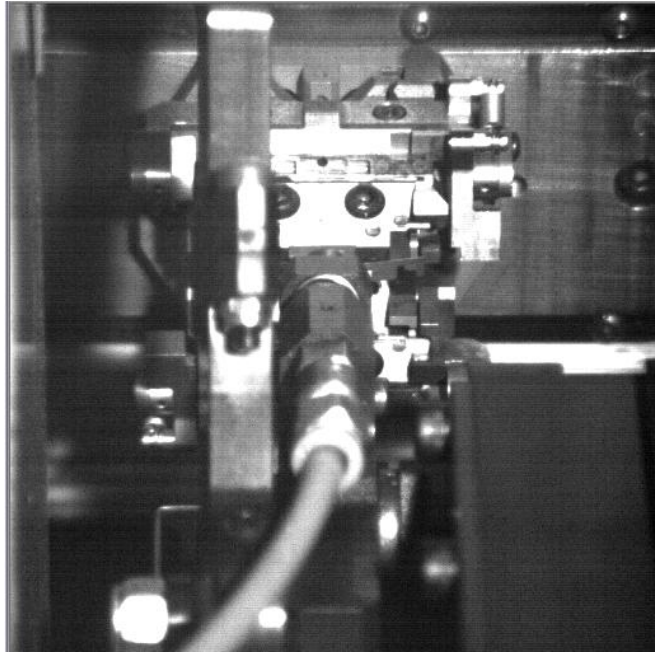
8.1.1 Shot 1



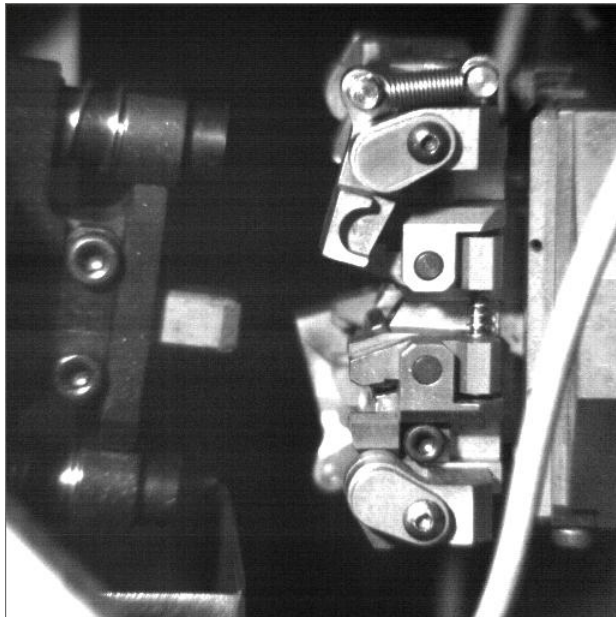
8.1.2 Shot 2



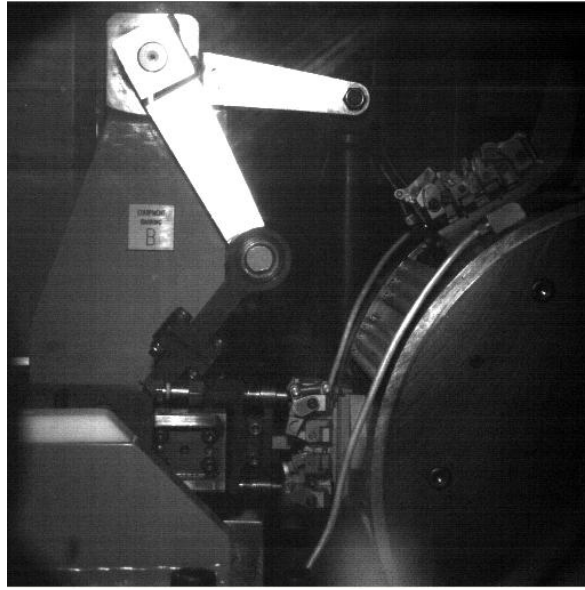
8.1.3 Shot 3



8.1.4 Shot 4



8.1.5 Shot 5



8.2 Appendix B: Effective Mass and Stiffness Calculations

Effective mass of the rotate linkage train

effective mass: lever cam follower

$$m_{lcf} := 1.573177\text{kg}$$

$$I_{lcf} := 5.17 \cdot 10^4 \text{ kg} \cdot \text{mm}^2$$

$$r_{lcf} := 330\text{mm}$$

$$m_{\text{eff1}} := \frac{I_{lcf}}{r_{lcf}^2} = 0.475 \text{ kg}$$

effective mass: ADN connecting rod

$$m_{\text{adn}} := 0.71132271\text{kg}$$

$$I_{\text{adn}} := 7.06 \cdot 10^4 \text{ kg} \cdot \text{mm}^2$$

$$r_{\text{adn}} := 511\text{mm}$$

$$m_{\text{eff2}} := m_{\text{adn}} = 0.711 \text{ kg}$$

effective mass: lever actuator

$$m_{lva} := 1.018975\text{kg}$$

$$I_{lva} := 1.08 \cdot 10^4 \text{ kg} \cdot \text{mm}^2$$

$$r_{lva} := 120\text{mm}$$

$$m_{\text{eff3}} := \frac{I_{lva}}{r_{lva}^2} = 0.75 \text{ kg}$$

effective mass: shaft offset

$$m_{\text{shoff}} := 0.27590143\text{kg}$$

$$I_{\text{shoff}} := 1.27 \cdot 10^2 \text{ kg} \cdot \text{mm}^2$$

$$r_{\text{shoff}} := 120\text{mm}$$

$$m_{\text{eff4}} := \frac{I_{\text{shoff}}}{r_{\text{shoff}}^2} = 8.819 \times 10^{-3} \text{ kg}$$

effective mass: connecting link asm

$$m_{\text{cla}} := 0.26288092\text{kg}$$

$$I_{\text{cla}} := 1.65 \cdot 10^3 \text{ kg} \cdot \text{mm}^2$$

$$r_{\text{cla}} := 124.4\text{mm}$$

$$m_{\text{eff5}} := m_{\text{cla}} = 0.263 \text{ kg}$$

TOTAL FOR ROTATE LINKAGE TRAIN

$$m_{\text{tot,eff}} := m_{\text{eff1}} + m_{\text{eff2}} + m_{\text{eff3}} + m_{\text{eff4}} + m_{\text{eff5}} = 2.208 \text{ kg}$$

Effective mass of slider linkage train

effective mass: lever cam follower + cam follower

$$m_{lcf} := 1.573177\text{kg} + 0.310\text{kg} = 1.883\text{kg}$$

$$I_{lcf} := 5.17 \cdot 10^4 \text{kg} \cdot \text{mm}^2$$

$$r_{lcf} := 330\text{mm}$$

$$m_{\text{eff1}} := \frac{I_{lcf}}{r_{lcf}^2} = 0.475\text{kg}$$

effective mass: AEG connecting rod

$$m_{aeg} := 0.3815992\text{kg}$$

$$I_{aeg} := 1.21 \cdot 10^4 \text{kg} \cdot \text{mm}^2$$

$$r_{aeg} := 275\text{mm}$$

$$m_{\text{eff2}} := m_{aeg} = 0.382\text{kg}$$

effective mass: lvr actuator

$$m_{lvr} := 1.018975\text{kg}$$

$$I_{lvr} := 1.08 \cdot 10^4 \text{kg} \cdot \text{mm}^2$$

$$I_{lvr} = 0.011 \text{m}^2 \cdot \text{kg}$$

big half $r_{lvr1} := 184\text{mm}$

small half $r_{lvr2} := 165\text{mm}$

$$m_{\text{eff3}} := \frac{I_{lvr}}{r_{lvr1}^2} = 0.319\text{kg}$$

$$m_{\text{eff4}} := \frac{I_{lvr}}{r_{lvr2}^2} = 0.397\text{kg}$$

effective mass: slider

$$m_{sl} := 0.63556\text{kg}$$

$$I_{sl} := 5.2697 \cdot 10^3 \text{kg} \cdot \text{mm}^2$$

$$r_{sl} := 1$$

$$m_{\text{eff5}} := m_{sl} = 0.636\text{kg}$$

effective mass: drive link

$$m_{dl} := 0.16612465 \text{ kg}$$

$$I_{dl} := 1.10 \cdot 10^{-2} \text{ kg} \cdot \text{mm}^2$$

$$r_{dl} := 32 \text{ mm}$$

$$m_{eff6} := m_{dl} = 0.166 \text{ kg}$$

TOTAL FOR SLIDER LINKAGE TRAIN

$$m_a := m_{eff4} + m_{eff5} + m_{eff6}$$

$$a := 165 \text{ mm}$$

$$b := 184 \text{ mm}$$

$$m_b := m_{eff1} + m_{eff2} + m_{eff3}$$

Lever ratio calculation

$$m_{tot,eff} := m_a + \left(\frac{b}{a}\right)^2 \cdot m_b = 2.66 \text{ kg}$$

Effective mass of the new system

effective mass: rocker

$$m_{\text{rock}} := 0.395 \text{ kg}$$

$$m_{\text{eff1}} := m_{\text{rock}} = 0.395 \text{ kg}$$

effective mass: coupler plus pickoff tool

$$m_{\text{coup}} := 0.976 \text{ kg}$$

$$m_{\text{eff2}} := m_{\text{coup}} = 0.976 \text{ kg}$$

effective mass: crank

$$m_{\text{crank}} := 0.738 \text{ kg}$$

$$m_{\text{eff3}} := m_{\text{crank}} = 0.738 \text{ kg}$$

lever ratio 1 a := 58.9 b := 52.9 c := 99.1

$$m_{\text{eff4}} := (m_{\text{eff1}} + m_{\text{eff2}}) \cdot \left(\frac{b}{c}\right)^2 + (m_{\text{eff3}}) \cdot \left(\frac{a}{c}\right)^2 = 0.651 \text{ kg}$$

effective mass: small conrod

$$m_{\text{conrod}} := 0.331 \text{ kg}$$

$$m_{\text{eff5}} := m_{\text{conrod}} = 0.331 \text{ kg}$$

effective mass: big half of bell crank

$$m_{\text{bell1}} := 0.894 \text{ kg}$$

+

$$m_{\text{eff6}} := m_{\text{bell1}} = 0.894 \text{ kg}$$

effective mass: small half of bell crank

$$m_{\text{bell2}} := 0.384 \text{ kg}$$

$$m_{\text{eff7}} := m_{\text{bell2}} = 0.384 \text{ kg}$$

lever ratio 2

d := 218.5 e := 100

$$m_{\text{eff8}} := (m_{\text{eff4}} + m_{\text{eff5}} + m_{\text{bell1}}) \cdot \left(\frac{d}{e}\right)^2 + m_{\text{bell2}} = 9.342 \text{ kg}$$

TOTAL FOR GREEN LINKS

$$m_{\text{tot.eff}} := m_{\text{eff4}} + m_{\text{eff8}} = 9.994 \text{ kg}$$

Effective Stiffness Redesign System

Stiffnesses

$$k_{\text{camlever}} := 5.12 \cdot 10^6 \cdot \frac{\text{N}}{\text{m}}$$

$$k_{\text{longconrod}} := 4.64 \cdot 10^7 \cdot \frac{\text{N}}{\text{m}}$$

$$k_{\text{bellcrankshort}} := 4.64 \cdot 10^7 \cdot \frac{\text{N}}{\text{m}}$$

$$k_{\text{bellcranklong}} := 9.82 \cdot 10^6 \cdot \frac{\text{N}}{\text{m}}$$

$$k_{\text{shortconrod}} := 4.30 \cdot 10^8 \cdot \frac{\text{N}}{\text{m}}$$

$$k_{\text{crank}} := 7.92 \cdot 10^7 \cdot \frac{\text{N}}{\text{m}}$$

$$k_{\text{coupler}} := 5.48 \cdot 10^7 \cdot \frac{\text{N}}{\text{m}}$$

$$k_{\text{rocker}} := 1.31 \cdot 10^8 \cdot \frac{\text{N}}{\text{m}}$$

Leveres

$$L_{\text{tbc}} := 218 \text{mm}$$

$$L_{\text{sbc}} := 100 \text{mm}$$

Rocker to Bell Crank Long Side

$$k_{\text{oneoverRBCH1}} := \frac{1}{k_{\text{rocker}}} + \frac{1}{k_{\text{coupler}}} + \frac{1}{k_{\text{crank}}} + \frac{1}{k_{\text{shortconrod}}} + \frac{1}{k_{\text{bellcranklong}}}$$

$$k_{\text{RBCH1}} := \frac{1}{k_{\text{oneoverRBCH1}}} = 7.009 \times 10^6 \frac{\text{N}}{\text{m}}$$

Lever Arm

$$k_{\text{la}} := \left(\frac{L_{\text{sbc}}}{L_{\text{tbc}}} \right)^2 \cdot k_{\text{RBCH1}} + k_{\text{bellcrankshort}} = 4.787 \times 10^7 \frac{\text{N}}{\text{m}} \quad +$$

To long conrod as cam lever is ground

$$k_{\text{oneovereff}} := \frac{1}{k_{\text{la}}} + \frac{1}{k_{\text{longconrod}}}$$

$$k_{\text{eff}} := \frac{1}{k_{\text{oneovereff}}} = 2.356 \times 10^7 \frac{\text{N}}{\text{m}}$$

8.3 Appendix C: MATLAB Code

8.3.1 Main MATLAB Code

```
1 %% Handout Norton 09/28/08
2 clear; clc; close all;
3 global k2 c2 m2 d2 j2 q mI2 I2 w r s1 s2 sidot s2dot ...
4 t1 t2 sigma1 sigma2 sigma1dot sigma2dot
5
6 %% system parameters
7
8 m1=1; k1=1; zeta1=0.05;
9
10 m2=2.675; k2=5.741e9; zeta2=0.05;
11 I2=633.3e2;
12 j2=263.9e9;
13 q=35;
14 mI2=1.673;
15 r=175;
16 omega1=sqrt(k1/m1);
17 c1=2*zeta1*omega1;
18 omega2=sqrt(k2/m2);
19 c2=2*zeta2*omega2;
20 d2=2*zeta2*sqrt(j2/I2);
21
22 w=220*2*pi/60;
23 T=2*pi/w;
24 dt=T/1440;
25 t=[0:dt:T]';
26
27 %% Cam profiles
28 dataCam1=dlmread('JG_cam_reengineered.dat','',6,0) % Re-engineered in Dynacam
29 dataCam2=dlmread('JH_engineered_Rev1.dat','',6,0) % Re-engineered in Dynacam
30 s=dataCam1(:,2); sdot=dataCam1(:,3);
31 sigma=dataCam2(:,2); sigmaDot=dataCam2(:,3);
32
33 %% Solve the system
34 y0=[s(1);0;sigma(1);0];
35 nip=3;
36 y(1,:)=y0;
37
38 for i=1:length(t)-1
39
40     t1=t(i); t2=t(i+1);
41     tspan = (t1:t2-t1)/nip:t2;
42
43     s1=s(i); s2=s(i+1);
44     sidot=sdot(i); s2dot=sdot(i+1);
45     sigma1=sigma(i); sigma2=sigma(i+1);
46     sigma1dot=sigmaDot(i); sigma2dot=sigmaDot(i+1);
47
48     [t_ode,yStep]=ode45('camSystem_11_18', tspan,y0);figure(30)
49
50     y0=yStep(nip+1,:);
51     y(i+1,:)=y0;
52
53 end
54
55 %% original notations
56 x=y(:,1);
57 xdot=y(:,2);
58 theta=y(:,3);
59 thetaDot=y(:,4);
60
61 %% Plot the results
62 subplot(2,2,1);
63 plot(t,x); xlabel('t(s)'); ylabel('x')
64 subplot(2,2,2);
65 plot(t,xdot); xlabel('t(s)'); ylabel('xdot')
66 subplot(2,2,3);
67 plot(t,theta); xlabel('t(s)'); ylabel('theta')
68 subplot(2,2,4);
69 plot(t,thetaDot); xlabel('t(s)'); ylabel('thetaDot')
70
71 %% Plot s and sigma
72 subplot(2,2,1)
73 hold on;
74 plot(t, s, '-r')
75 legend('x', 's')
76 subplot(2,2,3)
77 hold on;
78 plot(t, sigma,'-r'); legend('theta', 'sigma')
79 subplot(2,2,2)
80 hold on; plot(t, sdot, '-r')
81 legend('xDot', 'sdot')
82 subplot(2,2,4)
83 hold on; plot(t, sigmaDot,'-r');
```

```

84 -         legend('thetaDot', 'sigmaDot')
85
86
87     %% Calculate the acceleration
88
89     A=m2+mI2;
90     B=mI2*q*cos(y(:,3));
91     D=I2+mI2*q^2;
92     C=mI2*cos(y(:,3));
93     M=mI2.*y(:,4).^2*q.*sin(y(:,3))-c2*y(:,2)-k2*y(:,1)+k2*s+c2*sdot;
94     N=-d2*y(:,4)-j2*y(:,3)+j2*sigma+d2*sigmaDot;
95
96     xdotdot=(M.*D-N.*B)./(A*D-C.*B);
97     thetaDotdot=(N.*A-M.*C)./(A*D-C.*B);
98
99     figure
100    subplot(2,1,1)
101    plot(t, xdotdot); xlabel('t(s)'); ylabel('xdotdot')
102    subplot(2,1,2)
103    plot(t, thetaDotdot); xlabel('t(s)'); ylabel('thetaDotdot')
104

```

8.3.2 Cam Systems Code

```

1  function ydot=camSystem_11_18(t,y)
2
3  global k2 c2 m2 d2 j2 q mI2 I2 w r s1 s2 s1dot s2dot ...
4      t1 t2 sigma1 sigma2 sigma1dot sigma2dot
5
6
7  s=s1+((s2-s1)*(t-t1))/(t2-t1);
8  sdot=s1dot+((s2dot-s1dot)*(t-t1))/(t2-t1);
9  sigma=sigma1+((sigma2-sigma1)*(t-t1))/(t2-t1);
10 sigmaDot=sigma1dot+((sigma2dot-sigma1dot)*(t-t1))/(t2-t1);
11
12 % write the system in an explicit for: ydot=f(y,t)
13 % original eqs: A*xdotdot +B*theta_dotdot=M;
14 %              C*xdotdot+D*theta_dotdot=N;
15 A=m2+mI2;
16 B=mI2*q*cos(y(3));
17
18 D=I2+mI2*q^2;
19 C=mI2*cos(y(3));
20
21
22 M = mI2 * y(4)^2 * q * sin(y(3))- c2 * y(2) - k2 * y(1)+ k2 * s + c2 * sdot;
23 N = -d2 * y(4) - j2 * y(3) + j2 * sigma + d2 * sigmaDot;
24 ydot(1,1) = y(2);
25 ydot(2,1) = ( M * D - N * B ) / ( A * D - C * B );
26 ydot(3,1) = y(4);
27 ydot(4,1) = ( N * A - M * C ) / ( A * D - C * B );
28

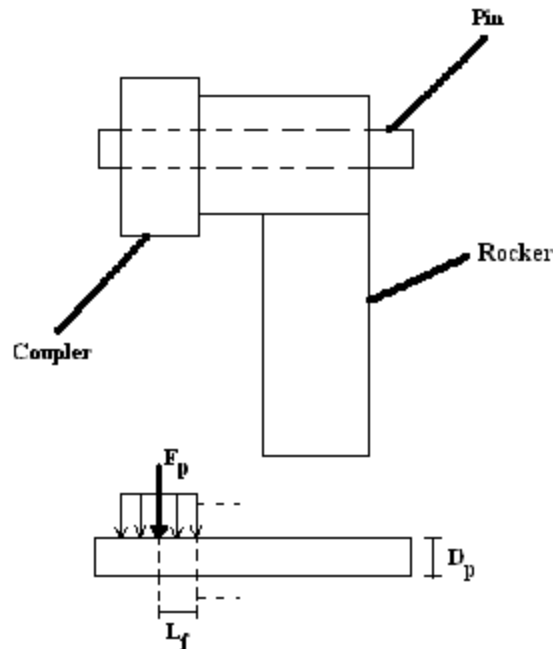
```

8.4 Appendix D: List of Drawings

<u>Part</u>	<u>Drawing File Name</u>
Bellcrank	lever_actuator_l218-100A90.pdf
Connecting Rod, Length 116.5mm	connecting_rod_body_116-5.pdf
Connecting Rod, Length 271mm	connecting_rod_body_271.pdf
Coupler Assembly	coupler_assembly.pdf
Coupler	coupler.pdf
Crank	crank.pdf
Height Adjustment Bracket	height_adjustment_bracket.pdf
Pickoff Tool Mounting Pin	pickoff_tool_mounting_pin.pdf
Pin, Crank	crank_pin.pdf
Pin, Rocker	rocker_pin.pdf
Redesigned Assembly	redesigned_excess_unload_assembly.pdf
Rocker	rocker.pdf
Weldment	bracket-unload-excess.pdf

8.5 Appendix E: Pin Fatigue Analysis MathCAD Sheet

Pin Fatigue Calculations

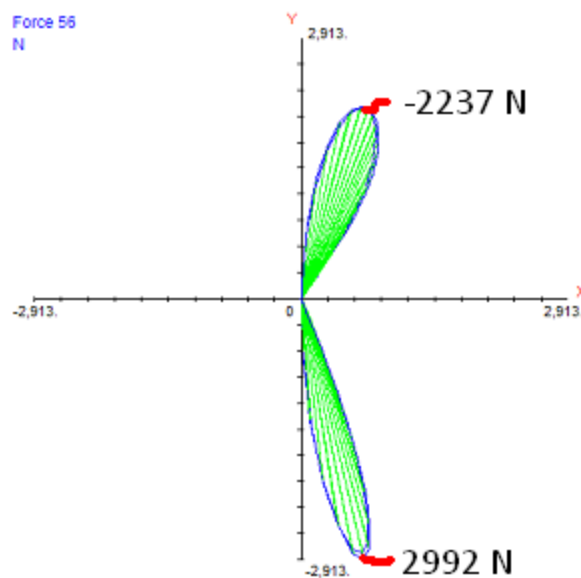


Input Variables

Material	Steel 1095 normalized at 1650 deg F
yield strength	$S_y := 496\text{MPa}$
ultimate tension	$S_{ut} := 1014\text{MPa}$
Max pin force	$F_{pmax} := 2991.6\text{N}$
Min pin force	$F_{pmin} := -2237.4\text{N}$
Pin Diameter	$D_p := 14\text{mm}$
Distance to force	$L_f := 7.5\text{mm}$

Correction Factor Variables

Type of load	load := "bending"
Surface	surface := "machined"
Temperate	$T_{err} := 80\text{f F}$
Reliability	$R := 0.5$
Size	$d := D_p$



pin force plot from Sixbar model

Alternating and Mean Stress

Area moment of inertia

$$I := \frac{\pi \cdot D_p^4}{64} = 1.886 \times 10^3 \cdot \text{mm}^4$$

Max and min bending moments

$$M_{\max} := F_{p\max} \cdot L_f = 22.437 \cdot \text{N} \cdot \text{m}$$

$$M_{\min} := F_{p\min} \cdot L_f = -16.78 \cdot \text{N} \cdot \text{m}$$

Max and min stresses

$$\sigma_{\max} := \frac{M_{\max} \cdot \left(\frac{D_p}{2}\right)}{I} = 83.288 \cdot \text{MPa}$$

$$\sigma_{\min} := \frac{M_{\min} \cdot \left(\frac{D_p}{2}\right)}{I} = -62.29 \cdot \text{MPa}$$

Alternating and Mean Stresses

$$\sigma_a := \frac{\sigma_{\max} - \sigma_{\min}}{2} = 72.789 \cdot \text{MPa}$$

$$\sigma_m := \frac{\sigma_{\max} + \sigma_{\min}}{2} = 10.499 \cdot \text{MPa}$$

Alternating and Mean von Mises Stresses

$$\sigma'_a := \sigma_a$$

$$\sigma'_m := \sigma_m$$

Corrected endurance strength

Correctional Factors:

Uncorrected endurance limit.

$$S'_e := \begin{cases} \text{return } 0.5 \cdot S_{ut} & \text{if } S_{ut} < 200 \cdot \text{ksi} \\ \text{return } (100 \text{ksi}) & \text{if } S_{ut} \geq 200 \cdot \text{ksi} \end{cases} = 5.07 \times 10^8 \text{ Pa}$$

Load factor

$$C_{\text{load}} := \begin{cases} \text{return } 1 & \text{if load} = \text{"bending"} \\ \text{return } 1 & \text{if load} = \text{"torsion"} \\ \text{return } 0.7 & \text{if load} = \text{"axial"} \end{cases} = 1$$

Size Factor

$$C_{\text{size}} := 0.869 \cdot \left(\frac{d}{\text{in}} \right)^{-0.097} = 0.921$$

Surface factor

$$A := \begin{cases} \text{return } 1.34 & \text{if surface} = \text{"ground"} \\ \text{return } 2.70 & \text{if surface} = \text{"machined"} \\ \text{return } 2.70 & \text{if surface} = \text{"cold_rolled"} \\ \text{return } 14.4 & \text{if surface} = \text{"hot_rolled"} \\ \text{return } 39.9 & \text{if surface} = \text{"forged"} \end{cases} = 2.7$$

$$b := \begin{cases} \text{return } -0.085 & \text{if surface} = \text{"ground"} \\ \text{return } -0.265 & \text{if surface} = \text{"machined"} \\ \text{return } -0.265 & \text{if surface} = \text{"cold_rolled"} \\ \text{return } -0.718 & \text{if surface} = \text{"hot_rolled"} \\ \text{return } -0.995 & \text{if surface} = \text{"forged"} \end{cases} = -0.265$$

$$C_{\text{surfl}} := A \cdot \left(\frac{S_{ut}}{\text{MPa}} \right)^b = 0.431$$

$$C_{\text{surf}} := \begin{cases} 1 & \text{if } C_{\text{surfl}} > 1 \\ C_{\text{surfl}} & \text{otherwise} \end{cases} = 0.431$$

Temp Factor

$$C_{\text{temp}} := \begin{cases} \text{return } 1 & \text{if } T \leq 840 \\ 1 - 0.0032 \cdot (T - 840) & \text{otherwise} \end{cases} = 1$$

Reliability

$$C_{\text{reliab}} := \begin{cases} \text{return } 1.000 & \text{if } R = 0.50 \\ \text{return } 0.897 & \text{if } R = 0.90 \\ \text{return } 0.814 & \text{if } R = 0.99 \\ \text{return } 0.753 & \text{if } R = 0.999 \\ \text{return } 0.702 & \text{if } R = 0.9999 \\ \text{return } 0.659 & \text{if } R = 0.99999 \end{cases} = 1$$

Corrected endurance strength:

$$S_e = C_{\text{load}} \cdot C_{\text{size}} \cdot C_{\text{surf}} \cdot C_{\text{temp}} \cdot C_{\text{reliab}} \cdot S'_e = 201.32 \text{ MPa}$$

Safety Factor

$$N_{F3} := \frac{S_e \cdot S_{\text{ut}}}{\sigma'_a \cdot S_{\text{ut}} + \sigma'_m \cdot S_e} = 2.689$$

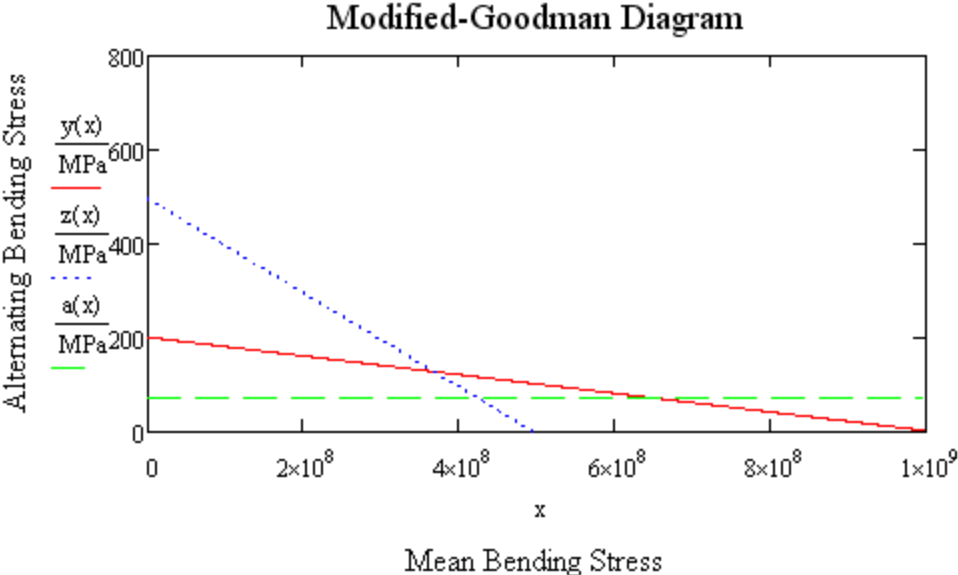
Goodman Diagram

$$y(x) := -\left(\frac{S_e}{S_{ut}}\right)x + S_e$$

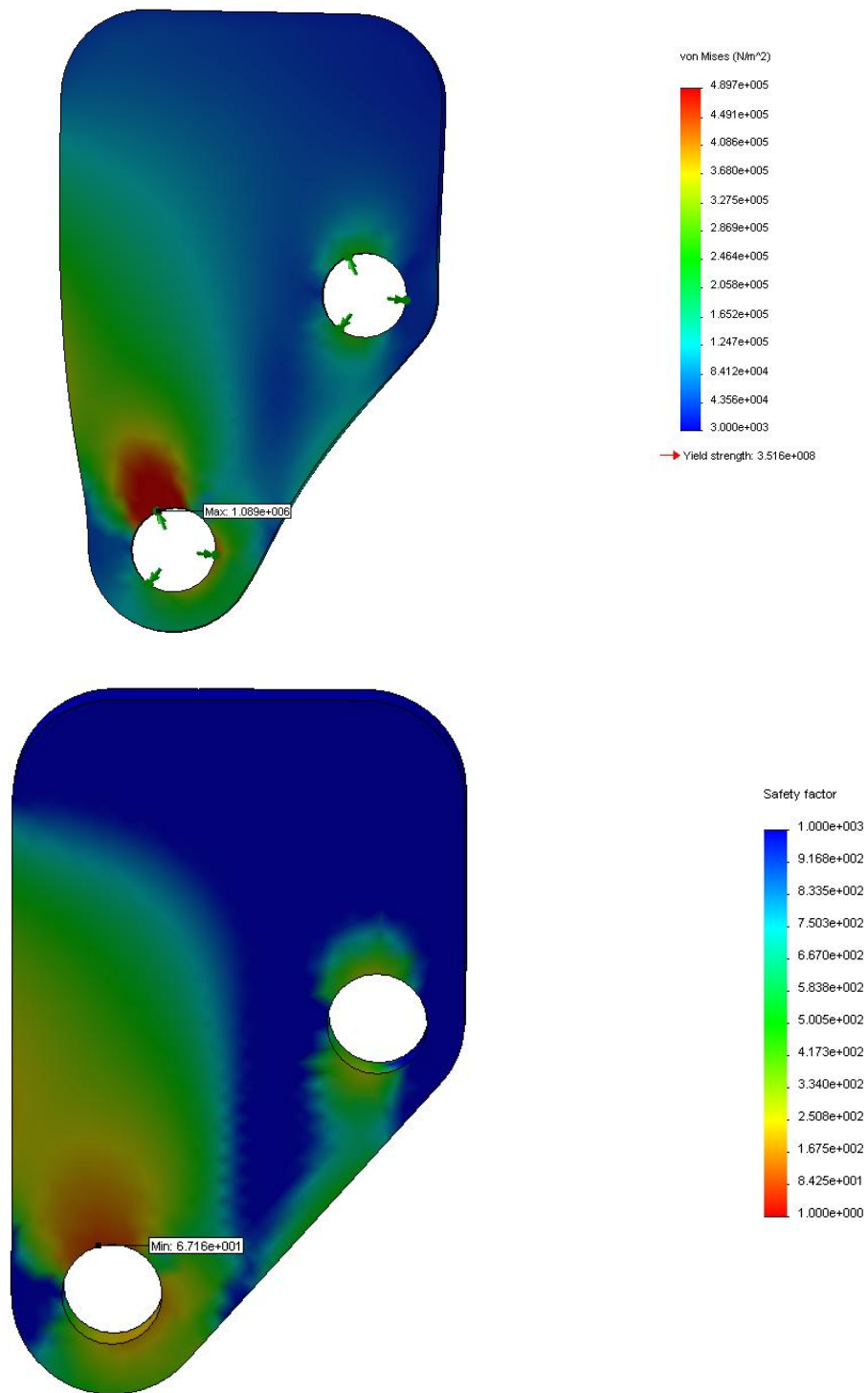
$$z(x) := -x + S_y$$

$$a(x) := \sigma'_a$$

$\sigma'_m = 10.499 \text{ MPa}$ (mean von Mises Stress not pictured, would be shown as $x = \sigma'_m$)



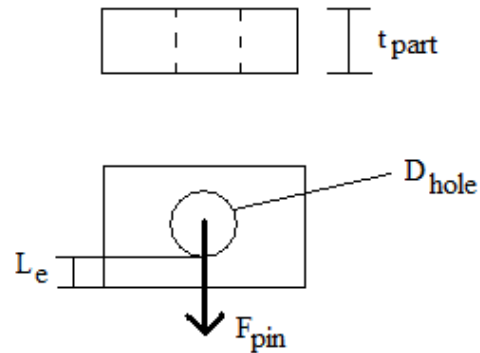
8.6 Appendix F: Coupler COSMOSWorks Screenshots



8.7 Appendix G: Tear out Analysis MathCAD Sheet

Tearout Stress in Pin 56 Join on Coupler

Picture



Inputs

Hole Diameter	$D_{hole} := 14\text{mm}$
Part Thickness	$t_{part} := 14\text{mm}$
Force on Pin from Sixbar Model	$F_{pin} := 2764\text{N}$
Distance from Hole Edge to Part Edge	$L_e := 16\text{mm} - \frac{D_{hole}}{2} = 9\text{mm}$
Material	Steel 1095 normalized at 1650 deg F
Yield Strength	$S_y := 496\text{MPa}$

Calculations

Cross-Sectional Area of Part Between Hole and Edge

$$A_{cs} := t_{part} \cdot L_e = 126 \cdot \text{mm}^2$$

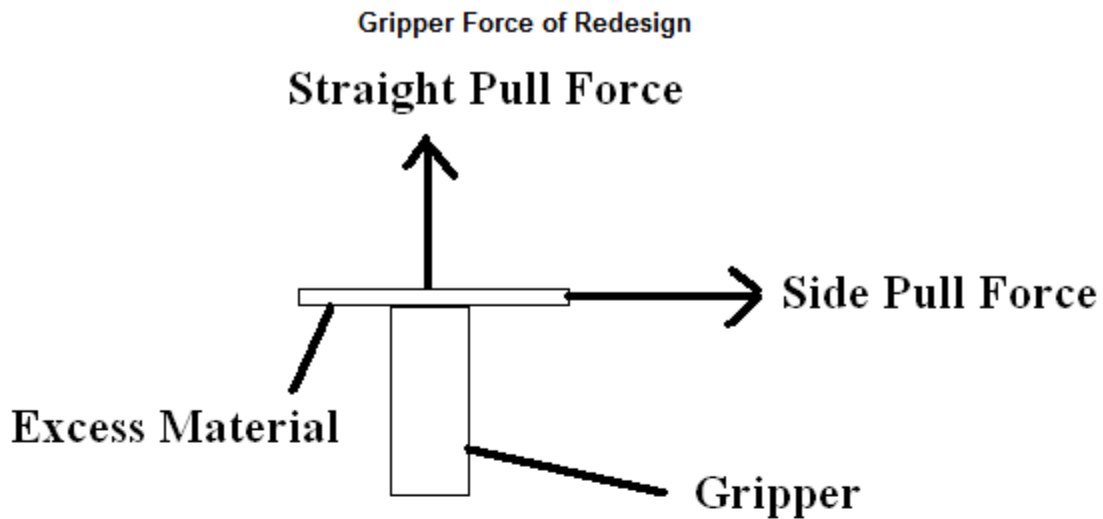
Tearout Stress

$$\tau_{tearout} := \frac{F_{pin}}{A_{cs}} = 21.937 \cdot \text{MPa}$$

Factor of Safety

$$SF := \frac{S_y}{\tau_{tearout}} = 22.611$$

8.8 Appendix H: Gripper Force Analysis MathCAD Sheet



Inputs

Max Acceleration of Blade on Grippers $a_{\text{straight}} := 618454 \frac{\text{mm}}{\text{s}^2}$

$$a_{\text{side}} := 370584 \frac{\text{mm}}{\text{s}^2}$$

Blade Mass $m_{\text{blade}} := 5.7821614 \cdot 10^{-5} \cdot \text{kg}$

Vacuum Pressure $p_v := -10 \cdot \text{psi}$

Gripper Area $a_g := 2.5 \text{mm} \cdot 7 \text{mm} = 17.5 \cdot \text{mm}^2$

Steel on Steel Static Friction Coeff $\mu_{\text{ss}} := 0.15$

Max Force of Blade

$$F_{\text{maxstraight}} := m_{\text{blade}} \cdot a_{\text{straight}} = 0.036 \text{ N}$$

$$F_{\text{maxside}} := m_{\text{blade}} \cdot a_{\text{side}} = 0.021 \text{ N}$$

Gripper Force

$$F_{\text{grip}} := a_g \cdot p_v = -1.207 \text{ N}$$

Factor of Safety Straight Pull

$$\text{SF}_p := \frac{-F_{\text{grip}}}{F_{\text{maxstraight}}} = 33.741$$

Factor of Safety Side Pull

$$\text{SF}_{\text{sp}} := \frac{-F_{\text{grip}} \cdot \mu_{\text{ss}}}{F_{\text{maxside}}} = 8.446$$